"Cytotoxicity and cell cycle effects of gold and silver nanoparticles in human intestinal epithelial Caco-2 cells"

Mariana Vinhas Fernandes

Master degree in Analytical, Clinical and Forensic Toxicology

Dissertation thesis for the Master Degree in Analytical, Clinical and Forensic Toxicology submitted to the Faculty of Pharmacy

Dissertação de candidatura ao grau de Mestre em Toxicologia Analítica, Clínica e Forense apresentada à Faculdade de Farmácia

Supervisors:

Doutora Sónia Alexandra Teixeira Fraga

Professora Doutora Helena Maria Ferreira da Costa Ferreira Carmo

Professora Doutora Maria de Lurdes Pinho de Almeida Souteiro Bastos

University of Porto

September 2014

IS AUTHORIZED THE INTEGRAL REPRODUCTION OF THIS THESIS FOR RESEARCH PURPOSES BY MEANS OF A WRITTEN DECLARATION FOR PERMISSION OF USE.

Experimental work carried out in REQUIMTE Laboratory, Department of Toxicology,

Faculty of Pharmacy, University of Porto

“Tell me and I forget.

Teach me and I remember.

Involve me and I learn.”

Benjamin Franklin

Aknowledgements

Agradecimentos

Com a finalização desta etapa da minha vida não podia deixar de agradecer a algumas pessoas que me apoiaram incondicionalmente nesta aventura que foi o Mestrado de Toxicologia Analítica Clínica e Forense:

Primeiro, queria agradecer à Professora Doutora Maria de Lourdes Bastos, Coordenadora do Mestrado em Toxicologia Analítica Clínica e Forense, agradeço pela criação e oportunidade de frequentar o curso que, já durante a primeira graduação, pretendia efectuar.

Agradeço em particular à Dra. Sónia Alexandra Teixeira Fraga, pela orientação e pela disponibilidade incondicional durante estes meses no laboratório e na realização desta dissertação. Agradeço a forma generosa como me recebeu e transmitiu os seus vastos conhecimentos.

À minha co-orientadora, Professora Doutora Helena Carmo, agradeço também pela orientação e pela sabedoria, dentro e fora do laboratório, onde aprendi a pensar por mim própria.

À Doutora Renata Silva, agradeço pelos ensinamentos de citometria de fluxo e pela paciência que teve comigo na realização das experiências de ciclo celular.

Aos meus colegas do Mestrado, (eles sabem quem são por isso não vou estar a mencionar nomes!) queria agradecer a amizade e o companheirismo que tivemos durante estes dois anos (e que vão durar por mais anos…).

Um especial agradecimento para seis pessoas, que me ajudaram a tornar-me numa pessoa melhor, que me desafiaram todos os dias, e que me ajudaram a passar à frente em alguns momentos maus, e que festejaram comigo nos momentos bons. Por isso agradeço à Ana Sofia Oliveira, Armanda Gomes, Débora Rios de Oliveira, Márcia Monteiro, Margarida Araújo e Ana Filipa Ferreira.

Um último agradecimento à minha família, em especial aos meus pais e irmão, que me ajudaram nas alturas de maior “stress” na realização desta dissertação e pelo apoio incondicional e carinho que me dão todos os dias.´

Abstract

Nanotechnology offers an infinite possibility of advance and innovation in many fields such as industry, cosmetics, biomedicine and food/feed. The production of nanoscaled particles has grown exponentially and this growth has raised several questions regarding the environmental and health impact of these nanoparticles from their production and uses in various areas. However, compared to other fields on which nanoparticles are applied, knowledge of their safety use in the food and feed area is still scarce. The toxicological studies performed so far, demonstrated that physicochemical properties of nanoparticles, such as size, shape, surface chemistry and agglomeration state play a key role in the biological effect induced by NPs.

In the present work it was studied the cytotoxic effect of gold and silver nanoparticles in a human epithelial colorectal adenocarcinoma (Caco-2) cell line. The nanoparticles were functionalized with either citrate or a pentapeptide (CALNN, CALNS or CALND). Cytotoxicity was evaluated using an array of assays to assess the effect of the nanoparticles in cell metabolic activity, plasma membrane integrity, reactive oxygen species (ROS) production, lysosomal membrane integrity and cellular morphology. The effect of these nanoparticles on the cell cycle progression was also evaluated by flow cytometry.

Our results showed that gold nanoparticles had no significant impact in the cells morphology and cytotoxicity endpoints mentioned above. However, silver nanoparticles induced ROS production, concentration-dependent reduction of mitochondrial activity and lysosomal membrane integrity, and loss of monolayer integrity compared to untreated cells. The results from flow cytometry showed no significant difference of cell cycle progression between the treated cells and untreated cells.

Keywords: gold nanoparticles, silver nanoparticles, cytotoxicity, uptake, cell cycle, flow cytometry

Resumo

A nanotecnologia oferece uma possibilidade infinita de avanço e inovação em diversas áreas, como a indústria, cosméticos, biomedicina e nutrição. A produção e aplicação de materiais à nanoescala tem crescido exponencialmente e com este crescimento várias questões têm-se levantado relativamente ao impacto ambiental e na saúde. No entanto, em comparação com outras áreas em que as nanopartículas são aplicadas, o conhecimento sobre o seu uso e potencial risco na área alimentar ainda é escassa. Os estudos toxicológicos realizados até agora demonstraram que as propriedades físico-químicas das nanopartículas, tais como tamanho, forma, química de superfície e do estado de aglomeração desempenham um papel chave no efeito biológico induzido pelas nanopartículas.

No presente trabalho, foi estudado o efeito citotóxico de nanopartículas de ouro e de prata numa linha celular epitelial do adenocarcinoma colo-rectal humano (Caco-2). As nanopartículas foram funcionalizadas com citrato ou um pentapeptídeo (CALNN, CALNS ou CALND). A citotoxicidade foi avaliada utilizando leque de ensaios para avaliar o efeito das nanopartículas na actividade metabólica celular, na integridade da membrana plasmática, na produção de espécies reactivas de oxigénio (ROS), na integridade da membrana lisossomal e morfologia celular. O efeito destas nanopartículas na progressão do ciclo celular foi avaliado por citometria de fluxo.

Os nossos resultados mostraram que nanopartículas de ouro não tiveram um impacto significativo na morfologia celular e parâmetros de citotoxicidade acima mencionados. No entanto, as nanopartículas de prata induziram a produção de ROS, a redução da actividade mitocondrial e integridade da membrana lisossomal dependente da concentração, e a perda de integridade da monocamada, em comparação com células controlo. Os resultados de citometria de fluxo não mostraram diferenças significativas relativamente à progressão do ciclo celular entre as células tratadas e as células controlo.

Palavras- chave: nanopartículas de ouro, nanopartículas de prata, citotoxicidade, internalização, ciclo celular, citometria de fluxo

Index

Aknowledgements V

Resumo IX

List of Tables XIII

List of Figures XV

Chapter 1 1

Introduction 1

1.1. Nanomaterials – overview 3

1.2. Properties and applications 4

1.3. Interactions of metallic nanoparticles with biological systems 8

1.3.1. Influence of the physicochemical properties of gold and silver nanoparticles in the cellular uptake 8

1.3.2. The interaction of metallic nanoparticles with the cellular organelles 11

1.3.3. Toxicity of metallic nanoparticles 12

1.4. Cell cycle effects of AuNPs and AgNPs 19

1.4.1. Cell cycle- overview 19

1.4.2. Cell cycle behaviour in response to DNA damage 21

1.4.3. Metallic nanoparticles and the cell cycle 22

Chapter 2 25

Scope and Aims 25

Chapter 3 29

Experimental section 29

3.1. Materials and methods 31

3.1.1. Reagents and Materials 31

3.1.2. Cell culture 31

3.1.3. AuNPs and AgNPs nanoparticles 31

3.2. Methods and procedures 33

3.2.1. Cytotoxicity assays 33

3.2.2. Flow cytometry analysis 37

3.2.3. Statistical analysis 38
Chapter 4 39
Results 39
4.1. Cytotoxicity of AuNPs and AgNPs 41
4.2. Morphological analysis of Caco – 2 cells by phase contrast microscopy 52
4.3. Results of flow cytometry analysis 55
4.3.1. AuNPs and AgNPs uptake in Caco-2 cells 55
4.3.2. Cell cycle analysis 58
Chapter 5 67
Discussion 69
Chapter 6 73
Conclusion 75
Chapter 7 77
References 79
Supplement 1 89

List of Tables

Table 1 - Main types of NMs based on the dimensions of their structural elements..... 3

Table 2 - Products on the market containing gold nanoparticles in their composition. 6

Table 3 - Products on the market containing silver nanoparticles in their composition. 7

Table 4 – Summary of some *in vitro* studies on the cytotoxicity of gold nanoparticles. 14

Table 5 - Summary of some *in vitro* studies on the genotoxicity of gold nanoparticles. ... 15

Table 6 - Summary of recent *in vitro* studies on the cytotoxicity of silver nanoparticles. .. 17

Table 7 - Summary of some *in vitro* studies on the genotoxicity of silver nanoparticles. .. 18

Table 8 - Cyclin and cyclin-dependent kinases (CDKs) involved in the cell cycle progression. 20

Table 9 - Main characteristics of AuNPs and AgNPs.The average size and zeta potential of the AuNPs were determined by DLS. The Au content of the suspensions was determined by GFAAS. The Ag content of the suspensions was determined by ICP-MS. 33

Table 10 - Gold nanoparticles (AuNPs) uptake determined by flow cytometry analysis of cell size (FSC) and complexity (SSC) in synchronized and non-synchronized cultures, after 24h of exposure. 55

Table 11 - Silver nanoparticles (AgNPs) uptake determined by flow cytometry analysis of cell size (FSC) and complexity (SSC) in synchronized and non-synchronized cultures, after 24h of exposure. 57

Table 12 - Effect of 24h-exposure to AuNPs on cell cycle distribution (%) in synchronized Caco-2 cultures. 59

Table 13 - Effect of 24h-exposure to AuNPs on cell cycle distribution (%) in non-synchronized Caco-2 cultures. 59

Table 14 - Effect of 24h-exposure to AgNPs and $AgNO_3$ on cell cycle distribution (%) in synchronized Caco-2 cultures. 60

Table 15 - Effect of 24h-exposure to AgNPs and $AgNO_3$ on cell cycle distribution (%) in non-synchronized Caco-2 cultures..... 61

List of Figures

Figure 1 - Illustrative image of endocytic pathways and intracellular interactions. The green dots are the representation of the nanoparticles or other coumpounds capable of being uptaken by endocytosis.Arf6 dependent (ADP-ribosylation factor 6) is implicated in endocytosis of plasma membrane proteins, caveolin – caveolae/lipid raft dependent leads to a local change in the morphology of the membrane,Cdc42 dependent (cell division control protein 42 homolog) - regulates signaling pathways that control cell morphology, migration, endocytosis and cell cycle progression, EE – endosomes, MP – macropinosomes, MVB – multivesicular bodies/late endosomes, Lys – lysosomes, RE – recycling endosomes, RhoA (ras homolog gene family, member A) - actson the reorganization of the actin cytoskeleton of the cell, - From (Iversen et al., 2011). 9

Figure 2 - Schematic representation of the cell cycle. Outer circle: I - interphase, M - mitosis. Inner circle: G1 - gap 1, S - synthesis, G2 - gap 2, G0 - resting phase, M – mitosis. 19

Figure 3 - Representative cell cycle histogram of Caco-2 cells analysed by flow cytometry. 21

Figure 4 - Diagram of cell cycle response triggered by DNA damage (From (Saidin, 2008)). 22

Figure 5 - Role of the cell cycle in the cellular uptake of NPs. Nanoparticle uptake in a cycling cell. The yellow-green circles represent the nanoparticles, which, inside cells, accumulate in the lysosomes, represented by the oval compartment. When the cell divides, the internalized nanoparticles are split between the two daughter cells (From (Kim et al., 2012)). 23

Figure 6 - Representation of the NPs used in this study: a) citrate-coated AuNPs, b) CALNN-coated AuNPs, c) CALNS- coated AuNPs, d) CALND-coated AuNPs and e) citrate-coated AgNPs. 32

Figure 7 - Cell staining mechanism of Calcein-AM in viable cells. 34

Figure 8 - Representation of the conversion of yellow tetrazolium,3-(4,5-dimethylthiazol-2-yl)-2,5-diphenyltetrazolium bromide, into the insoluble formazan crystal. 35

Figure 9 - Representation of the mechanism of the 2', 7'-dichlorofluorescein-diacetate (DCFH-DA) assay. 36

Figure 10 - Esterase activity of Caco-2 cells at (A) 6 h, (B) 24 h, (C) 48 h and (D) 72 h after exposure to Citrate-, CALNN-, CALNS-, CALND-AuNPsas assessed by the Calcein- AM assay. Results were calculated as percentage of control (untreated cells). Data is presented as mean ± SEM (n = 12-16). Data was analysed by one-way ANOVA with post-hoc Dunnet's tests applied for multiple comparisons * P<0.05, # P<0.01; significantly different from the control value. 42

Figure 11 - Effects of Cit-, CALNN-, CALNS-, CALND-AuNPs in the plasma membrane integrity, determined by the propidium iodide (PI) assay, after (A) 6 h, (B) 24 h, (C) 48 h and (D) 72 h. Results were calculated as percentage of control (untreated cells). Data is presented as mean ± SEM (n = 12-16). Data was analysed using one-way ANOVA with post-hoc Dunnet's tests applied for multiple comparisons. * P<0.05, # P<0.01, $ P<0.001, & P<0.0001 significantly different from the control value. 44

Figure 12 - Effects of Cit-, CALNN-, CALNS-, CALND-AuNPs in the lysosomal integrity, determined by the neutral red absorbance assay, after (A) 6 h, (B) 24 h, (C) 48 h and (D) 72 h. Results were calculated as percentage of control (untreated cells). Data is presented as mean ± SEM (n = 12-16). Data was analysed using one-way ANOVA with post-hoc Dunnet's tests applied for multiple comparisons. * P<0.05, # P<0.01, $ P<0.001, & P<0.0001 significantly different from the control value. 46

Figure 13 - Effects of Cit-AgNPs and $AgNO_3$ in lysosomal integrity, determined by neutral red absorbance, after (A) 6 h, (B) 24 h, (C) 48 h. Results were calculated as percentage of control (untreated cells). Data is presented as mean ± SEM (n = 9 per group). Data was analysed using one-way ANOVA with post-hoc Dunnet's tests applied for multiple comparisons. * P<0.05, & P<0.0001; significantly different from the control value. 47

Figure 14 - Effects on the Cit-AgNPs and $AgNO_3$ in activity of mitochondrial enzymes, determined by the MTT assay, after (A) 6 h, (B) 24 h and (C) 48 h. Results were calculated as percentage of control (untreated cells). Data is presented as mean ± SEM (n = 9 per group). Data was analysed using one-way ANOVA

with post-hoc Dunnet's tests applied for multiple comparisons. * P<0.05, # P<0.01, & P<0.0001; significantly different from the control value. 48

Figure 15 - Effects of Cit-, CALNN-, CALNS-, CALND-AuNPs in the production of reactive oxygen species, determined by the DCFH-DA assay, after (A) 6 hours, (B) 24 hours, (C) 48 hours, (D) 72 hours. Results were calculated as percentage of control (untreated cells). Data is presented as mean ± SEM (n = 12-16). Data was analysed using one-way ANOVA with post-hoc Dunnet's tests applied for multiple comparisons. * P<0.05, # P<0.01, $ P<0.001, & P<0.0001 significantly different from the control value. 50

Figure 16 - Effects of Cit-AgNPs and $AgNO_3$ in the production of reactive oxygen species, determined by the DCFH-DA assay, after (A) 6 hours, (B) 24 hours, (C) 48 hours and (D) 72 hours. Results were calculated as percentage of control (untreated cells). Data is presented as mean ± SEM (n = 12 per group). Data was analysed using one-way ANOVA with post-hoc Dunnet's tests applied for multiple comparisons. * P<0.05, # P<0.01, $ P<0.001, & P<0.0001 significantly different from the control value. 52

Figure 17 - Representative phase contrast microscopy images of Caco-2 cells at 72 h after incubation with: a) control, b) Vehicle (H2O), c) 1 μM of Cit - AuNPs, d) 10 μM of Cit - AuNPs, e) 100 μM of Cit - AuNPs, f) 1 μM of CALNN - AuNPs, g) 10 μM of CALNN - AuNPs, h) 100 μM of CALNN - AuNPs, i) 1 μM of CALNS - AuNPs, j) 10 μM of CALNS - AuNPs, k) 100 μM of CALNS - AuNPs, l) 1 μM of CALND – AuNPs, m) 10 μM of CALND – AuNPs and n) 100 μM of CALND – AuNPs (100 X magnification).. 53

Figure 18 - Representative phase contrast microscopy images of Caco-2 cells at 72 h after incubation with: a) control, b) vehicle (citrate), c) 1 μM of Cit - AgNPs, d) 10 μM of Cit - AgNPs, e) 40 μM Cit - AgNPs, f) 1 μM of $AgNO_3$, g) 10 μM of $AgNO_3$, h) 40 μM of $AgNO_3$ (100x magnification). 54

Figure 19 - Caco-2 cells histograms of size (FSC) and complexity (SSC) of synchronized (a and b) and non-synchronized (c and d) cultures obtained after exposure to differently coated AuNPs. 1) vehicles (H_2O and citrate), 2) Cit-AuNPs, 3) CALNN-AuNPs, 4) CALNS-AuNPs, 5) CALND-AuNPs, at the concentrations of 1 μM (red line), 3 μM (green line) and 10 μM (blue line) compared to control cells (black line). 57

Figure 20 - Representative histograms of AuNPs uptake in Caco-2 cells by flow cytometry analysis of cell size (FSC) and complexity (SSC) of synchronized(a and b) and non-synchronized culture (c and d), after exposure of 6) Cit-AgNPs and 7) $AgNO_3$at the concentrations of 1 µg/mL (red line), 2.5µg/mL (green line) and 5µg/mL (blue line) comparing to control cells (black line). 58

Figure 21 - Representative PI fluorescence (DNA content) histograms of the Caco-2 cells (synchronized and non-synchronized cultures) after 24 h of exposure to AuNPs (10 µM). 62

Figure 22 - Representative PI fluorescence (DNA content) histograms of the Caco-2 cells (synchronized and non-synchronized cultures) after 24 h of exposure to 1, 2.5 and 5 µM Cit-AgNPs and $AgNO_3$ comparing to control cells (synchronized and non-synchronized cultures). 65

Figure 23 - Representative histograms of the Caco-2 cell cycle analysis by flow cytometry after 24 h of exposure with Cit-, CALNN-, CALNS- and CALND-AuNPs (1, 3 and 10 µM), comparing to control cells (synchronized and non-synchronized culture). 94

Abbreviations and Symbols

0-D -	zero dimensional
1-D -	one dimensional
2-D -	two dimensional
3-D -	three dimensional
11-MUA -	11-mercaptoundecanoic acid
µM -	micromolar
Ag -	bulk silver
AgNPs -	silver nanoparticles
$AgNO_3$ -	silver nitrate
ATP -	adenosine triphosphate
Au -	bulk gold
AuNPs -	gold nanoparticles
BSA -	bovine serum albumin
BSNPs -	AgNPs synthesized with sodium borohydride
Ca^{2+} -	calcium ions
CALND -	pentapeptide of Cysteine–Alanine-Leucine– Asparagine – Aspartate
CALNN -	pentapeptide of Cysteine–Alanine-Leucine– Asparagine–Asparagine
CALNS -	pentapeptide of Cysteine–Alanine-Leucine–Asparagine–Serine
CDKs -	cyclin-dependent kinases
CdSe -	cadmium selenide quantum dot
CHKs	checkpoint homolog kinases
Cit -	citrate
CNTs -	carbon nanotubes
CO_2-	carbon dioxide
CTAB -	cetyl trimethylammonium bromide
DCFH-DA -	dichloro-dihydro-fluorescein diacetate
DLS -	dynamic light scattering
DMEM	Dulbecco's modified Eagle's medium
DMSO -	dimethyl sulfoxide
DNA -	deoxyribonucleic acid
DTAF -	4,6-dichlorotriazinyl aminofluorescein
EDX -	energy - dispersive X-ray
EE -	endosomes
FBS	fetal bovine serum
GFAAS -	graphite furnace atomic absorption spectrometry

GLU - glucose
GSH - glutathione
HBSS Hank's balanced salt solution
HEPES *N*-2-hydroxyethylpiperazine-*N'*-2-ethanosulfonic acid
HER2 - human epidermal growth factor receptor 2
HIV-1 - human immunodeficiency virus 1
ICP-MS - inductively coupled plasma mass spectrometry
IgG - immunoglobulin G
LDH - lactate dehydrogenase
Lys - lysosomes
MN - micronucleus
MP - macropinosomes
MTS - 3-(4,5-dimethylthiazol-2-yl)-5-(3-carboxymethoxyphenyl)-2-(4-sulfophenyl)-2H-tetrazolium
MTT - 3-(4,5-dimethylthiazol-2-yl)-2,5-diphenyltetrazolium bromide
MVB - multivesicular bodies/late endosomes
NIST - National Institute of Standards and Technology
NMs - nanomaterials
nm - nanometer
nM - nanomolar
NPs - nanoparticles
NR - neutral red
PAA - poly (allyamine hydrochloride)
PAMAM - poly (amido amine) dendrimers,
PBS phosphate buffered saline
PEG - poly(ethylene) glycol
PI - propidium iodide
PVP - polyvinylpyrrolidone
RE - recycling endosomes
Rho A - ras homolog gene family, member A
ROS - reactive oxygen species
SEM - standard error of the mean
SERS - Surface-Enhanced Raman Spectroscopy
TEM - transmission electron microscopy
TiO_2 - titanium dioxide nanoparticles
TSNPs - AgNPs synthesized by reduction with tannic acid

U251 -	human glioblastoma cells
UV/VIS -	Ultraviolet – visible
XTT -	2,3-bis-(2-methoxy-4-nitro-5-sulfophenyl)-2H-tetrazolium-5-carboxanilide
WST-8 -	2-(2-methoxy-4-nitrophenyl)-3-(4-nitrophenyl)-5-(2,4-disulfophenyl)-2H-tetrazolium

Chapter 1

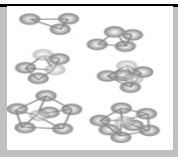
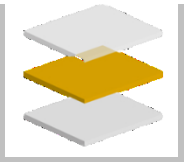
Introduction

1.1. Nanomaterials – overview

The definition of nanomaterials (NMs) is far from being consensual. According to the European Commission, the adopted definition of NM is based only on size and covers different types of materials. Within this definition, NMs are natural, incidental or manufactured material containing particles, in an unbound state, as an aggregate or as an agglomerate and where, for 50 % or more of the particles in the number size distribution, one or more external dimensions is in the size range of 1 nm - 100 nm (European Commission, 2011).

In order to better understand the diversity and complexity of the NMs it is essential to organize them into some form of categorization. Therefore, NMs can be classified according to their structure in amorphous or crystalline (Ashby et al., 2009). Furthermore, as described in **Table 1**, NMs can also be classified according to the dimension of their structural elements in zero-(0-D), one–(1-D), two–(2-D) and three-dimensional (3-D) (Siegel, 1994).

Table 1 - Main types of NMs based on the dimensions of their structural elements.

NMs dimension	Characteristics	Examples
0D (zero-dimensional)	All the measured dimensions are within the nanoscale; NPs are isolated from each other.	 NPs
1D (one-dimensional)	One dimension is outside the nanoscale; needle-*like* shaped NMs.	 nanotubes, nanorods and nanowires
2D (two-dimensional)	Two dimensions are outside the nanoscale; plate-*like* shaped NMs.	 nanofilms, nanolayers and nanocoatings
3D (three-dimensional)	Three dimensions outside the nanoscale; bulk materials with a nanocrystalline structure and arrangement.	 Dispersions of NPs, bundles of nanowires, nanotubes, multinanolayers

According to their chemical nature, NMs may also be categorized as organic or inorganic(Peralta-Videa et al., 2011). Among the organic are the carbon-based NMs that include fullerenes, carbon nanotubes (CNTs) and nanofibers. However, organic NPs can also be originated from organic polymers or even be biologically inspired, in which a biological substance is encapsulated, trapped or adsorbed, namely lipids, peptides or polysaccharides. On the other hand, quantum dots (CdSe), metals (Ag, Au), metal oxides (TiO2, ZnO, MgO and Fe3O4) or ceramics (SiO2) fall into the category of inorganic NMs. Organic NMs are often considered “soft” materials, whether inorganic materials are considered to be “hard” materials (Elsaesser and Howard, 2012).

1.2. Properties and applications

Decreasing particle size from bulk to nanoscale alters the physicochemical properties (optical, magnetic, electrical and catalytic) of the materials, metallic nanoparticles included, by increasing the number of surface atoms and energy, and consequently reactivity, thus providing the attractive possibility of application of these materials in many fields (Faramarzi and Sadighi, 2013). Over the past years, the development of new methods for synthesis and modification of metallic NPs allowed the rapid evolution of the nanotechnology world. These new methods of synthesis originated NPs with different physicochemical properties that can potentially lead to distinct biological and toxicological responses.

Shape is also a characteristic that can influence the physicochemical properties and applications of the NMs in general, including gold (AuNPs) and silver (AgNPs) nanoparticles. Owing to their shape along with the possibility of surface modification, Au and Ag nanorods have potential for biomedical applications such as drug delivery, photothermal therapy, chemical sensing and biological imaging (Alkilany et al., 2012, Gao et al., 2012). On the other hand, nanoplates due to their sharp edges can produce high electric field gradients combined with illumination, which is useful for optical biosensors and Surface-Enhanced Raman Spectroscopy (SERS) (Sun and Wiederrecht, 2007, Grzelczak et al., 2008). Au and Ag nanostars due to their unique shape possess optical properties that are useful for biomedical applications such as tumor imaging using SERS (Khoury and Vo-Dinh, 2008, Garcia-Leis et al., 2013).

Surface modification and/or bio-functionalization of these metallic NPs is expected to contribute for nanotechnology advancement, namely for implementation of these materials in the food industry and biomedical field (Kim et al., 2013).

Due to the bioinert nature of the bulk gold (Au), ease of synthesis and stability, AuNPs have been regarded as good candidates to be used in medicine and other biological applications (Balansky et al., 2013). Regarding AgNPs, their enhanced plasmonic properties have proven useful for SERS applications, making them a sensitive tool to trace single molecules (Ravindran et al., 2013).

Gold nanoparticles have been used since ancient times to produce the red color in the medieval stained windows glass and ceramic objects. Recently, AuNPs have become the center of attention not only due to their potential for biomedical application in the diagnostics and therapeutics of a number of diseases including cancer, Alzheimer's disease, hepatitis, arthritis and diabetes (Balansky et al., 2013) but also in the industry as a catalyst in a number of chemical reactions (Corma and Garcia, 2008) or even in the cosmetics field as a facial mask component to improve blood circulation and skin elasticity (Fathi-Azarbayjani et al., 2010).

In the first half of the 20th century, silver (Ag) was largely used in order to prevent infections. However, its use was often associated with argyria, a condition caused by excessive exposure and gradual accumulation of Ag compounds in various parts of the body that may cause spasms, and ultimately death. Around that time, the topical used of silver nitrate ($AgNO_3$) was indicated for the therapy of eye infections in newborns but it was believed that consumption of large doses would lead to corneal damage (Chernousova and Epple, 2013).

Recently due to its enhanced physicochemical and biological properties compared to the bulk silver, interest in the application of Ag in the nanoparticulate form has peaked (Tolaymat et al., 2010).

Currently, it is estimated that of all the NMs used in consumer products, AgNPs have the highest degree of commercialization (Ahamed et al., 2010). In cosmetics, AgNPs are being applied as an active ingredient for physical UV shielding, skin whitening, hair and dental care and as antibactericidal agent (Mihranyan et al., 2012). In fact, the antimicrobial properties of the AgNPs have been successfully explored for biomedical purposes (Bystrzejewska-Piotrowska et al., 2009). At present, AgNPs are constituents of catheters, implant surfaces or dental alloys and are expected to be employed in cancer and retinal therapy (Dziendzikowska et al., 2012). Interestingly, it has been reported that AgNPs could interact with HIV-1 virus inhibiting its capacity to bind to host cells *in vitro* (Elechiguerra et al., 2005).

Nanotechnology is also expected to greatly benefit the food and feed sector. The NPs are being applied for sensory improvement (e.g. flavor enhancement), specific and accurate delivery/targeting of bioactive compounds and nutrients, stabilization of active ingredients, packaging and product innovation to extend shelf-life, improvement of food safety and antimicrobial action to kill pathogens in food, decreasing health risks. Nevertheless, a recent report from the Food Safety Authority of Ireland stated that only a small number of products have been commercialized (I. Pratt, 2008). Still, the value of nanotechnology in the food market may have reached 19.4 million euros in 2010 and 740 billion euros in 2013.

While organic NPs are essentially used to alter the normal structure of biocompounds or food additives to improve or create new properties, inorganic NPs such as AuNPs and AgNPs, are mainly used for the preservation of prepared foods. These NPs are included in food containers, food contact materials, food supplements or food additives.

In **Table 2** and **3** are presented some products currently available on the market containing AuNPs and AgNPs in their composition, respectively.

Table 2 - Products on the market containing gold nanoparticles in their composition.

Gold	Product Example		Company	Origin	Application
	MesoGold		Purest Colloids, Inc.	USA	Food supplements,
	Nutri-Nano™ CoQ-10 3.1x Softgels		Solgar	USA	Food supplement

Table 3 - Products on the market containing silver nanoparticles in their composition.

Silver	Product Example		Company	Origin	Application
	MesoSilver		Purest Colloids, Inc.	USA	Food supplements
	Silver-22TM		RBC Life Sciences®, Inc.	USA	Antimicrobial protection, food supplements
	SilverBiotics		American Biotech Labs	USA	Food supplement
	Colloidal silver		Fairvital	Germany	Food supplement
	Sovereign Silver™		Natural-Immunogenics Corp.	USA	Food supplement
	MARATHON Household Water Purifiers (Model : silverdyn type)		Katadyn Asia Inc.	Korea	Water filtration
	Nano Silver Baby Mug Cup		Baby Dream® Co., Ltd.	Korea	Antimicrobial protection
	BlueMoonGoods™ Fresh Box Silver Nanoparticle Food Storage Containers		BlueMoonGoods, LLC	USA	Antimicrobial protection, storage material
	Nano Silver NS-315 Water Bottle		A-DO Global	Korea	Antimicrobial protection, storage
	Nano-Silver Cutting Board		Pro-Idee GmbH & Co. KG	Germany	Antimicrobial protection, cooking

1.3. Interactions of metallic nanoparticles with biological systems

Owing to their interactions with the biological systems, NPs can acquire a surface corona mainly constituted of biomolecules such as lipids and proteins, that will influence their behavior and effects (Fadeel et al., 2013). Thus, it has been recently proposed that interactions of engineered NPs with cells or tissues, and subsequent effects, are a combination of material-intrinsic and context-dependent properties determined, in part, by the bio-corona of a given biological compartment (Elsaesser and Howard, 2012). Therefore, identifying and characterizing the nature of these interactions will provide a conceptual basis for the rational design and safe use of these NPs in biology and medicine (Zhang et al., 2012).

1.3.1. Influence of the physicochemical properties of gold and silver nanoparticles in the cellular uptake

The physicochemical properties play a major role on NPs interactions with the biological systems (Zhang et al., 2012). Shape, size and surface chemistry have been found to greatly influence NP uptake and cellular toxicity (Nel et al., 2009).

The size and surface characteristics are key points for the process of opsonization (i.e. binding of opsonins on the surface of NPs, promoting phagocyte recognition) and clearance of NPs. Differential opsonization might explain different clearance rates and macrophage sequestration of NPs (Arora et al., 2012). The suppression of these opsonization processes at desired sites or anatomical compartments can increase the passive retention of NPs in bloodstream. For that purpose, surface coating with poly(ethylene) glycol (PEG) has been found to effectively increase the systemic circulation time of hydrophobic NPs (Arora et al., 2012). Also, the contact of NPs with biological fluids and consequent formation of a protein corona can modify the NPs properties (shape, surface charge, aggregation status),and thus influence NP uptake into the cells and performance in the organism (i.e. biodistribution and cell/organ specificity) (Zhang et al., 2012).

In phagocytic cells, NPs can be internalized by passive penetration or phagocytosis/macropinocytosis, two specific forms of endocytosis, involving actin polymerization. In non-phagocytic cells, NPs are internalized by endocytosis, independent-or receptor-dependent, involving clathrin or caveolin pathways (Roy et al.,

2014). While most studies focused on NP uptake in non-polarized cells, the complexity of internalization in polarized cells is now being studied, namely, the uptake differences between the apical (clathrin–mediated endocytosis) and basolateral (caveolae–mediated endocytosis) domains(Iversen et al., 2011). Recently, new mechanisms of clathrin–independent endocytosis have been reported and are described in **Figure 1**.

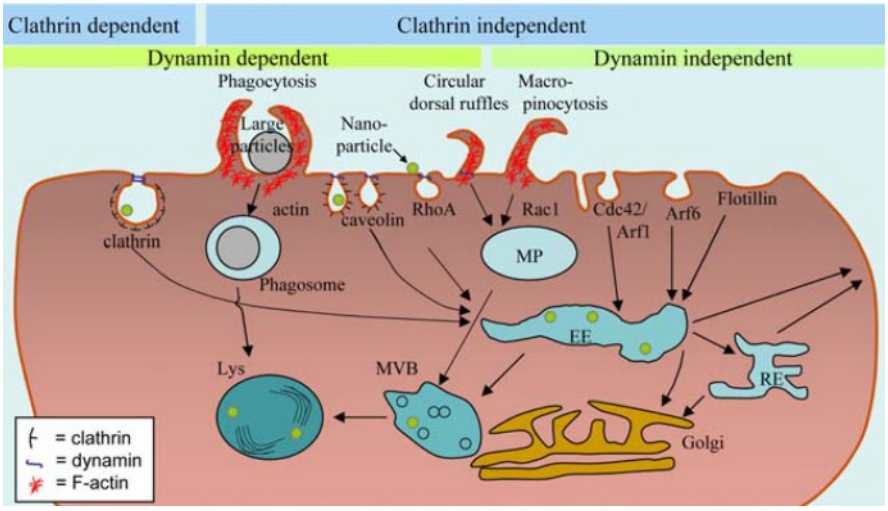


Figure 1 - Illustrative image of endocytic pathways and intracellular interactions. The green dots are the representation of the nanoparticles or other coumpounds capable of being uptaken by endocytosis.Arf6 dependent (ADP-ribosylation factor 6) is implicated in endocytosis of plasma membrane proteins, caveolin – caveolae/lipid raft dependent leads to a local change in the morphology of the membrane, Cdc42 dependent (cell division control protein 42 homolog) - regulates signaling pathways that control cell morphology, migration, endocytosis and cell cycle progression, EE – endosomes, MP – macropinosomes, MVB – multivesicular bodies/late endosomes, Lys – lysosomes, RE – recycling endosomes, RhoA (ras homolog gene family, member A) - actson the reorganization of the actin cytoskeleton of the cell, - From (Iversen et al., 2011).

NPs can cause disturbances in the plasma membrane structure (Verma and Stellacci, 2010), through interactions with membrane proteins, ion channels, cytoskeleton, and thus can interfere with cellular functions such as molecular transport and signal transduction (Wu et al., 2012).

In spite of the increasing number of studies regarding NPs uptake, the knowledge of cellular uptake of NPs is far from being completely understood due to the complexity and variety of mechanisms involved, making it difficult to extrapolate between *in vitro* and *in vivo* (Iversen et al., 2011).

1.3.1.1. Gold nanoparticles

Chithrani and Chan, have evaluated the role of size (14, 50 and 74 nm) on the uptake of AuNPs in an immortalized cervical cancer (HeLa) cell line. These authors have

found that saturation kinetics varied among differently sized AuNPs, being the 50 nm the most efficiently internalized, indicating there might exist an optimal size for efficient AuNPs uptake into cells (Chithrani and Chan, 2007). In the same study, the effect of shape on AuNPs internalization was also evaluated. The results indicated that spherical-shaped AuNPs seem to be more easily internalized comparing with rod-shaped particles, which might be explained by greater membrane wrapping time required for elongated particles (Chithrani and Chan, 2007).

The surface chemistry significantly contributes to NPs interactions with cells since the surface functional groups are primary dictators of many important NP properties such as solubility and cell surface (Verma and Stellacci, 2010). Cho et al., investigated the influence of the surface coating on the AuNPs uptake in the breast cancer cell line (SK-BR-3). Three differently coated [PEG, anti-human epidermal growth factor receptor–2 (HER2) and poly(allyamine hydrochloride) (PAA)] AuNPs were studied. The tested surface coatings conferred different surface charges to the AuNPs. While PEG-, anti-HER2-coated AuNPs were neutral/negatively charged, PAA-AuNPs were positively charged. The authors concluded that positively charged NPs easily bind to the cell surface comparing with neutral or negatively charged NPs, resulting in a more effective translocation across the plasma membrane (Cho et al., 2010). These results are representative of the importance of surface modification towards the efficiency of AuNPs uptake.

Kim et al. have also investigated the influence of surface charge on membrane integrity/perturbation of ovarian cancer cells (CP70 and A2780), human bronchial epithelial cells (BECs), and human airway smooth muscle cells (ASM). These authors have tested four types of AuNPs (cationic, anionic, zwitterionic[1] and neutral) and demonstrated that positively charged NPs could depolarize the membrane potential leading to lipid bilayer disruption and loss of membrane integrity. The authors also found that positively charged NPs increased the intracellular levels of Ca^{2+}, which combined with alterations of the membrane potential and integrity induced cytotoxicity (Kim et al., 2013).

The cytoskeleton is an important piece for cellular mechanical stability, integrity, trafficking and migration (Wu et al., 2012). Exposure of human lung carcinoma cells (A549) to AuNPs has proven to induce changes in the cytoskeleton arrangement and alterations in cellular morphology (Pernodet et al., 2006). In addition, AuNPs have also been reported to induce cell death after 48 h of exposure, in a concentration-dependent manner, by acting on the actin fibrils of human dermal fibroblasts (Patra et al., 2007).

[1] Zwitterionic – neutral molecule with both positive and negative electrical charge.

1.3.1.2. Silver nanoparticles

Available literature supports that AgNPs could be easily internalized by cells. In a study on human epidermal keratinocyte cells (HEK) incubated with differently sized and coated AgNPs (20 and 110 nm citrate-coated and40 and 120 nm silica-coated), the authors evaluated the effect of pre-exposure to human proteins (albumin, IgG and transferrin) to create a protein-NP corona, in the AgNPs uptake into the cells(Monteiro-Riviere et al., 2013). The results showed that there was a significant change in the cellular uptake of all NPs studied. The difference of the cellular uptake of citrated-coated AgNPs was essentially related to the size of the NP, since for 20 nm citrate-coated NPs a reduction of intracellular concentration was observed after pre-exposure of albumin and IgG, while for 110 nm this reduction was observed exclusively after the pre-exposure of IgG. The opposite conclusion was obtained for the silica-coated AgNPs The greatest uptake of IgG during the experience was observed upon exposure with 20 nm silica-coated AgNPs. However, the authors emphasized the need for additional studies to prove this data (Monteiro-Riviere et al., 2013).

Greulich et al. evaluated the uptake of polyvinylpyrrolidone (PVP)-coated AgNPs on human mesenchymal stem cells (hMSC), in particular the mechanism/pathways involved in NPs endocytosis. Based on combined focused ion beam/scanning electron microscopy (FIB/SEM) experiments, energy-dispersive X-ray (EDX) analysis and flow cytometry, the authors showed that NPs were internalized by macropinocytosis and clathrin-dependent endocytosis (Greulich et al., 2011).

Singh et al. also investigated the uptake of 43.9 nm AgNPs in a mouse leukaemic monocyte macrophage cell line (RAW 264.7). The authors used confocal microscopy to monitor the uptake of AgNPs labeled with a fluorescein derivative (DTAF) and found that the NPs were efficiently transported during the 3 h of experiment (Singh and Ramarao, 2012).

1.3.2. The interaction of metallic nanoparticles with the cellular organelles

After cellular internalization, NPs can be transported to intracellular organelles such as lysosomes, mitochondria and nucleus.

Lysosomes are organelles whose function involves the digestion of waste materials and cellular debris. Endo-lysosomal pathways and autophagy are emerging mechanisms to capture and degrade NPs internalized by cells. However, recent studies showed that NPs have a negative impact on these mechanisms. NPs can induce lysosomal oxidative stress affecting lysosomal stability and promoting lysosomal

dysfunction. Lysosomal membrane permeabilization, a consequence of lysosomal dysfunction, can lead to mitochondrial permeabilization, which can induce the ROS production and ultimately cell apoptosis (Stern et al., 2012).

Mitochondria targeting by NPs, either directly or indirectly, remains an open discussion. However, it is known that NP-induced disturbance of this organelle has biological effects that can be translated into toxicity. The primary role of mitochondria is the production of ATP, still, mitochondria has also key roles in other metabolic tasks such as signaling through mitochondrial-derived reactive oxygen species (ROS) (Li et al., 2013), programmed cell death (Green, 1998), calcium signaling (Hajnóczky et al., 2006) and regulation of cellular metabolism (McBride et al., 2006). Damage of mitochondrial function induced by NPs can decrease the mitochondrial membrane potential, increase ROS production and cause depletion of GSH. Studies regarding AuNPs and AgNPs interactions with mitochondria have already been performed. Exposure for 48 h to 1.4 nm AuNPs was found to induce oxidative stress, which associated with protein and lipid oxidation led to mitochondrial damage in HeLa cells (Pan et al., 2009). On the other hand, Wistar rat liver mitochondria exposure to 40 and 80 nm AgNPs led to a reduction of mitochondrial function associated with a decrease of mitochondrial membrane potential and ADP-induced depolarization.

Finally, NPs can also interact with the cell nucleus. Given their small size, charge and surface area, NPs can also enter the nucleus and induce DNA damage. DNA damage can be produced either by direct interaction between the DNA and the NPs, which can result in mutations or hinder the chromosomal DNA replication , or indirectly through ROS production or release of toxic ions from soluble NPs (Wu et al., 2012).

1.3.3. Toxicity of metallic nanoparticles

The knowledge of the mechanisms involved in the cellular uptake of metallic NPs and interaction with intracellular organelles can lead to a better understanding of the toxicity induced by metallic NPs.

The mechanisms involved in the toxicity of NPs can be either of chemical or physical nature. Among the chemical mechanisms are the production of ROS, dissolution and release of toxic ions, disturbance of the activity of electron/ion cell membrane transport and lipid peroxidation (Kamat et al., 2000, Foley et al., 2002, Nel et al., 2006, Xia et al., 2008). On the other hand, disruption of membranes affecting transport and trafficking processes, alterations of protein conformation/folding and protein aggregation/fibrillation phenomena are some of the physical mechanisms that might be involved in NPs toxicity (Elsaesser and Howard, 2012).

As previously mentioned, NPs might also induce genotoxicity through direct or indirect mechanisms (Dusinska et al., 2013). NPs can reach the cell nucleus and bind to DNA, affecting replication of chromosomal DNA or causing mutations (Wu et al., 2012). In addition, some NPs are known to cause DNA damage by increasing oxidative stress and inflammatory responses (Meng et al., 2009). NP-induced DNA damage often leads to activation of the cytoplasmic protein p53 (Ng et al., 2011). In ROS-mediated DNA damage, an increased expression of antioxidant genes has been observed, which can culminate in cell death (apoptosis or necrosis) if the DNA damage exceeds the reparable limits (Sablina et al., 2005, Ng et al., 2011).

1.3.3.1. Gold nanoparticles

As previously mentioned, AuNPs were initially considered non-toxic due to the bioinert character of the bulk Au. In spite of the large number of studies conducted so far to assess their safety, toxicity of AuNPs is still controversial. While some studies demonstrated the biocompatibility of AuNPs, others have reported the existence of toxicity events associated with AuNPs exposure. Khlebtsov and Dykman hypothesized that contradictory data on AuNPs toxicity may arise from the experimental design, namely differences in the particle size, shape, and surface chemistry, animal and cellular models used, tested doses and administration routes (Khlebtsov and Dykman, 2011).

In **Table 4** are summarized some studies regarding the cytotoxic effects of AuNPs. The physicochemical properties of the NPs, adopted cell model, type of assay and tested concentrations, as well as the main findings are described.

Different cell models may exhibit different sensitivity to AuNPs. This fact may also account for the discrepancy in AuNPs cytotoxicity data found in literature and is reflected in **Table 4**. Indeed, Patra et al. demonstrated that AuNPs induced a concentration-dependent toxicity response in A549 cells but not in baby hamster kidney (BHK21) or in liver hepatocellular carcinoma (HepG2) cells (Patra et al., 2007).

Another interesting finding is that surface modification also influences the toxicological potential of the AuNPs. As demonstrated by Connor et al, a high concentration of citrate coating resulted in higher levels of toxicity (Connor et al., 2005). In addition, Freese et al reported that CTAB-AuNPs but not Cit-and biotin-AuNPs produced toxicity in human myelogenous leukemia (K562) cells (Freese et al., 2012).

Table 4 – Summary of some *in vitro* studies on the cytotoxicity of gold nanoparticles.

NP tested	Cell model	Concentration	Assay	Main findings	Reference
Cit–AuNPs (10, 11 nm, 25 nm)	HDMEC hCMEC/D3 A549 NCIH441	50 – 1000 µM	MTS	Higher concentration of citrate coating led to higher incidence of cytotoxicity in endothelial and epithelial cells	(Freese et al., 2012)
Au–Nanorods (10 – 40 nm)	PK-15 Vero NIH3T3 MRC5	36 - 1000 ng/mL	MTS	Induction of apoptosis in Vero cells; Attenuation of cell growth in NIH3T3 cells through the process of autophagy	(Chueh et al., 2014)
Cit–AuNPs (17 nm)	A549 A431	0 – 80 µg/mL	MTT, LDH	Significant cytotoxic effect in both cell lines after 24 h of exposure.	(Choi et al., 2012)
Cit-, biotin-, CTAB-AuNPs	K562	0.002 – 250 µM	MTT	No cytotoxic effect for cit- or biotin-AuNPs in all concentration range; CTAB - AuNPs caused cytotoxicity at 0.05 µM	(Connor et al., 2005)
CALNN-AuNPs (13, 30 and 60 nm)	HeLa	0.02 – 0.32 nM	Trypan Blue	From 0.02 to 0.08 nM the survival rate varies from 80 to 95 %; 0.16 nM led to a survival rate of 60 %; 0.32 nM led to a survival rate less than 10 %	(Sun et al., 2008)
AuNPs (33 nm)	BHK21 HepG2 A549	10 – 120 nM	MTT	No evidence of toxicity in BHK21 and HepG2; concentration – dependent toxicity in A549 cells	(Patra et al., 2007)
AuNPs (10 and 50 nm)	HDF-f	10 – 300 µM	MTT	Absence of cytotoxicity up to 300 µM but accompanied by changes in the cell morphology.	(Qu and Lu, 2009)
Cit-, 11-MUA-AuNPs (20 nm)	HepG2	0 – 200 µM	MTT, LDH	No significant cytotoxicity was observed.	(Fraga et al., 2013)

Note: **11-MUA**: 11-mercaptoundecanoic acid, **Cit**: Citrate, **CALNN**: a pentapeptide ligand (Cys-Ala-Leu-Asn-Asn), **CTAB**: Cetyl trimethylammonium bromide, **MTT** - 3-(4,5-dimethylthiazol-2-yl)-2,5-diphenyltetrazolium bromide, **LDH** - lactate dehydrogenase, **MTS** - (3-(4,5-dimethylthiazol-2-yl)-5-(3-carboxymethoxyphenyl)-2-(4-sulfophenyl)-2H-tetrazolium).

Several studies have proven that NPs may induce genotoxicity, i.e. DNA damage, even in the absence of clear cytotoxic effects. The comet assay is one of the most frequently used tests to assess DNA damage induced by chemical agents. A recent review on the subject reported DNA strand breaks or DNA lesions resulting from exposure to NMs including metal-based NPs (Karlsson, 2010) According to this author, this assay may provide useful information for hazard identification of NMs.

Regarding AuNPs, it has been shown that can induce DNA damage caused by a concentration-dependent oxidative stress(Singh et al., 2009). However, Nelson et al. have demonstrated that different-sized (10, 30 and 60 nm) National Institute of Standards and Technology (NIST) AuNPs reference materials did not cause DNA damage both in HepG2 cells and calf-thymus DNA exposed for 24 h. Furthermore, no significant increase in ROS production was observed (Nelson et al., 2013).

In **Table 5** is presented a brief summary of some studies regarding the genotoxic effect of AuNPs.

Table 5 - Summary of some *in vitro* studies on the genotoxicity of gold nanoparticles.

NP tested	Cell model	Concentration	Assay	Main findings	Reference
Cit-, PAMAM-AuNPs	PBMC, HepG2	1 and 50 μM	Comet assay	Evidence of DNA damage induced by both tested NPs	(Paino et al., 2012)
Glycolipid-AuNPs	HepG2	0.0005 - 50 μg/mL	Comet assay	No genotoxic effect observed	(Singh et al., 2010)
Cationic AuNPs	HeLa	100 – 165 nM	Comet assay	Increase of NP hydrophobicity led a decrease of DNA damage. High levels of ROS were found	(Chompoosor et al., 2010)
Cit-, 11-MUA-AuNPs (20 nm)	HepG2	0.1 - 100 μM	Comet assay	Evidence of DNA damage on the citrate-AuNPs exposed cells, but not on 11- MUA - AuNPs treated cells; inverse concentration-dependent genotoxic effect	(Fraga et al., 2013)
AuNPs (15 nm)	HeLa	20 μg/mL	Comet assay	DNA damage and apoptosis	(Jeyaraj et al., 2014)
AuNPs (8 nm)	MonoMac 6, NR8383	3.2 – 10.2 $\mu g/cm^2$	Alkaline comet assay	Positive results; DNA damage	(Grigg et al., 2009)

Note: **PAMAM** - Poly (amido amine) dendrimers, **11-MUA**: 11-mercaptoundecanoic acid, **Cit**: Citrate.

Surface chemistry has also an important role in NMs DNA damaging potential. Fraga et al reported that 20 nm Cit-AuNPs but not MUA-AuNPs induced DNA damage in HepG2 cells at 24h of exposure. Interestingly, the DNA damaging effect of Cit-AuNPs followed an inverse concentration-dependent trend (Fraga et al., 2013).

As previously stated, ROS are a major source of DNA damage. Still, an interesting yet confusing finding contradicts, somewhat, this premise. Chompoosor et al. have investigated the genotoxic effect of AuNPs coated with alkyls with different tail chain lengths on HeLa cells. The obtained data indicated that increasing of NP hydrophobicity produced an increase in ROS production accompanied by a decrease in DNA damage. The authors suggested that oxidative environment could activate the process of autophagy, thus explaining the observed decrease in the DNA damage (Chompoosor et al., 2010).

1.3.3.2. Silver nanoparticles

Toxicological studies on AgNPs have also been conducted. Mechanistic studies have shown that exposure to AgNPs is associated with the generation of ROS, DNA damage, lipid peroxidation that often lead to cytotoxicity, and ultimately cell death (de Lima et al., 2012). As observed for other types of NMs, the physicochemical properties of the AgNPs influence their toxicological potential (de Lima et al., 2012). Also, the AgNPs are very prone to dissolve and release Ag^+ ions. This Ag ion release can be controlled by NP surface modification with polymers or biomolecules (Kittler et al., 2010), that can also influence NPs toxicity.

Several studies have investigated whether the toxicity induced by the AgNPs was caused by the NPs themselves orby the released Ag+ ions (Beer et al., 2012). Furthermore, an Ag salt, usually $AgNO_3$, is often tested to compare the Ag effects between bulk and nanoscale.

In **Table 6** are represented some studies on the cytotoxicity of AgNPs. Piao et al. observed higher NPs induced-toxicity compared to $AgNO_3$ (Piao et al., 2011). On the other hand, Beer et al. have found that toxicity of the AgNPs was dependent of the amount of Ag ions in the solution (Beer et al., 2012).

In some of the studies, the response of the cells to AgNPs was found to be concentration-dependent (Arora et al., 2009, Kaur and Tikoo, 2013).

Table 6 - Summary of recent *in vitro* studies on the cytotoxicity of silver nanoparticles.

NP tested	Cell model	Concentration	Assay	Main findings	Reference
AgNPs (BSNPs, TSNPs)	A431, A549, RAW264.7	5 - 100 µg/mL	MTT, DCFH-DA	**TSNPs** – concentration-dependent toxicity characterized by cellular disruption and ROS generation; **BSNPs** – cytotoxic effect observed up at 50 µg/mL, for 50 – 100 µg/mL range the cytotoxic effect was attenuated	(Kaur and Tikoo, 2013)
AgNPs (7 - 20 nm)	Swiss albino mice primary cells, primary fibroblasts cells	1.56 - 100 µg/mL	XTT	Concentration–dependent response of cell viability (61 µg/mL and 449 µg/mL, for primary fibroblasts and primary liver cells, respectively)	(Arora et al., 2009)
AgNPs (30 – 50 nm)	A549	0 – 1.5 µg/mL	MTT, WST-8	Toxicity of AgNPs dependent on Ag^+ percentage in the suspensions	(Beer et al., 2012)
AgNPs (10, 50 and 100 nm) $AgNO_3$ (Ag^+ ions source)	Human Chang liver cells	0 – 10 µg/mL	MTT	Higher toxicity of AgNPs compared to $AgNO_3$	(Piao et al., 2011)
AgNPs (10, 50 and 100 nm) $AgNO_3$(Ag^+ ions source)	RBE-4	1 – 25 µg/mL	NR, LDH	AgNPs decreased NR uptake; Increase of NR uptake after 1 h of exposure to Ag^+ ions, followed by a decrease in the uptake after 24 h of exposure; Smaller particles (10 nm) increased LDH leakage compared to larger particles (100 nm)	(Grosse et al., 2013)
Starch-Capped AgNPs (6-20 nm)	IMR-90 U251	25- 400 µg/mL	ATP, DCFH-DA	Positive cytotoxic effect. ATP depletion, mitochondrial dysfunction and ROS formation	(AshaRani et al., 2009)

Note: **TSNPs** - AgNPs synthesized by reduction with tannic acid (TSNPs), **BSNPs** – AgNPs synthesized with sodium borohydride, **NR** – neutral red assay, **MTT** - 3-(4,5-dimethylthiazol-2-yl)-2,5-diphenyltetrazolium bromide, **WST – 8** - (2-(2-methoxy-4-nitrophenyl)-3-(4-nitrophenyl)-5-(2,4-disulfophenyl)-2H-tetrazolium), **XTT** - (2,3-bis-(2-methoxy-4-nitro-5-sulfophenyl)-2H-tetrazolium-5-carboxanilide), **LDH** - lactate dehydrogenase, **DCFH-DA** - Dichloro-dihydro-fluorescein diacetate.

Nevertheless, Bohmert et al. reported that increased ROS production and cytotoxic effects in human epithelial colorectal adenocarcinoma (Caco-2) cells, following exposure to differently sized (20 and 40 nm) peptide-coated (Cys-Lys-Lys) AgNPs, were concentration-, time- and particle size-independent (Bohmert et al., 2012). AshaRani et al. showed that AgNPs interaction with normal human lung fibroblast cells (IMR-90) and human glioblastoma cells (U251) induced cytotoxicity through ATP depletion, mitochondrial dysfunction and ROS formation (AshaRani et al., 2009).

Overall, AgNPs can induce cytotoxicity through the release of Ag^+ ions into the cellular environment or by themselves by interacting with intracellular components, promoting the formation of ROS, ultimately conducting to cell death.

Along with other types of NMs (metal-based, metal oxide-based, QDs, fullerenes and CNTs), AgNPs can also induce genotoxicity through their interaction of DNA and ROS or free radicals formed upon cell uptake (Elsaesser and Howard, 2012, Roy et al., 2014).

In **Table 7** includes some in vitro studies conducted to assess AgNPs genotoxicity.

Table 7 - Summary of some *in vitro* studies on the genotoxicity of silver nanoparticles.

NP tested	Cell model	Concentration	Assay	Main findings	Reference
Glycolipid - AgNPs	HepG2	0.0005 - 50 µg/mL	Comet assay	No genotoxic effect observed	(Singh et al., 2010)
Bare AgNPs (5 nm)	TK6	10 – 30 µg/mL	Ames test MN test	Positive genotoxic effect	(Li et al., 2012)
Polysaccharide – AgNPs Bare AgNPs	mES MEF	50 µg/mL	Annexin-V	Coated-NPs caused a more severe DNA damage than uncoated-NPs.	(Ahamed et al., 2008)
BSA-AgNPs $AgNO_3$ (Ag^+ ions source)	CHO-K1	0 – 20 µg/ml	Annexin-V/propidium iodide	Positive genotoxic effect	(Jiang et al., 2013)
PVP-AgNPs	BEAS-2B	2.5 – 240 µg/ml	Comet assay, MN, CA	Concentration-dependent DNA damage; MN and CA were not observed in all the experimental conditions	(Nymark et al., 2013)
Bare AgNPs (20 or 200 nm)	HepG2 HT-29 A549	10, 50 and 100 µg/mL	Comet assay	Evidence of DNA damage	(Kruszewski et al., 2013)

Note: **BSA** – bovine serum albumin, **PVP** – polyvinylpyrrolidone, **MN** – micronucleus, **CA** – chromosome aberration.

Several studies showed contradiction regarding the role of the surface coating on the genotoxicity potential of AgNPs. Ahamed et al. reported that polysaccharide-coated AgNPs caused more DNA damage than uncoated NPs in mouse embryonic fibroblasts (Ahamed et al., 2008). However, this observation was contradicted by other studies. Singh et al. demonstrated that coated NPs had no genotoxic potential, while Li et al. study results showed a positive genotoxic effect in human lymphoblastoid (TK6) cells exposed to bare AgNPs (Li et al., 2012). Furthermore, concentration also influences the genotoxic effect of NPs. Nymark et al. showed that exposure to polyvinylpyrrolidone (PVP)–AgNPs for 4 and 24 h produced a concentration-dependent DNA damage in human bronchial epithelial cells (Nymark et al., 2013).

1.4. Cell cycle effects of AuNPs and AgNPs

1.4.1. Cell cycle- overview

The cell cycle corresponds to a series of events that lead to cell division and duplication, as represented in **Figure 2**. This phenomenon is divided in two major periods: interphase and mitosis

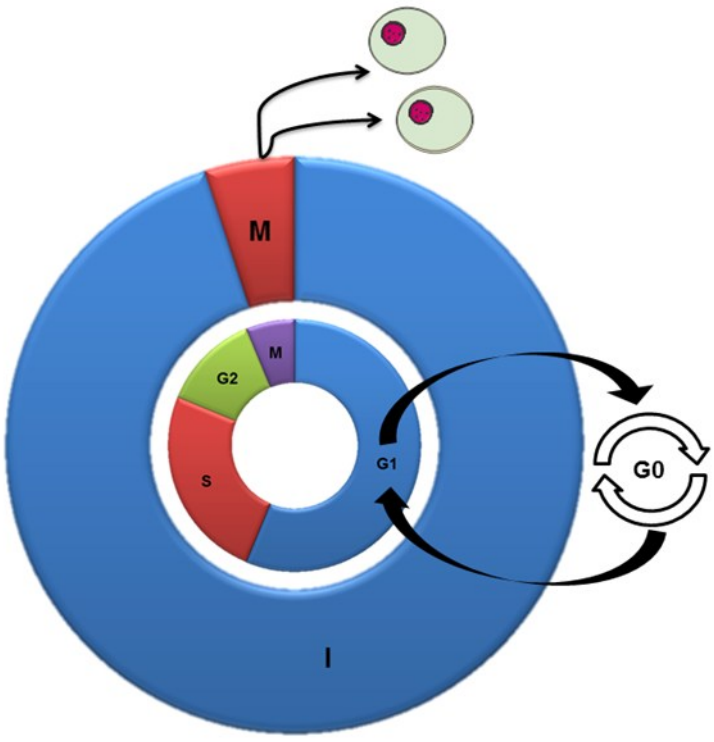


Figure 2 - Schematic representation of the cell cycle. Outer circle: I - interphase, M - mitosis. Inner circle: G1 - gap 1, S - synthesis, G2 - gap 2, G0 - resting phase, M – mitosis.

Interphase, in which the cell spends most of its lifetime, is divided in three phases. Thus, the *first gap phase*, **G1**, is characterized by an increase of the cell size, due to the production of cellular components such as membranes, organelles and ribosomes. In the *synthesis* or **S** phase, the replication of DNA occurs. In the *second gap phase*, **G2**, the cell produces proteins and continues to grow. The period of mitosis, **M**, is characterized by cell division into two different cells which, in turn, enter the interphase period. After cell division, the cell can also stop dividing, and enter into a quiescent state, the G0 phase(Mahmoudi et al., 2011).

The two cell cycle checkpoints, **G0/G1** and **G2/M** are determined by factors that control progression through the cell cycle, particularly the cyclin-cyclin-dependent kinases (CDKs) complexes. Upon activation of the complex cyclin-CDKs, the kinases initiate a biochemical reaction of phosphorylation, which may lead to the activation or inactivation of proteins that coordinates cell cycle progression.

At the beginning of the cell cycle, the G1 cyclin-CDKs complex is activated in order to prepare the cell to enter S phase, through the induction of transcription factors, which, in turn, allow the expression of S cyclins and enzymes essential to DNA replication.

Phosphorylation of the active S cyclins creates the pre-replication complexes gathered during G1 phase, in order to ensure that all cell's genome is replicated only once.

Mitotic cyclin-CDKs complexes, which remain inactive in G1 and S phases, induce the mitotic process through the stimulation of proteins that leads to chromosome condensation and the completion of mitotic spindle formation. After the completion of the spindle assembly checkpoint, M cyclins are destroyed during metaphase and anaphase, which causes the exit of mitosis and cytokinesis (Mahmoudi et al., 2011).

The specific cyclin-CDKs complexes involved in the cell cycle progression are represented in **Table 8.**

Table 8 - Cyclin and cyclin-dependent kinases (CDKs) involved in the cell cycle progression.

Cell cycle phase	Cyclin-CDKs	Action
G1/ S	Cyclin A - CDK2	Active in S phase
	Cyclin D - CDK4, Cyclin D - CDK6, and Cyclin E - CDK2	Regulation of the transition from G_1 to S phase
G2/M	Cyclin B - CDK1	Regulation of the progression from G_2 to M phase

Cell cycle analysis can be performed by flow cytometry. This technique is based on the evaluation of the cell properties in a flow, after staining the cells with propidium iodide (PI), a nucleic acids-binding dye. In **Figure 3** is represented a typical histogram of the cell cycle analysis by flow cytometry. The first peak of the histogram is related to the cells in the G0/G1 phase. The cells in G2/M phase are represented in the second peak of the histogram. The space between the peaks corresponds to the cells that are in the S phase. When is present, the sub-G1 area corresponds to cellular debris and late apoptotic and necrotic cells.

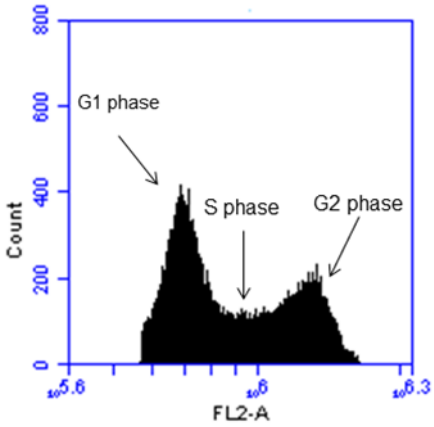


Figure 3 - Representative cell cycle histogram of Caco-2 cells analysed by flow cytometry.

1.4.2. Cell cycle behaviour in response to DNA damage

In a normal state, the cell behavior is regulated not only by cell genetic programing and cellular factors (size of the cell can dictate cell division), but also by a large spectrum of extra-cellular factors such as physicochemical nature of the medium involving the cells, interaction between cells and the extracellular matrix, expression of adhesion molecules, and the presence of growth factors in the involving medium.

The cells response to DNA damage may involve the activation of cell cycle checkpoint, initiation of DNA repair, and if the damage is irreversible, activation of the apoptotic process, which involves both p53 and E2F1 transcription factors. Indeed, Vousden and Lane., have shown that high levels of p53 resulted in irreversible apoptosis and low levels of p53 lead to transient growth arrest and cell survival (Vousden and Lane, 2007).

Thus, upon DNA damage, p53 is activated inhibiting E2F1 via p21 **(Figure 4)**, resulting in the cell cycle arrest in the G1 phase. If the DNA damage is repairable, the cell will continue the cell cycle progression to the S phase and, mainly due to the activation of E2F1 and inactivation of p53. However, if the DNA damage is irreparable, both p53 and

E2F1 will be activated leading to the initiation of the apoptotic process. Zhang et al. demonstrated that E2F1 promoted apoptosis by the up-regulation of p53 pro-apoptotic cofactors (Zhang et al., 2010).

The ATM (ataxia telangiectasia mutated) and ATR (ATM and Rad3-related) protein kinases also play a key role in the progression of the cell cycle. This role is more prominent in the S phase and G2 phase checkpoints. The S phase regulation is characterized by the activation of Chk2 kinase by the ATM kinase, followed by the destabilization of Cdc25A, leading to the inactivation of the Cdk2/Cyclin E and Cdk2/Cyclin A complexes (S phase arrest).

G2 phase arrest is caused by the cyclin-dependent kinase CdC2 (or Cdk1) inactivation through the sequestration of the Cdc25A in the cytoplasm. This process causes the Cdc2/Cyclin B1 to remain inactive and thus blocking the mitotic process. The cell cycle checkpoints signaling pathways can be visualized in **Figure 4**.

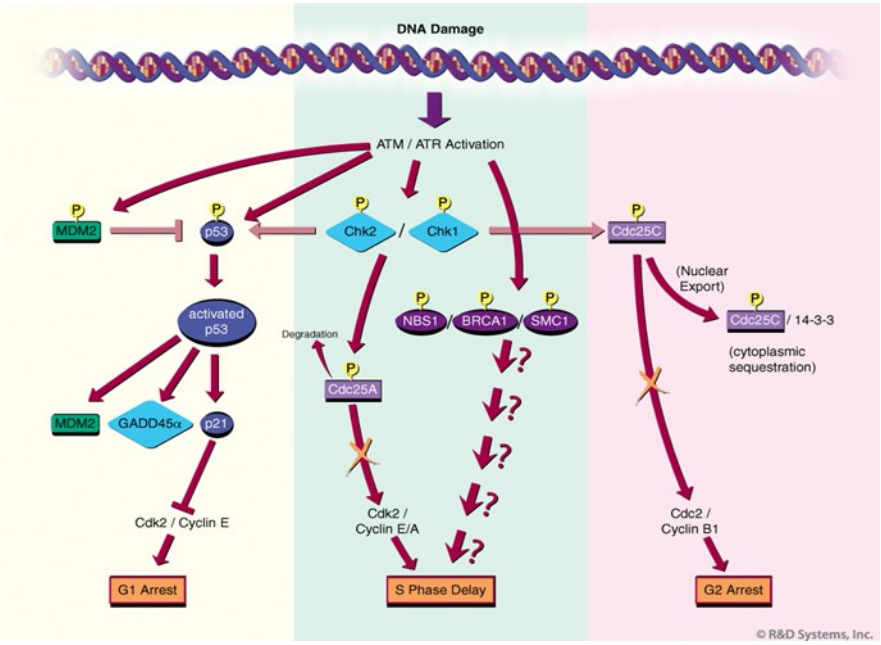


Figure 4 - Diagram of cell cycle response triggered by DNA damage. ATM - ataxia telangiectasia mutated protein kinases, ATR - ATM and Rad3-related protein kinases, Cdc25A - cell division control 25A protein-coding gene, Cdk2 - cyclin-dependent kinase 2, Cdc2 - cell division control protein 2 homolog, Chk – checkpoint homolog kinases, p53 - tumor suppressor protein (From (Saidin, 2008).

1.4.3. Metallic nanoparticles and the cell cycle

Similarly to other xenobiotics, metallic NPs can also have a significant impact on the cell cycle progression. The flow cytometry technique is a valuable tool to analyze the impact of the NPs on the cell cycle. Any kind of dysregulation in the cell cycle will become

evident by changes in the areas of the peaks corresponding to the different phases, resulting in the accumulation of cells in one or more phases of the cell cycle.

The rate of NPs uptake can also be influenced by the cell cycle phase. In this context, Kim et al. investigated the relationship between NP cellular uptake and cell cycle phase. The authors showed that as long as NPs are not extruded from the cell, they are passed onto the daughter cells. Thus, this process dilutes the concentration of the NPs inside the cell (**Figure 5**). The formation of protein-NP corona also varies during the cell cycle as the production of membrane proteins is different among phases (Kim et al., 2012).

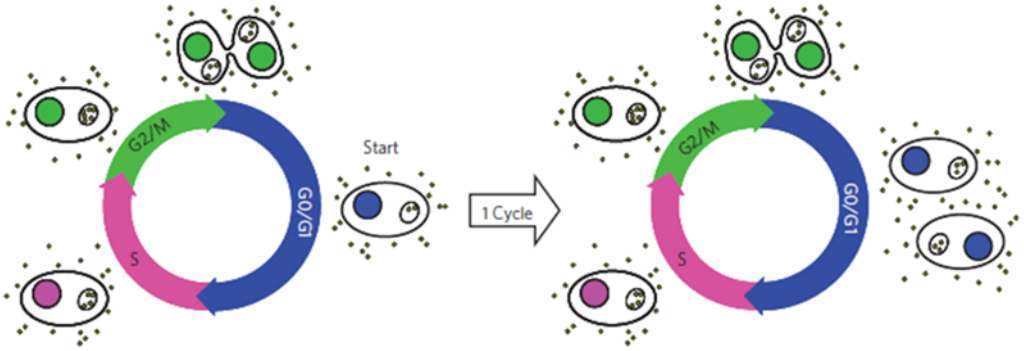


Figure 5 - Role of the cell cycle in the cellular uptake of NPs. Nanoparticle uptake in a cycling cell. The yellow-green circles represent the nanoparticles, which, inside cells, accumulate in the lysosomes, represented by the oval compartment. When the cell divides, the internalized nanoparticles are split between the two daughter cells (From (Kim et al., 2012)).

1.4.3.1. Gold nanoparticles

Studies on the effects of AuNPs in the cell cycle are still scarce. However, it has already been reported that AuNPs can interfere in the cell cycle (Mahmoudi et al., 2011). Roa et al. demonstrated that exposure for 24h to glucose capped-AuNPs (Glu-AuNPs) accelerated the G0/G1 phase transition in human prostate cancer cells (DU-145) and resulted in the accumulation of cells in the G2/M phase (29.8%) comparing with control cells (18.4%)(Roa et al., 2009). Choi et al. have also evaluated the effect of serum protein coated AuNPs in the cell cycle of human lung carcinoma and human epidermoid carcinoma cell lines. The authors observed an increase in the sub-G1 population in the AuNPs-exposed cells compared to control cells, where most cells were in the G1 phase (Choi et al., 2012). Also, Chuang et al. performed an extensive evaluation of 10 nm x 45 nm Au nanorods in human lung adenocarcinoma epithelial (A549) and gastric adenocarcinoma (AGS) cells. They have demonstrated that in A549 cells, the tested Au-nanorods stimulated the accumulation in the G1 phase in a concentration-dependent manner and no cell death was observed after 24 h of exposure. However, the opposite findings were observed in AGS cells, incubation with the Au-nanorods for 24 h induced an

increase of ROS levels and cell death, however no effect in the cell cycle of AGS cells was observed (Chuang et al., 2013).

1.4.3.2. Silver nanoparticles

The effect of AgNPs on the cell cycle has also been studied. In A549 cells, incubation for 24 h with a low concentration (2 μg/mL) of AgNPs did not alter the cell cycle progression (Beer et al., 2012). However, at a higher concentration (3 μg/mL), a decrease of the cell number in the G1/G0 phase was obtained (Beer et al., 2012). In mouse peritoneal macrophage (RAW264.7) cells, exposure to 69 nm AgNPs for 24 h resulted in cell arrest at the G1 phase hindering the S phase, followed by cell apoptosis (Park et al., 2010). In addition, AshaRani et al. employed the cell cycle analysis as a complementary study of the oxidative stress caused by starch-coated AgNPs. Based on the fact that cells with DNA damage can accumulate in G1, S and G2/M phase, and cells in an irreversible state of damage will accumulate in sub-G1 phase, the authors reported that these NPs caused cell arrest at the G2/M phase of human lung fibroblast (IMR-90) and human glioblastoma (U251) cells (AshaRani et al., 2008).

Zheng et al. used both AuNPs and AgNPs to study their role in enhancement of radiosensitivity in hepatocellular cells (HepG2). In this study, they have combined AgNPs and AuNPs with irradiation and evaluated whether this combination (AgNPs-irradiation and AuNPs-irradiation) could induce changes in cell cycle compared to control cells (the cells treated with irradiation alone). It was concluded that both combinations had no impact in the various phases of cell cycle (Zheng et al., 2013).

Overall, the physicochemical properties and experimental conditions underlie the differences in the observed toxic response of these NPs. More studies have to be conducted in order to overcome these difficulties in interpreting the toxicity of the NPs. Also, the better understanding of NPs *in vitro* effects can be useful to predict their *in vivo* outcomes.

Chapter 2

Scope and Aims

Nanotechnology is growing at an exponential rate, which raises concerns about the effects that NMs can bring to the human health and environment. The NMs are being applied in many areas, including industry, biomedicine and food and feed. In the field of human nutrition, NMs can be used as dietary supplements, incorporated in food packaging materials and also to preserve prepared foods. These applications offer potential benefits but have also raised concerns about their possible health and safety risks to consumers.

Surface modification and/or bio-functionalization of metallic NPs has been proven to influence the NPs properties and opens new doors for the development of nanotechnology.

Following this line of thought, in this thesis, the cytotoxic effects of AuNPs and AgNPs with potential application in the food and feed industries were studied in human epithelial colorectal adenocarcinoma Caco-2 cells. This cell line is a well-characterized and accepted model of the human intestinal barrier, thus in the present study it has been selected to assess the interaction of the NPs with the gastrointestinal tract. The tested AuNPs were capped with citrate (Cit-AuNPs) and three pentapeptides, CALNN (Cys – Ala – Leu – Asn - Asn), CALND (Cy – Ala – Leu – Asn – Asp) and CALNS (Cys – Ala – Leu – Asn - Ser), whereas AgNPs were capped with citrate (Cit-AgNPs). Both AuNPs and AgNPs had the size of ~20 nm.

Cell cycle deregulation is one of the major hallmarks of cancer. Therefore, uptake of the differently capped AuNPs and Cit-AgNPs, and their effect on the cell cycle progression was also addressed by the flow cytometry analysis. This analysis can provide useful information on cells ability to handle with metal-based NPs exposure.

Chapter 3

Experimental section

3.1. Materials and methods

3.1.1. Reagents and Materials

The Dulbecco's modified Eagle's medium (DMEM) with or without phenol red, Triton X-100, Calcein-AM, Neutral red, *N*-2-hydroxyethylpiperazine-*N'*-2-ethanosulfonic acid (HEPES) and 3-(4,5-dimethylthiazol-2-yl)-2,5-diphenyltetrazolium bromide (MTT) were purchased from Sigma-Aldrich (Madrid, Spain).

The fetal bovine serum (FBS), penicillin-streptomycin solution (10000 U/mL), Fungizone® antimycotic solution (250 µg/mL of amphotericin B), trypsin (0.25%) - EDTA (0.53 mM) solution and Hank's balanced salt solution (HBSS) were obtained from Gibco ® Life Technologies (Madrid, Spain). The phosphate buffered saline (PBS) without Ca^{2+} and Mg^{2+}, was obtained from Biochrom (Cambridge, United Kingdom). RNase A (DNase-free) was obtained from Panreac AppliChem (Darmstadt, Germany).

The Biopure^{TM} 20 nm silver nanoparticles (1 mg/mL) were purchased from nanoComposix (California, USA).

3.1.2. Cell culture

Caco - 2 (HTB 37 - HTB; passages 68 – 81) cells were obtained from the American Type Culture Collection (Rockville, MD, USA) and maintained in a humidified atmosphere of 5% CO_2 – 95% air at 37ºC. The cells were kept in culture in DMEM, supplemented with 10 % FBS, 1% penicillin-streptomycin (100 U/mL), 2.5 % Fungizone and 25 mM of HEPES. For subculture, the cells were dissociated with trypsin (0.25%) - EDTA (0.53 mM) solution and cultured in T-25 (2.5×10^5 cells) and T-75 (7.5×10^5 cells) flasks, respectively. The medium was replaced 1-2- times per week.

3.1.3. AuNPs and AgNPs nanoparticles

Gold nanoparticles (AuNPs) were synthesized and characterized in the department of Chemistry and Biochemistry of the Faculty of Sciences of the University of Porto. The citrate capped AuNPs (Cit-AuNPs) were synthesized according to the protocol developed by Turkevich and collaborators (Enustun and Turkevich, 1963, Kimling et al., 2006), with slight modifications (Morais et al., 2012). To exchange the capping of Cit-AuNPs to pentapeptide-AuNPs (CALNN-, CALNS-, and CALND-AuNPs), it was used a molar ratio

of [AuNP]/capping agent of 1:5000, as previously described (Morais et al., 2012). The structures of the AuNPs and respective coatings are represented in **Figure 6**.

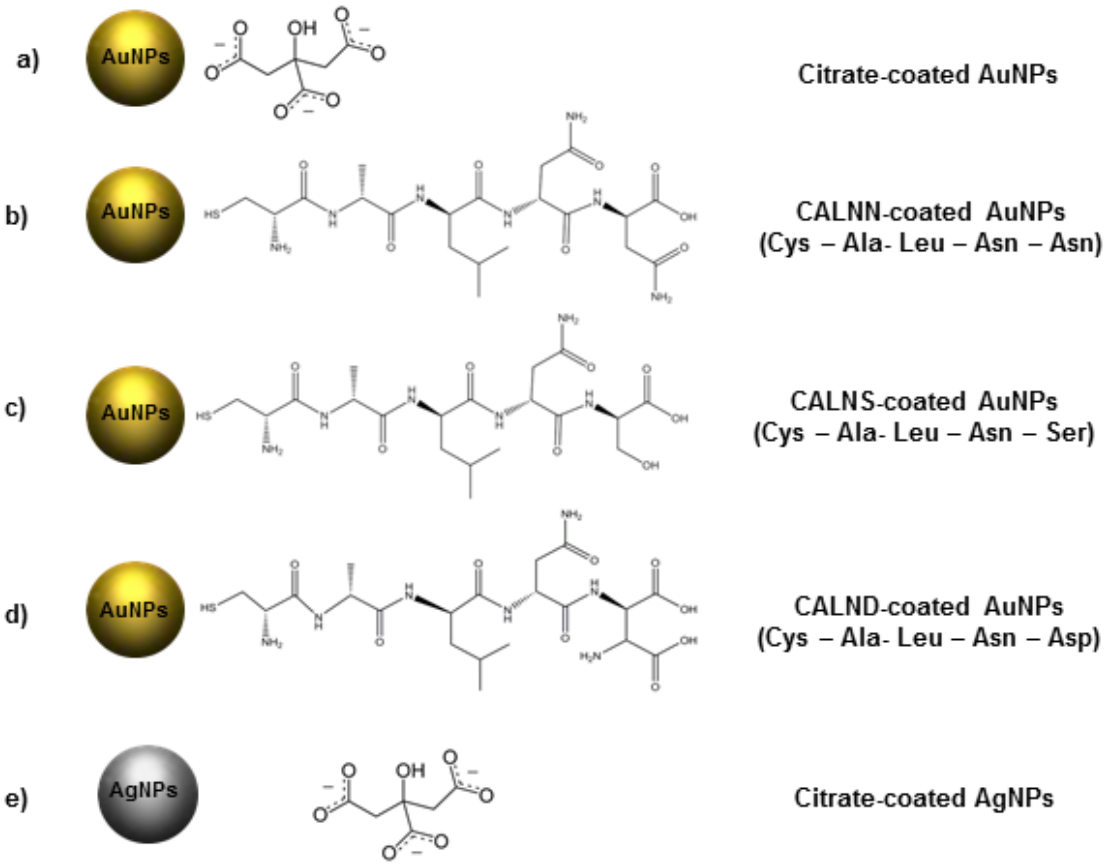


Figure 6 - Representation of the NPs used in this study: a) citrate-coated AuNPs, b) CALNN-coated AuNPs, c) CALNS- coated AuNPs, d) CALND-coated AuNPs and e) citrate-coated AgNPs.

Characterization of the AuNPs and AgNPs was performed using three techniques: UV/Vis spectroscopy to assess the colloidal suspensions concentration and optical properties, transmission electron microscopy (TEM) to determine the morphology and average particle size, and dynamic light scattering (DLS) to determine the hydrodynamic diameter and zeta potential of AuNPs. To calculate the mass concentration of AuNPs and AgNPs it was used the graphite furnace atomic absorption spectrometry (GFAAS) and inductively coupled plasma-mass spectrometry (ICP-MS), respectively. The main characteristics of AuNPs and AgNPs are represented in **Table 9**.

Table 9 - Main characteristics of AuNPs and AgNPs.The average size and zeta potential of the AuNPs were determined by DLS. The Au content of the suspensions was determined by GFAAS. The Ag content of the suspensions was determined by ICP-MS.

NP	Descriptions	Hydrodynamic radius[a] (nm)	Zeta potential[b] (mV)	[Au][c] (µg/mL) [Ag][d] (µg/mL)
AuNPs	Citrate-coated (synthesized)	22.4 (5.7)	-44.7± 7.5	249.0
	CALNN-coated (synthesized)	33.7 (9.6)	-47.1± 6.0	152.2
	CALNS-coated (synthesized)	35.1 (9.9)	-43.1± 9.2	184.0
	CALND-coated (synthesized)	34.9 (9.6)	-40.5± 7.0	158.1
AgNPs	Citrate-coated (acquired from nanoComposix)	32.0(4.0)	-21.4 ± 2.7	1000

[a]The values in parenthesis are polydispersion indexes.
[b] Results are expressed as means ± standard deviation.
[c]The concentration of Au of the injected colloidal suspensions were determined by GFAAS. Results are expressed as means ± standarderror of the mean.
[d]The concentration of Au of the injected colloidal suspensions were determined by ICP-MS.

All procedures, including cell culture, incubation with the NPs and cytotoxicity assays were standardized. The same batches of AuNPs and AgNPs were used for all the experiments. The NPs stock suspensions were stored at 4ºC, protected from light. The NPs working suspensions used in the experiments were prepared by direct dilution of the stock suspensions in FBS-free, phenol red-free DMEM.

3.2. Methods and procedures

3.2.1. Cytotoxicity assays

To assess the cytotoxic effect of AuNPs and AgNPs, a series of assays were performed. For AuNPs, three fluorescent assays were conducted to assess metabolic activity, plasma membrane integrity, reactive oxygen species (ROS) production, namely the Calcein-AM, propidium iodide (PI) and 2', 7'-dichlorofluorescein-diacetate (DCFH-DA) assay, respectively. A colorimetric assay, the Neutral Red uptake (NR) was also performed to evaluate the lysosomal integrity. To measure the fluorescence signal and reduce the NP interference, bottom readings were performed. For AgNPs, DCFH-DA, NR and MTT assays were used to assess their cytotoxicity. The Calcein-AM and PI assays

were not used due to the signal interference caused by the deposition of AgNPs suspension on top of the cells. Potential morphological changes induced by NP exposure and NP aggregation/agglomeration were also investigated. For that purpose, cells were monitored using an inverted phase contrast microscope throughout the incubation period.

All experiments were repeated three times, using different cell passages. All results from the cytotoxicity assays were expressed in percentage relatively to control (untreated cells).

3.2.1.1. Cell metabolic activity (Calcein-AM assay)

This assay evaluates the cell metabolic activity through the conversion of a non-fluorescent (Calcein-AM) into a fluorescent dye, Calcein, by the intracellular esterases in live cells, as represented in **Figure 7**.

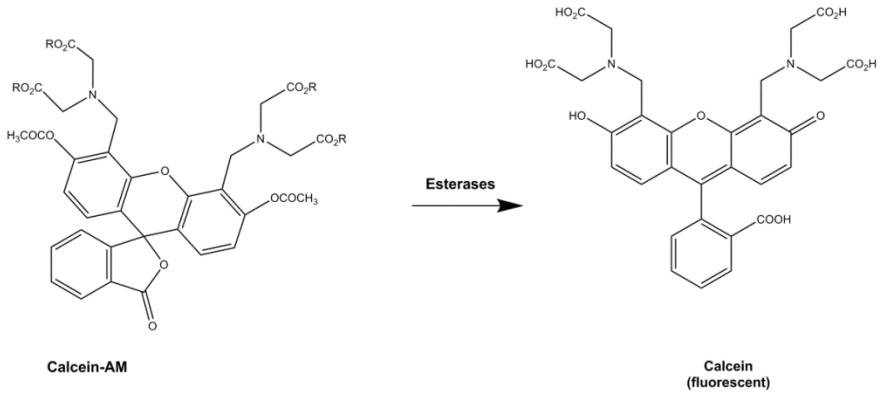


Figure 7 - Cell staining mechanism of Calcein-AM in viable cells.

The cells were seeded in 96-well plates at a density of 10000 cells/well. After reaching confluence, the cells were incubated with increasing concentrations (0, 1, 3, 10, 30, 60, 100 µM) of Cit-, CALNN-, CALNS- and CALND-AuNPs for 6, 24, 48 and 72 h at 37ºC, 5% CO_2.At each time-point, the medium was discarded and replaced with 150 µL of Calcein-AM 1 µM in each well and incubated for 60 min at room temperature, protected from light. Afterwards, the medium was once more discarded and 150 µL of HBSS (with Ca^{2+}/Mg^{2+}) was added to each well. As a positive control, cells were incubated with 70 % ethanol solution for 30 min. The fluorescence was measured in a microplate reader (spectrophotometer *Sinergy HT microplate reader*) with the excitation and emission wavelengths of 485 ± 10 nm and 530 ± 12.5 nm respectively.

3.2.1.2. Mitochondrial activity (MTT assay)

The MTT assay is based on the activity of mitochondrial enzymes. If cells are viable they can properly metabolize the MTT to its insoluble crystal, formazan, as represented in **Figure 8**.

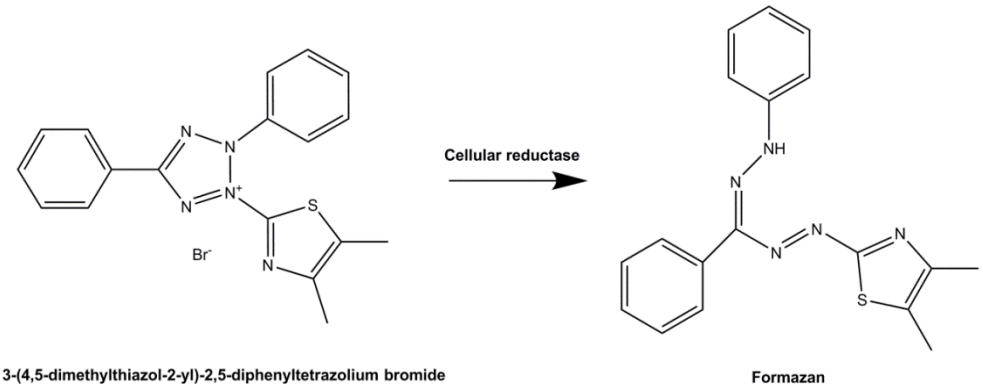


Figure 8 - Representation of the conversion of yellow tetrazolium,3-(4,5-dimethylthiazol-2-yl)-2,5-diphenyltetrazolium bromide, into the insoluble formazan crystal.

Cells were seeded in 96-well plates (10000 cells/cm^2) and after reaching confluence, were incubated with increasing concentrations (0, 1, 3, 10, 30, 60, 100 µM) of Cit-, CALNN-, CALNS-, CALND-AuNPs, for 6, 24, 48 and 72 h at 37ºC, 5% CO_2. Regarding AgNPs exposure, the cells were incubated with increasing concentrations (0, 1, 2.5, 5, 10, 20, 40 µg/mL) of Cit-AgNPs for 6, 24 and 48 h at 37ºC, 5% CO_2. After the exposure time was completed, the media were discarded and 150 µL of MTT solution (0.5 mg/mL) was added to the cells for 60 min. Then, the media was once again discarded and 150 µL of dimethylsulfoxide (DMSO) was added to dissolve the formazan. The solution was carefully mixed before the absorbance reading. Cells exposed to 70% ethanol were used as a positive control. The absorbance measurement was carried out in a microplate reader (spectrophotometer *Sinergy HT microplate reader*) at the wavelength of 560 nm (reference wavelength of 690 nm).

3.2.1.3. Plasma membrane integrity (iodide propidium assay)

The propidium iodide (PI) assay is used to evaluate the plasma membrane integrity and to discriminate live from necrotic cells. The PI binds to nucleic acids in plasma membrane compromised cells, which enhances its fluorescent signal.

Cells were seeded in 96-well plates (10000 cells/cm^2) and after reaching confluence, the cells were incubated with increasing concentrations (0, 1, 3, 10, 30, 60, 100 µM) of Cit-, CALNN-, CALNS-, CALND-AuNPs, for 6, 24, 48 and 72 h at 37ºC, 5% CO_2. After each time of incubation has been completed, 50 µL of 16 µM PI was added to

each well and incubated for 60 min at room temperature, protected from light. Cell exposed for 30 min to a solution of ethanol 70 % were used as a positive control. The fluorescence was measured in a microplate reader (spectrophotometer *Sinergy HT microplate reader*) with the excitation and emission wavelengths of 540 ± 25 nm and 605 ± 55 nm, respectively.

3.2.1.4. Reactive oxygen species levels (DCFH-DA assay)

The production of reactive oxygen species (ROS) can be evaluated by the 2',7'-dichlorofluorescein-diacetate (DCFH-DA) assay. The mechanism of this assay involves deacetylation followed by oxidation of this probe resulting in the conversion of a non-fluorescent into a fluorescent dye, as represented in **Figure 9**.

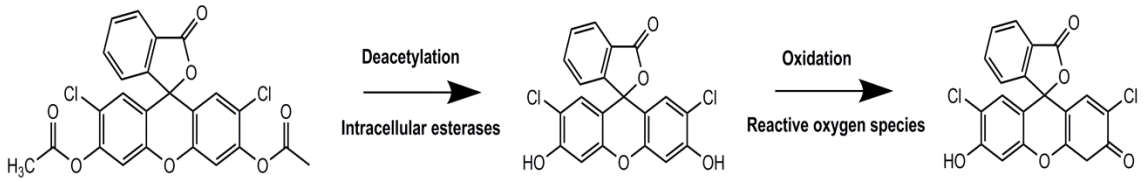


Figure 9 - Representation of the mechanism of the 2', 7'-dichlorofluorescein-diacetate (DCFH-DA) assay.

In this assay, two different protocols were tested. The first protocol consisted in the incubation of NPs suspensions followed by the incubation with the probe. Briefly, the cells were seeded in 96-well plates (10000 cells/cm^2), and at confluence incubated with increasing concentrations (0, 1, 3, 10, 30, 60, 100 µM) of Cit-, CALNN-, CALNS-, CALND-AuNPs, for 6, 24, 48 and 72 h at 37ºC, 5% CO_2. After the exposure period has been completed, the cells were incubated with 40 µM DCFH-DA for 1 h at 37 ºC, 5% CO_2. In this assay, cells were exposed for 60 min to hydrogen peroxide (H_2O_2) as a positive control.

The second protocol was used to evaluate the cells response to exposure to citrate-AgNPs. Firstly, the confluent cells were incubated with the probe for 1 h. Then, the media were discarded followed by incubation with increasing concentrations of 0, 1, 2.5, 5, 10, 20 and 40 µg/mL of Cit-AgNPs for 6, 24, 48 and 72 h at 37ºC, 5% CO_2. After each time of incubation has been completed, the media were discarded and 150 µL of HBSS (with Ca^{2+}/ Mg^{2+}) was added to the cells. The fluorescence was measured in a microplate reader (spectrophotometer *Sinergy HT microplate reader*) with the excitation and emission wavelengths of 485 ± 10 nm and 530 ± 12.5 nm, respectively.

3.2.1.5. Lysosomal membrane integrity (neutral red uptake assay)

The Neutral Red (NR) dye can be incorporated into the lysosomes of viable cells through active transport. If the lysosomes are in an unstressed state, they can retain the NR for a long period of time, and if not, the dye will be leaked into the cytosol. Upon the completion of the exposure time, the dye is liberated from the cells in an acidified ethanol solution.

Briefly, the cells were seeded in 96-well plates (10000 cells/cm^2) and at confluence, cells were incubated with increasing concentrations of Cit-, CALNN-, CALNS-, CALND-AuNPs (0, 1, 3, 10, 30, 60, 100 µM) and Cit-AgNPs (0, 1, 2.5, 5, 10, 20, 40 µg/mL) for 6, 24, 48 and 72 hours at 37ºC, 5% CO_2.

After completing the incubation time, the media were discarded and 150 µL of 0.33 mg/mL of NR solution was added to each well for 2 h at 37ºC, 5% CO_2. Then, NR solution was discarded and 150 µL of solubilization solution (1 % acetic acid in 50 % ethanol) was added to each well. The content of each well was carefully mixed before the plate reading. A solution of ethanol (70 %) was used a positive control. The absorbance measurement was carried out in a microplate reader (spectrophotometer *Sinergy HT microplate reader*) at the wavelength of 540 nm (reference wavelength of 690 nm).

3.2.2. Flow cytometry analysis

The impact of the tested NPs in the cell cycle was analysed by flow cytometry using a solution of PI to determine the number of cells in each phase of the cell cycle. Cellular uptake was also assessed by flow cytometry after PI staining.

The studies were performed both in synchronized and non-synchronized cell cultures in order to understand whether the cell cycle phase could influence the the uptake of the tested NPs oran eventual NP-induced cell arrest.

3.2.2.1. Cellular synchronization protocol

To acquire a synchronized cell population, Caco-2 cells were seeded in 12-well plate (240000 cells/well) for 24 h in complete DMEM at 37 ºC, 5 % CO_2. Then, the cells were maintained with FBS-free DMEM for another 24 h. After the period of starvation completed, cells were incubated with the NPs in complete DMEM for 24 h at 37 ºC, 5 % CO_2.

To compare synchronized and non-synchronized populations, the non-synchronized population was seeded with half density (120000cells/well) in complete

DMEM for 48 h at 37 ºC, 5 % CO_2, followed by the NPs incubation (in complete DMEM) for another 24 h at 37 ºC, 5 % CO_2.

3.2.2.2. Cellular uptake and cell cycle analysis

For the flow cytometry experiments, synchronized and non-synchronized cultures were incubated with non-toxic concentrations of AuNPs (0, 1, 3 and 10 μM) and AgNPs (0, 1, 2.5 and 5 μg/mL) in complete DMEM for 24 h at 37 ºC, 5 % CO_2. Then, cells were trypsinized, collected, washed two times with PBS pH 7.4 solution. Between washes, the cells were centrifuged (7 min, 300 *g*). Then, the cells were fixated with a solution of 70 % ethanol, for at least 12 h at 4ºC. After fixation, the pellet was washed two times with PBS pH 7.4 and stained with a PI solution (5 μg/mL of PI, 200 μg/mL of RNAse A and 0.1 % Triton-X). Total cellular DNA content of the samples was analysed using BD Accuri 6 flow cytometer (20 000 events). Data was analysed using FlowJo

The uptake of AuNPs and AgNPs in Caco-2 cells was analysed by flow cytometry, a laser-based technology useful for cell counting, cell sorting and biomarker detection. The cellular uptake was estimated based on the measurement of the light scattering, which is affected by the cellular shape and topography. This analysis comprised two measurements: the forward-scattered light (FSC), which is related to the size of the cell and the side-scattered light (SSC) that provides an insight on the complexity of the cell. The experimental design of the allowed the study of the NPs uptake either in synchronized or non-synchronized cultures.

3.2.3. Statistical analysis

All the experiments were carried out three times. The data obtained were expressed in terms of mean ± standard error of the mean (SEM).

The GraphPad 6 prism program was used to perform the statistical analysis of all data. Normality was tested using the D'Agostino-Pearson, Shapiro-Wilk and Kolmogorov-Smirnov normality tests. Parametric analyses were performed using the one-way ANOVA with post-hoc Dunnet's tests applied for multiple comparisons. Significance was accepted at a $P_{value} < 0.05$.

Non-parametric analysis of the cell cycle and cellular uptake results was performed using the Kruskal-Wallis test followed by the post-hoc Dunn's test applied for multiple comparisons. Significance was accepted at a $P_{value} < 0.05$.

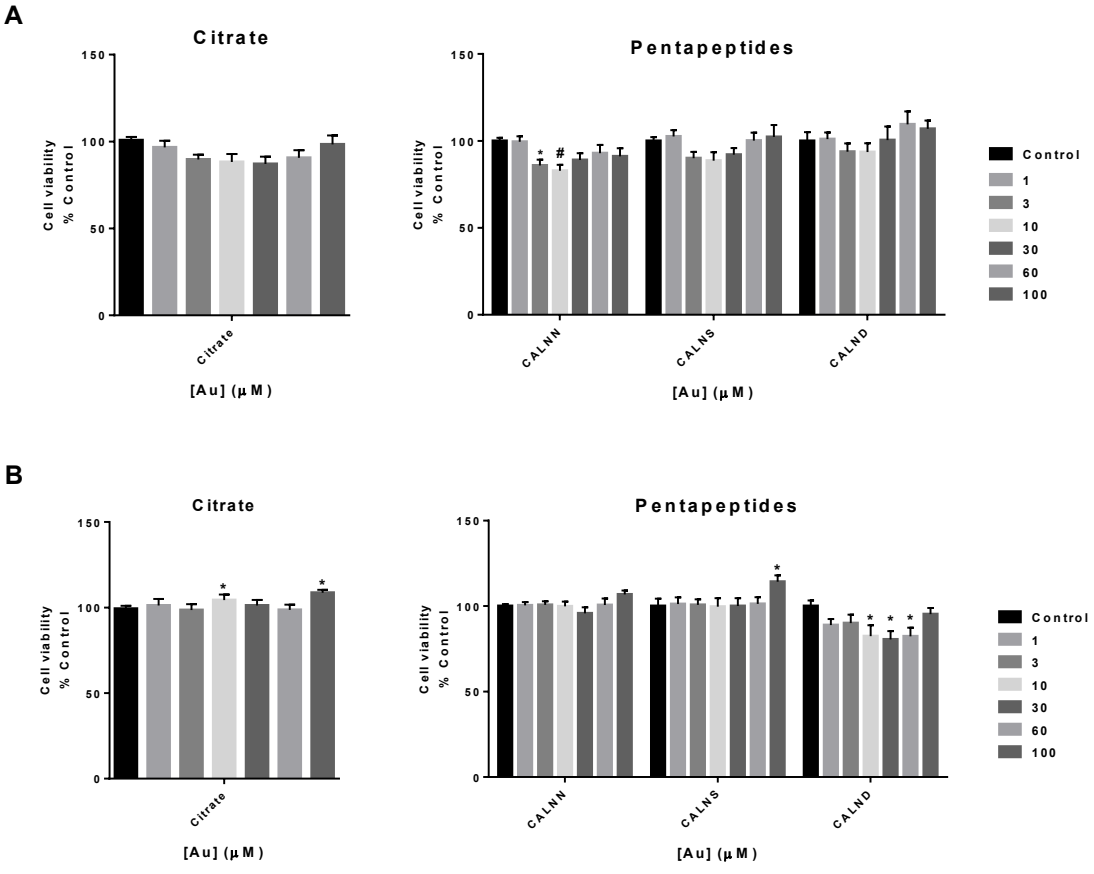
Chapter 4

Results

4.1. Cytotoxicity of AuNPs and AgNPs

Intracellular esterase activity, plasma membrane integrity and lysosomal membrane integrity were the endpoints used to evaluate the effect of the differently capped AuNPs on the viability of Caco-2 cells, at 4 different time-points: 6, 24, 48 and 72 h.

As shown in **Figure 10**, a significant decrease in cell viability, as assessed by the Calcein-AM assay, has been detected in cells exposed for 24 h to 10 and 100 μM of Cit-AuNPs. However, in general, Cit-AuNPs did not induce significant alterations of Caco-2 cells viability. Similar results were obtained in cells incubated with pentapeptide CALNN-, CALNS-, and CALND-coated AuNPs. However, at some points, small significant decreases in cell viability were observed: exposure for 6 h to 3 and 10 μM CALNN-AuNPs, incubation for 24 h with 10, 30 and 60 μM CALND-AuNPs and 100 μM CALNS-AuNPs. Nevertheless, after 48 and 72 h of incubation with any type of tested AuNPs, no alterations in the esterase activity of Caco-2 cells were observed, under the present experimental conditions.



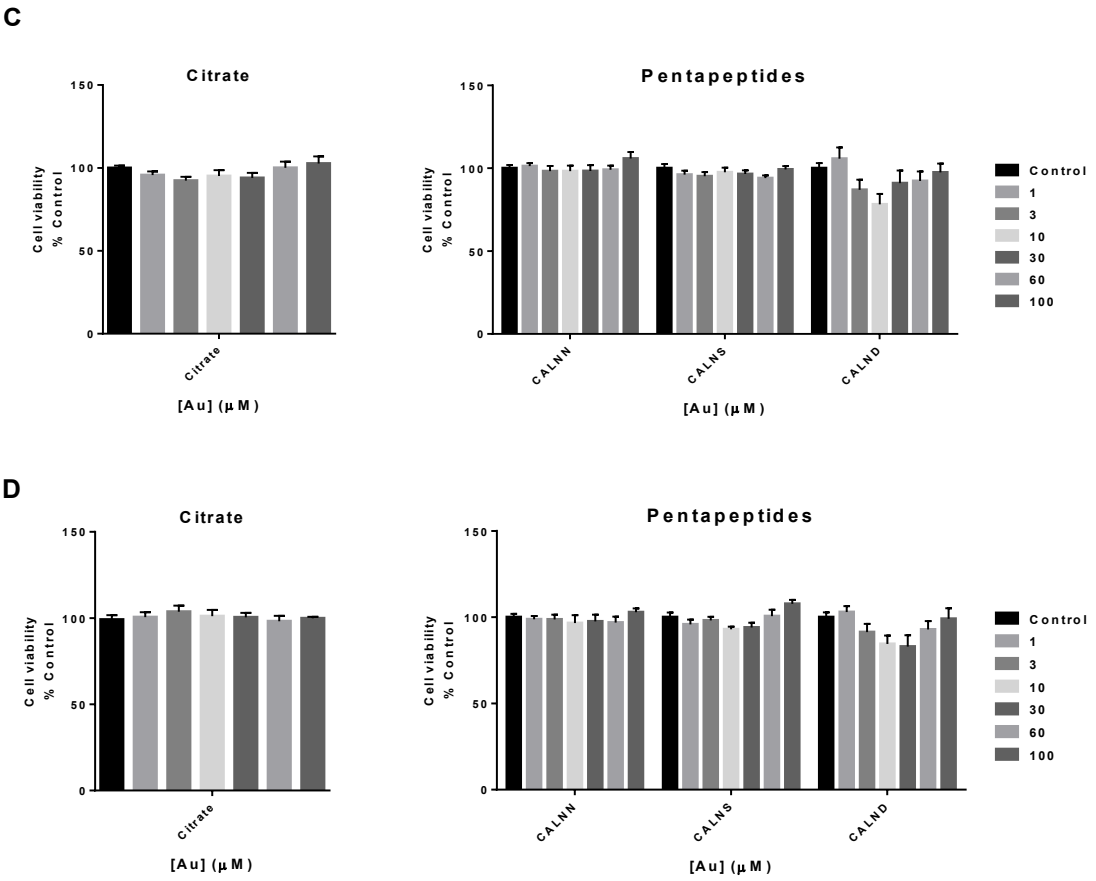
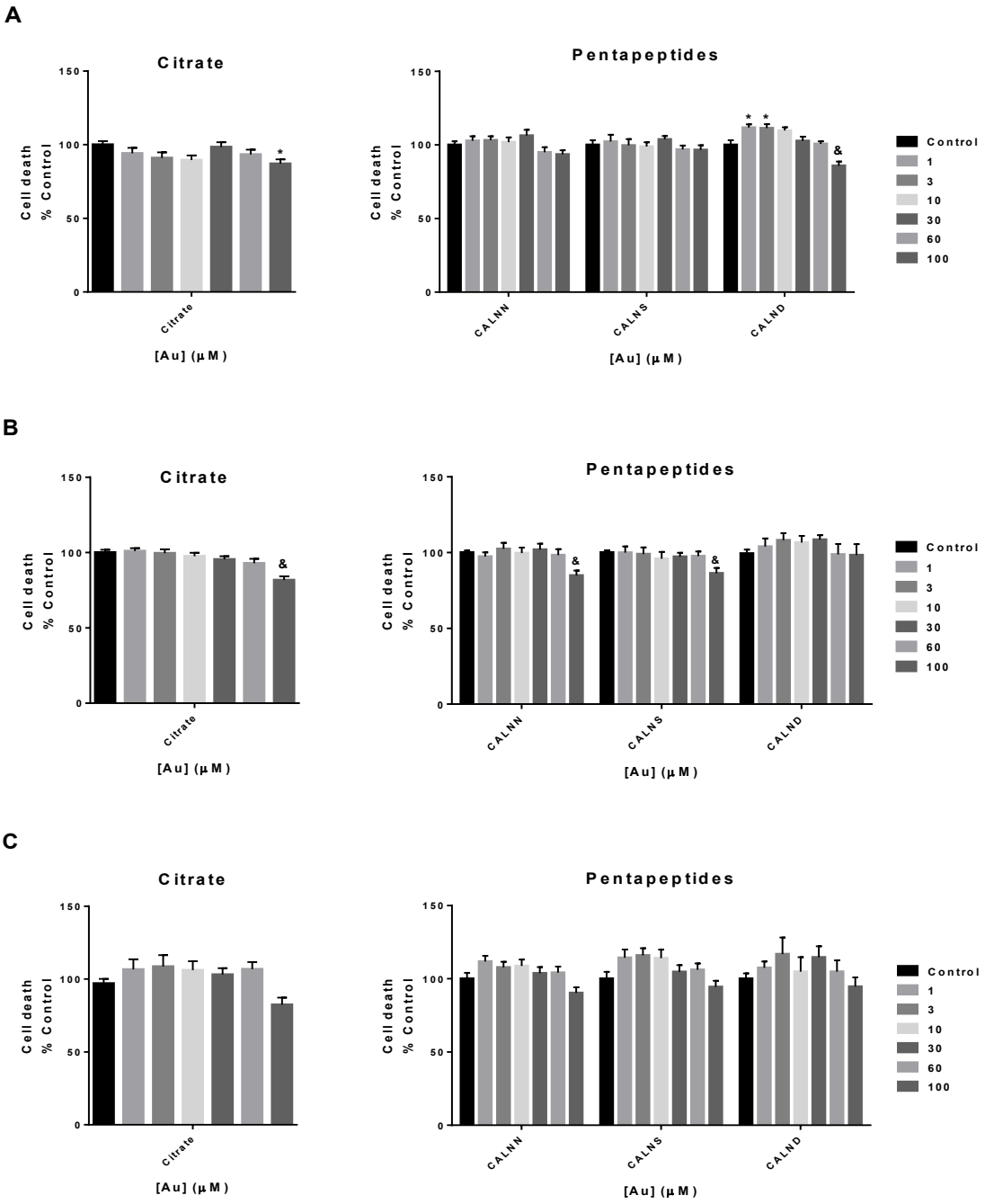


Figure 10 - Esterase activity of Caco-2 cells at (A) 6 h, (B) 24 h, (C) 48 h and (D) 72 h after exposure to Citrate-, CALNN-, CALNS-, CALND-AuNPsas assessed by the Calcein- AM assay. Results were calculated as percentage of control (untreated cells). Data is presented as mean ± SEM (n = 12-16). Data was analysed by one-way ANOVA with post-hoc Dunnet's tests applied for multiple comparisons * P<0.05, # P<0.01; significantly different from the control value.

Viability of Caco-2 cells after exposure to the differently-coated AuNPs was also estimated based on plasma membrane integrity, assessed by the PI assay. This assay differentiates necrotic from live cells. Dead cells emit greater PI fluorescence comparing with viable cells. As shown in **Figure 11**, after 6 h of exposure to 1 and 3 µM CALND-AuNPs a significant increase of cell death occurred compared to control cells **(Figure 11 A)**. At the same-time point, the cells incubated with 100 µM Cit-AuNPs and 100 µM CALND-AuNPs showed a significant decrease in cell death, which may be the result of signal interference from the interaction between the probe and the NPs and does not have any biological significance. The same effect could be observed after 24 h of exposure to the highest tested concentration (100 µM) in Cit-AuNPs-, CALNN-AuNPs- and CALNS-AuNPs-exposed cells **(Figure 11 B)**, or, after 72 h, in Cit-AuNPs- and CALNS-AuNPs-exposed cells **(Figure 11 D)**. In addition, at 72 h, an increase of cell death was observed

in cells exposed to 3 and 30 μM of CALNN-AuNPs. Nevertheless, taken together, the results indicate that the tested AuNPs did not cause significant cell death, which is in agreement with the results of the Calcein-AM assay.



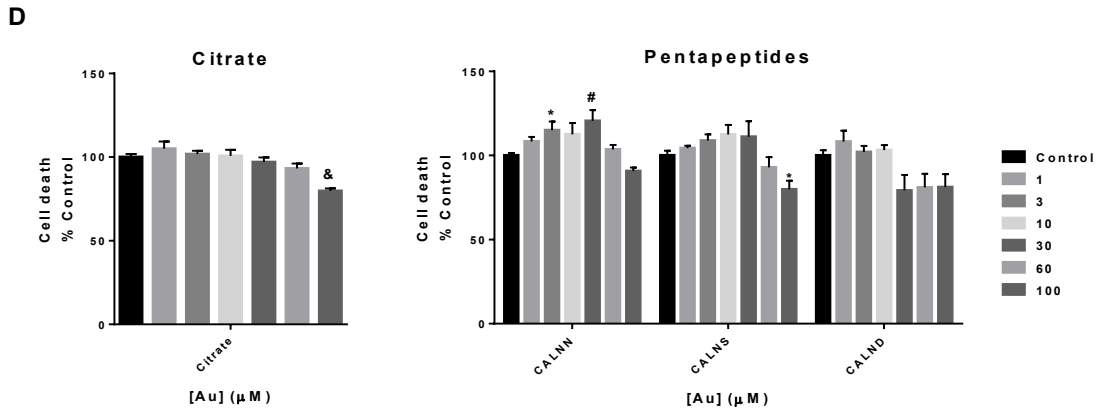


Figure 11 - Effects of Cit-, CALNN-, CALNS-, CALND-AuNPs in the plasma membrane integrity, determined by the propidium iodide (PI) assay, after (A) 6 h, (B) 24 h, (C) 48 h and (D) 72 h. Results were calculated as percentage of control (untreated cells). Data is presented as mean ± SEM (n = 12-16). Data was analysed using one-way ANOVA with post-hoc Dunnet's tests applied for multiple comparisons. * P<0.05, # P<0.01, $ P<0.001, & P<0.0001 significantly different from the control value.

The Neutral Red (NR) uptake assay was used to assess the integrity of the lysosomal membrane. Viable cells take up the dye by active transport and incorporate the dye into lysosomes, whereas non-viable cells do not take up the dye.

Thus, a decrease in NR cell content indicates damage of the lysosome and suggests a decrease in cell viability.

The results presented in **Figure 12 (A-D)** show that exposure for 6 h to Cit-AuNPs (10, 30 and 60 µM), CALNN-AuNPs (3, 10, 30, 60 and 100 µM), CALNS-AuNPs (10, 30, 60 and 100 µM) and CALND-AuNPs (30 and 100 µM) caused a decrease in the cell viability compared to control cells **(Figure 12 A)**. This decrease in cell viability was also observed after 24 h exposure to all tested concentrations of Cit-AuNPs, to 3, 10, 30, 60 and 100 µM CALNN-AuNPs, to 3, 10, 30 and 60 µM CALNS-AuNPs and to 10, 60 and 100 µM CALND-AuNPs **(Figure 12 B)**. At 48 h, only cells exposed to 60 µM Cit-AuNPs showed a significant decrease in the viability. However, cells incubated with CALND-AuNPs showed significant changes in cell viability compared to control **(Figure 12 C).**

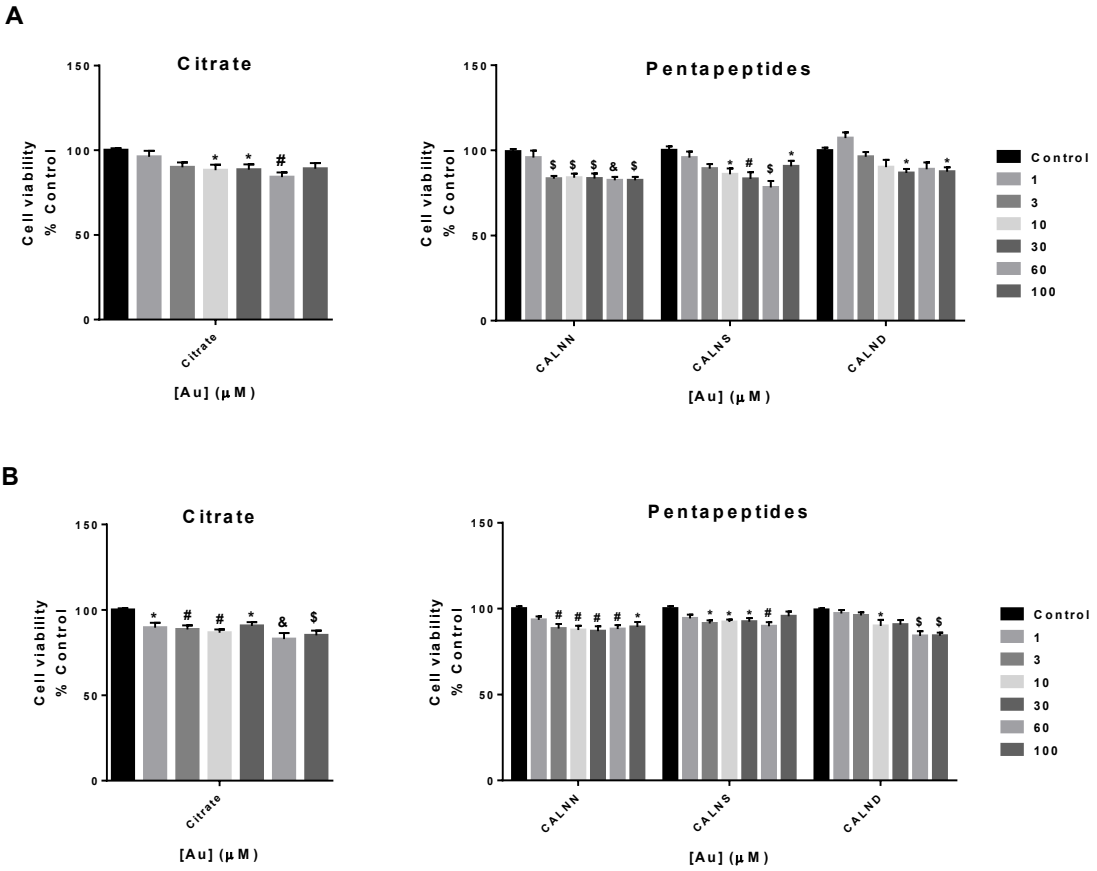
At 72 h, a significant decrease of cell viability was observed in Caco-2 cells incubated with 60 µM Cit-AuNPs, 3, 30, 60 and 100 µM CALNN-AuNPs, 3, 10, 30, 60 and 100 µM CALNS-AuNPs, at, and with 100 µM CALND-AuNPs **(Figure 12 D)**.

Regarding Cit-AgNPs, lysosomal membrane integrity and mitochondrial activity were the endpoints used to evaluate their impact on cell viability at three different time-points: 6, 24 and 48 h. The PI and Calcein-AM assays were not used to assess Cit-AgNPs cytotoxicity due to fluorescence quenching caused by the AgNPs.

As shown in **Figure 13 (A)**, after 6 h of incubation with 5 and 40 µg/mL of Cit-AgNPs, the NR incorporation into the lysosomes significantly decreased compared to control cells. Silver nitrate ($AgNO_3$) was also tested, and, at the same time-point, the highest tested concentrations (10, 20 and 40 µg/mL) led to a significant decrease of the cell viability, comparing with control cells, that can be interpreted as loss of integrity of the lysosomal membrane.

After 24 h of incubation (**Figure 13 B**), the cells incubated with 40 µg/mL Cit-AgNPs exhibited significantly decreased viability. . The cells incubated with 10, 20 and 40 µg/mL of $AgNO_3$ also showed a significant decrease viability compared to controls. This statistical significant decrease in viability was observed up to 48 h of exposure (**Figure 13 C**).

The decrease of viability was significantly more marked in Ag^+-treated cells compared to AgNPs-treated cells, at all time-points, after exposure to the highest tested concentrations (10, 20 and 40 µg/mL).



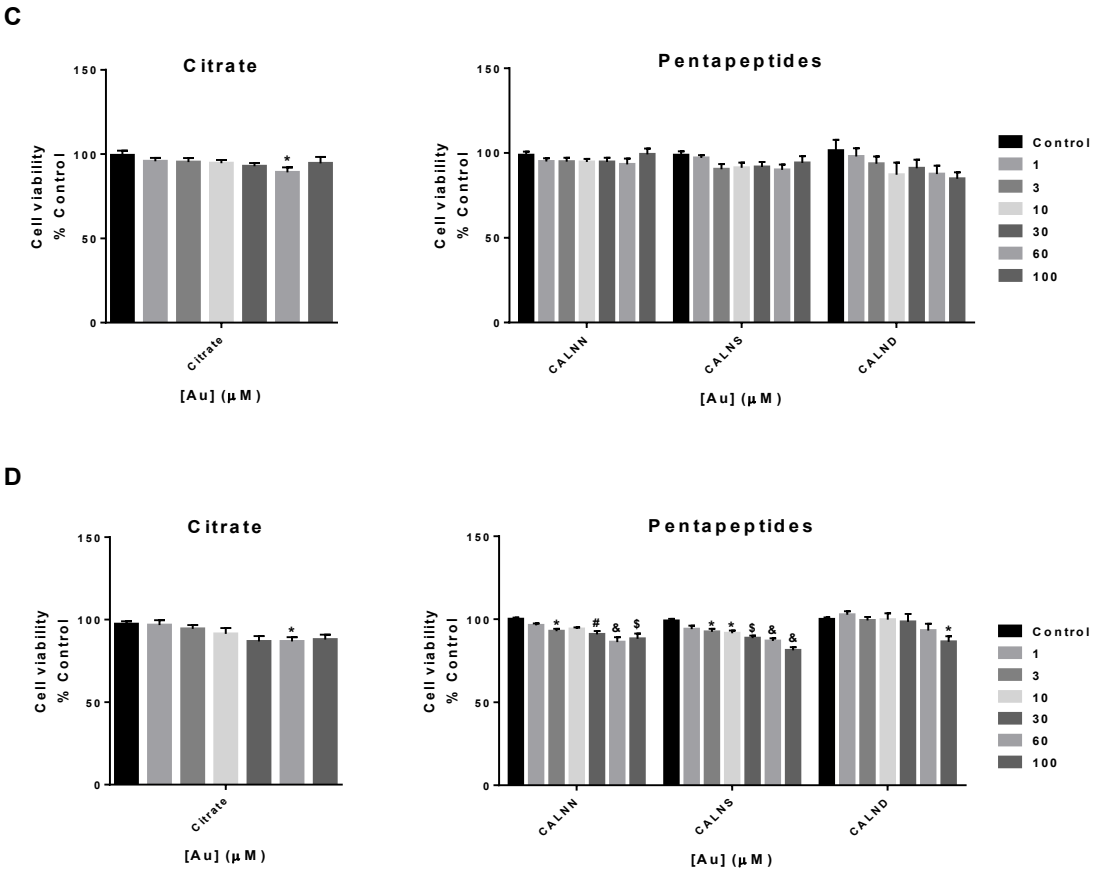
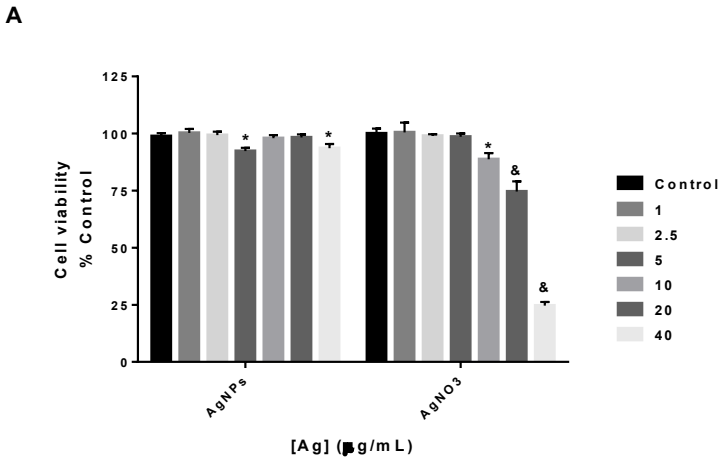


Figure 12 - Effects of Cit-, CALNN-, CALNS-, CALND-AuNPs in the lysosomal integrity, determined by the neutral red absorbance assay, after (A) 6 h, (B) 24 h, (C) 48 h and (D) 72 h. Results were calculated as percentage of control (untreated cells). Data is presented as mean ± SEM (n = 12-16). Data was analysed using one-way ANOVA with post-hoc Dunnet's tests applied for multiple comparisons. * P<0.05, # P<0.01, $ P<0.001, & P<0.0001 significantly different from the control value.



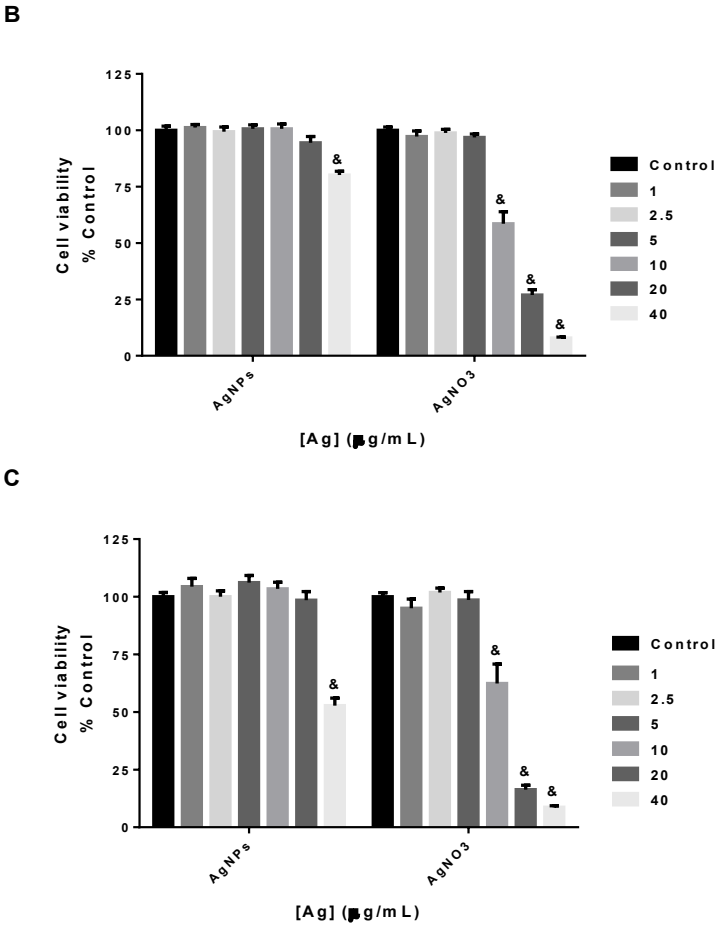


Figure 13 - Effects of Cit-AgNPs and $AgNO_3$ in lysosomal integrity, determined by neutral red absorbance, after (A) 6 h, (B) 24 h, (C) 48 h. Results were calculated as percentage of control (untreated cells). Data is presented as mean ± SEM (n = 9 per group). Data was analysed using one-way ANOVA with post-hoc Dunnet's tests applied for multiple comparisons. * $P<0.05$, $^{\&}$ $P<0.0001$; significantly different from the control value.

The MTT reduction assay was also used to evaluate cell viability in Caco-2 cells after exposure to the Cit-AgNPs and $AgNO_3$, based on the mitochondrial enzymes activity. As previously mentioned in the Experimental section, the reduction of MTT dye to formazan depends on the mitochondrial enzymes activity. Therefore, a decrease in the absorbance (formazan) corresponds to a decrease in the mitochondrial activity, indicative of decreased cell viability.

As shown in **Figure 14 A**, after 6 h of incubation with AgNPs, Caco-2 cells did not exhibit any loss of mitochondrial activity (cell viability) comparing with control cells., However, at the same time-point, treatment with 10, 20 and 40 µg/mL of $AgNO_3$ led to a significant decrease of cell viability. At 24 h (**Figure 14 B**), cells exposed to 10, 20 and 40 µg/mL $AgNO_3$ also showed a significant decreased viability. This phenomenon was also observed after 24 h of treatment with 40 µg/mL Cit-AgNPs. At 48 h of exposure (**Figure**

14 C), the results showed a significant decrease in the cell viability after treatment with 20 and 40 µg/mL AgNPs, and 10, 20 and 40 µg/mL $AgNO_3$.

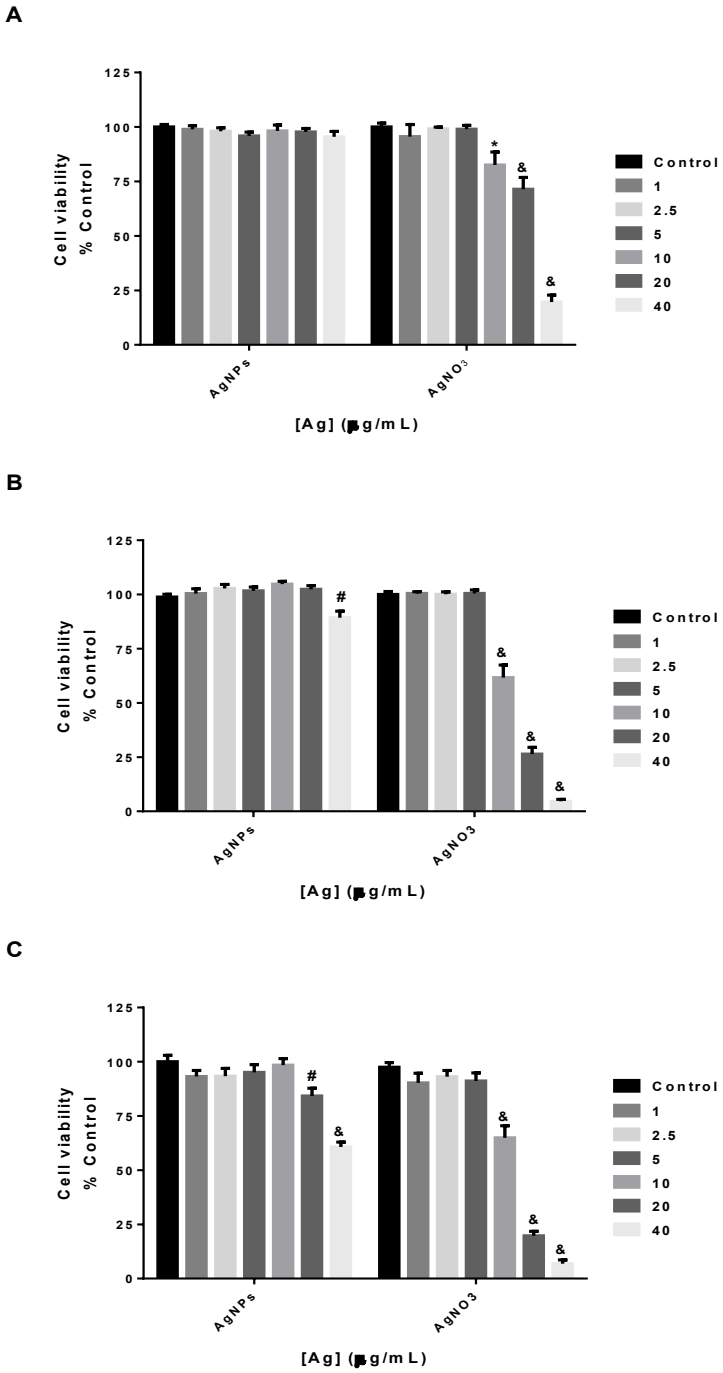
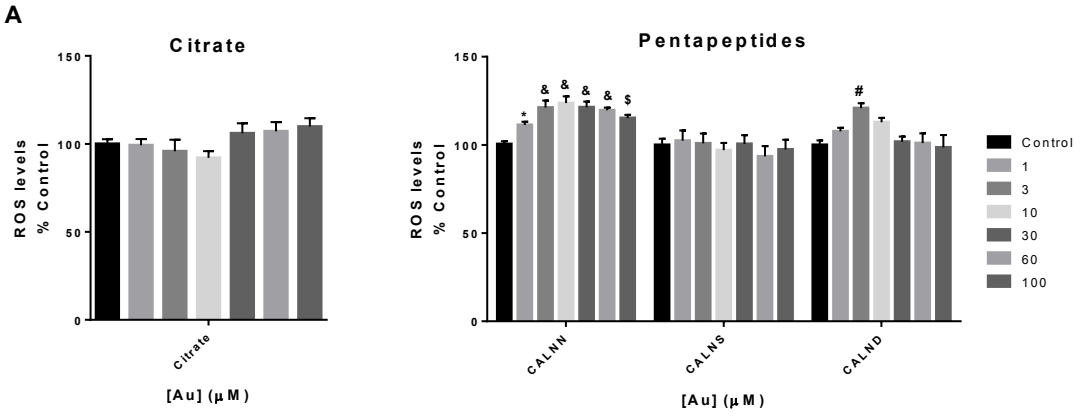


Figure 14 - Effects on the Cit-AgNPs and $AgNO_3$ in activity of mitochondrial enzymes, determined by the MTT assay, after (A) 6 h, (B) 24 h and (C) 48 h. Results were calculated as percentage of control (untreated cells). Data is presented as mean ± SEM (n = 9 per group). Data was analysed using one-way ANOVA with post-hoc Dunnet's tests applied for multiple comparisons. * $P<0.05$, # $P<0.01$, & $P<0.0001$; significantly different from the control value.

ROS production is often associated with exposure to metallic NPs. Therefore, the production of ROS following incubation with the differently coated AuNPs and Cit-AgNPs was evaluated by the DCFH-DA assay.

In **Figure 15 (A-D)** the results from the DCFH-DA assay after the incubations with the tested AuNPs are represented. As shown, CALNN-AuNPs, at all concentrations, induced a significant increase in ROS levels after 6 h of exposure **(Figure 15 A)**. At the same time-point, cells treated with 3 μM CALND-AuNPs also showed a significant increase of ROS levels comparing with control cells After 24 h of exposure **(Figure 15 B)**, cells treated with 3, 10 and 30 μM CALNN-AuNPs maintained the higher ROS levels compared to control. On the other hand, cells incubated with Cit-AuNPs (10 and 30 μM) also showed high ROS levels. At 48 h of exposure, only cells incubated with 30 μM CALND-AuNPs showed an increase of ROS production **(Figure 15 C)**. After 72 h, no significant increase of ROS levels was observed at all concentrations tested for all tested AuNPs **(Figure 15 D)**. Overall, the results suggest that Cit- and pentapeptide-coated AuNPs do not increase ROS levels in Caco-2 cells.

Regarding the levels of ROS production upon treatment with AgNPs and $AgNO_3$, the results are presented in n **Figure 16 (A-D)**. After 6 h (**Figure 16 A**) of cells incubation with 40 μg/mL Cit-AgNPs, a significant decrease in the ROS levels was observed On the other hand, at the same time of incubation, the cells treated with 10, 20 and 40 μg/mL Cit-$AgNO_3$ showed a significant increase in the levels of ROS when compared to the control. At 24 (**Figure 16 B**) and 48 h (**Figure 16 C**), cells incubation with Cit-AgNPs did not exhibit any changes in the ROS levels, whereas cells treated with 10, 20 and 40 μg/mL $AgNO_3$ showed a very noticeable and significant increase in the ROS levels comparing with control cells. These high levels of ROS levels were maintained up to 72 h of exposure (**Figure 16 D**). The incubation with 20 μg/mL Cit-AgNPs also led to a significant increase in the ROS levels. Moreover, is can be observed that ROS levels of $AgNO_3$-treated cells are much higher than AgNPs-treated cells.



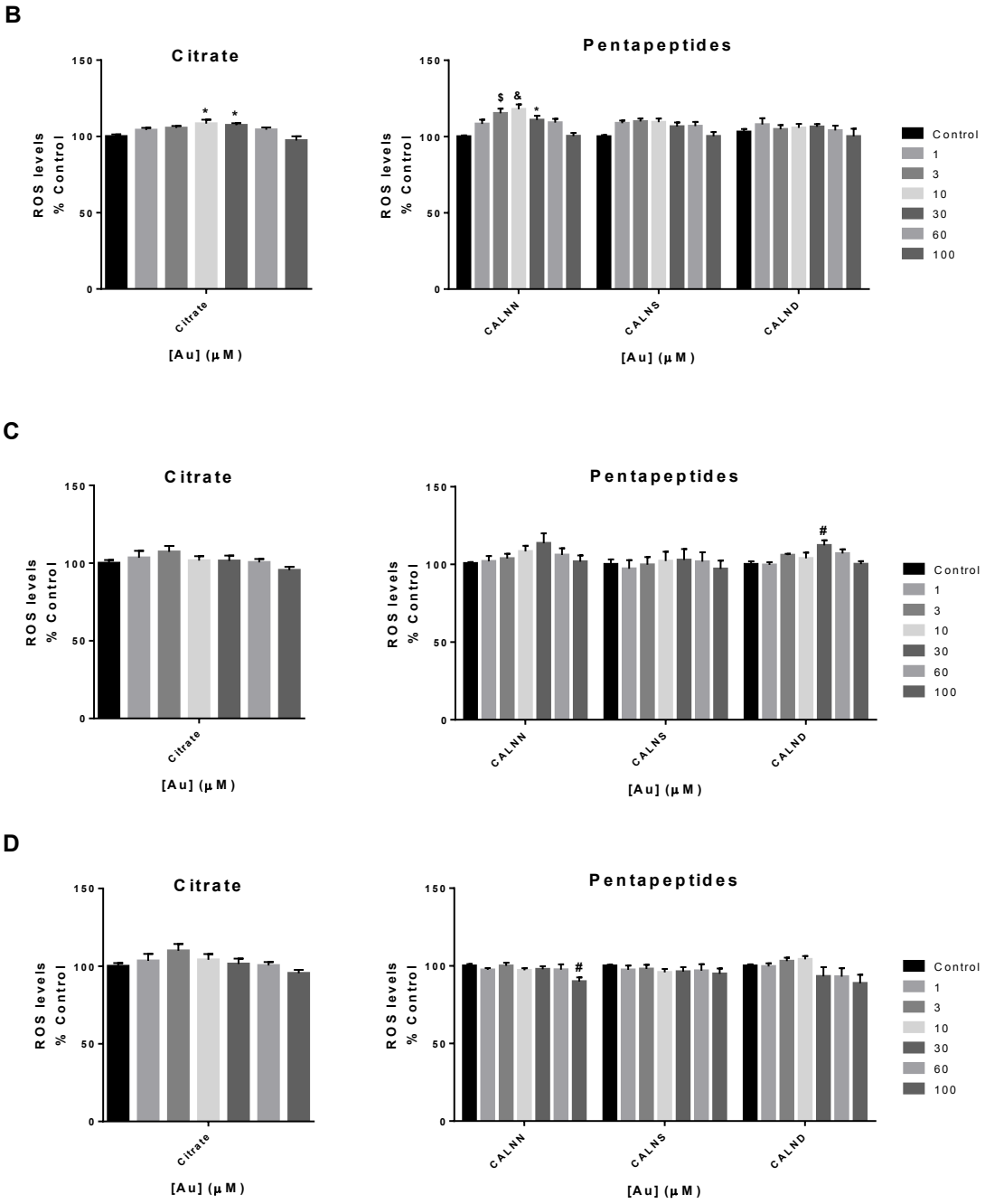
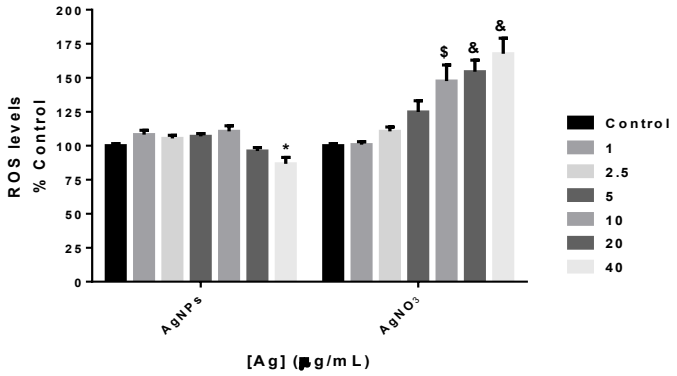
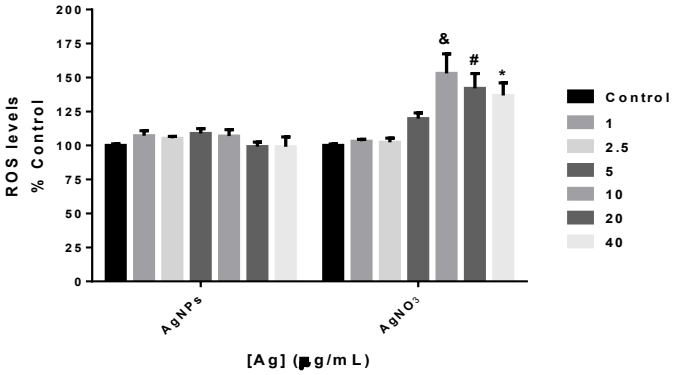


Figure 15 - Effects of Cit-, CALNN-, CALNS-, CALND-AuNPs in the production of reactive oxygen species, determined by the DCFH-DA assay, after (A) 6 hours, (B) 24 hours, (C) 48 hours, (D) 72 hours. Results were calculated as percentage of control (untreated cells). Data is presented as mean ± SEM (n = 12-16). Data was analysed using one-way ANOVA with post-hoc Dunnet's tests applied for multiple comparisons. * P<0.05, # P<0.01, $ P<0.001, & P<0.0001 significantly different from the control value.

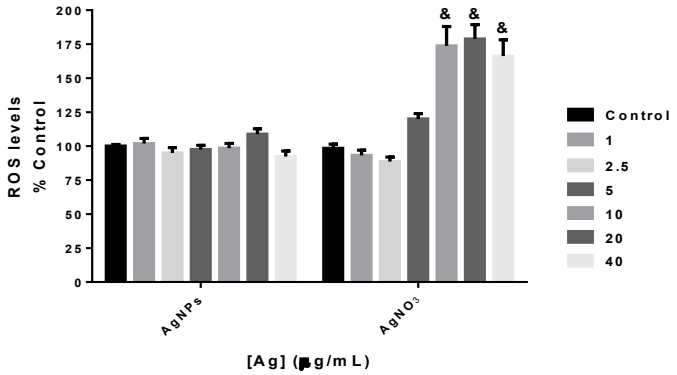
A


ROS levels
% Control
200
175
150
125
100
75
50
25
0
*
$
&
&
&
AgNPs
AgNO3
[Ag] (µg/mL)
Control
1
2.5
5
10
20
40

B


ROS levels
% Control
200
175
150
125
100
75
50
25
0
&
#
*
AgNPs
AgNO3
[Ag] (µg/mL)
Control
1
2.5
5
10
20
40

C


ROS levels
% Control
200
175
150
125
100
75
50
25
0
&
&
&
AgNPs
AgNO3
[Ag] (µg/mL)
Control
1
2.5
5
10
20
40

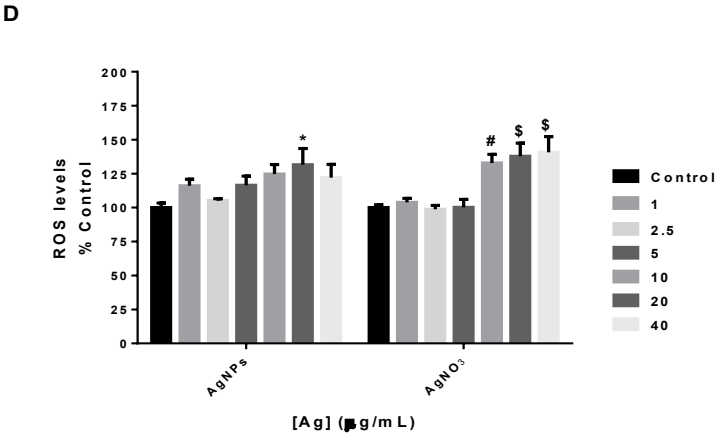


Figure 16 - Effects of Cit-AgNPs and $AgNO_3$ in the production of reactive oxygen species, determined by the DCFH-DA assay, after (A) 6 hours, (B) 24 hours, (C) 48 hours and (D) 72 hours. Results were calculated as percentage of control (untreated cells). Data is presented as mean ± SEM (n = 12 per group). Data was analysed using one-way ANOVA with post-hoc Dunnet's tests applied for multiple comparisons. * $P<0.05$, $^{\#}$ $P<0.01$, $^{\$}$ $P<0.001$, $^{\&}$ $P<0.0001$ significantly different from the control value.

4.2. Morphological analysis of Caco – 2 cells by phase contrast microscopy

Throughout the incubation time, cells were monitored to evaluate the potential effects of the tested NPs on Caco-2 morphology. As shown in **Figure 17**, both Cit- and pentapeptide-coated AuNPs did not induce any significant changes in the cells morphology, at all concentrations tested, comparing with control cells. However, at the highest concentration tested (100 µM), it is possible to visualize the formation of NPs aggregates on top of the cells monolayer (marked by white arrow). This phenomenon occurred in both Cit- and pentapeptide-coated AuNPs-exposed cells, even though, Cit-AuNPs have higher tendency to form agglomerates than pentapeptides-AuNPs. This fact is probably related with the high stability of pentapeptide-coated AuNPs in solution.

On the other hand, as shown in **Figure 18**, treatment with 1 µg/mL Cit-AgNPs did not induce any changes in the cellular morphology. However, presence of Cit-AgNPs aggregates and loss of monolayer integrity was observed in cells exposed to the highest tested concentrations (10 and 40 µg/mL). Regarding the cells incubated with $AgNO_3$, the same results were observed, i.e. the lowest concentration (1 µg/mL) did not induce any changes in Caco-2 morphology, whereas 10 and 40 µg/mL led to the loss of monolayer integrity (marked by orange arrow) and the presence of NPs aggregates was also visible (marked by white arrow).

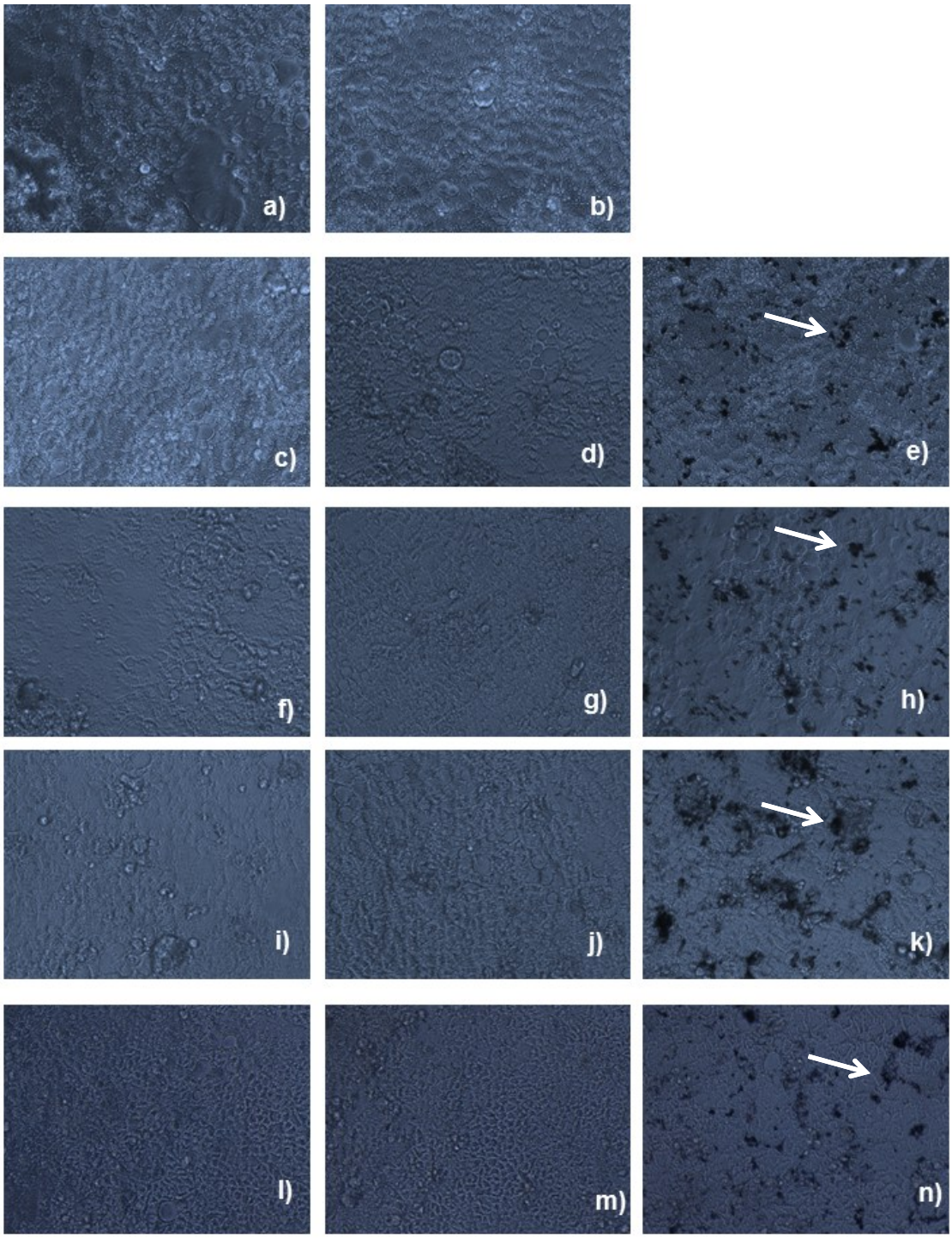


Figure 17 - Representative phase contrast microscopy images of Caco-2 cells at 72 h after incubation with: a) control, b) Vehicle (H2O), c) 1 μM of Cit - AuNPs, d) 10 μM of Cit - AuNPs, e) 100 μM of Cit - AuNPs, f) 1 μM of CALNN - AuNPs, g) 10 μM of CALNN - AuNPs, h) 100 μM of CALNN - AuNPs, i) 1 μM of CALNS - AuNPs, j) 10 μM of CALNS - AuNPs, k) 100 μM of CALNS - AuNPs, l) 1 μM of CALND – AuNPs, m) 10 μM of CALND – AuNPs and n) 100 μM of CALND – AuNPs (100 X magnification).

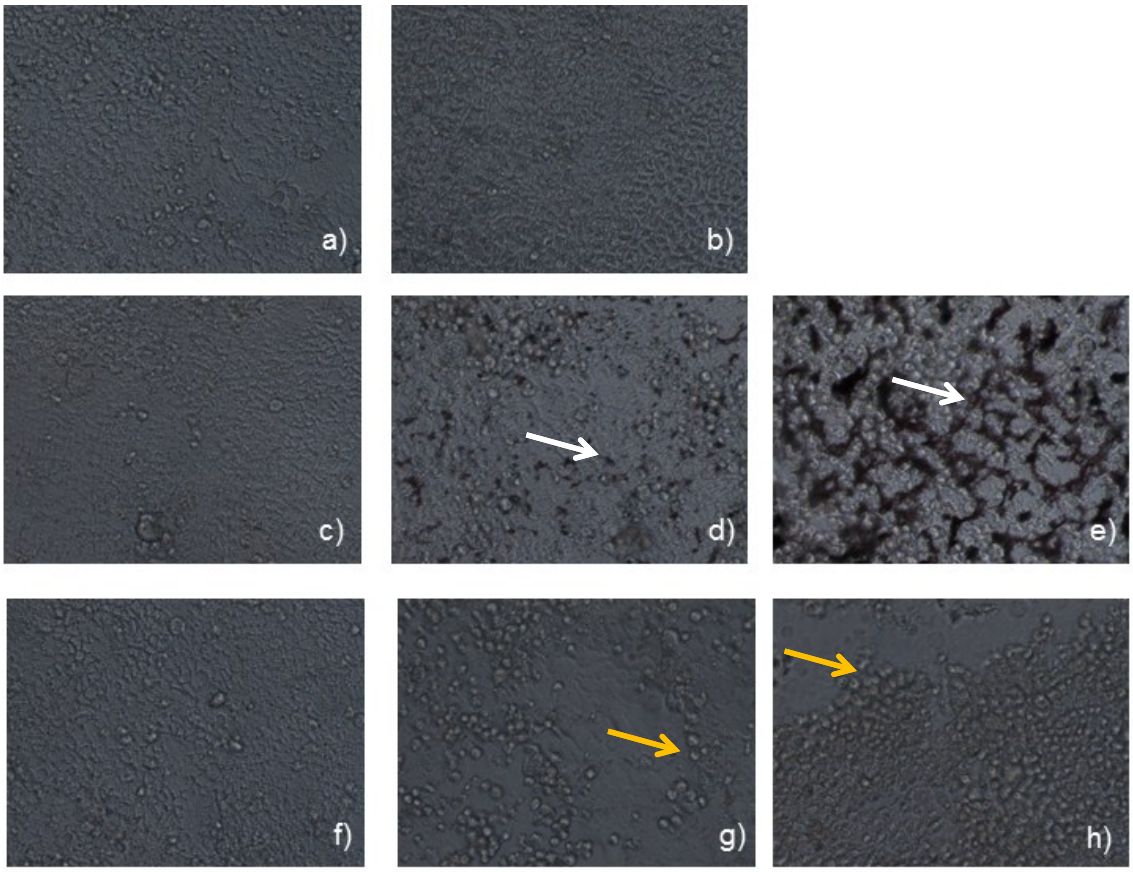


Figure 18 - Representative phase contrast microscopy images of Caco-2 cells at 72 h after incubation with: a) control, b) vehicle (citrate), c) 1 µM of Cit - AgNPs, d) 10 µM of Cit - AgNPs, e) 40 µM Cit - AgNPs, f) 1 µM of $AgNO_3$, g) 10 µM of $AgNO_3$, h) 40 µM of $AgNO_3$ (100x magnification).

4.3. Results of flow cytometry analysis

4.3.1. AuNPs and AgNPs uptake in Caco-2 cells

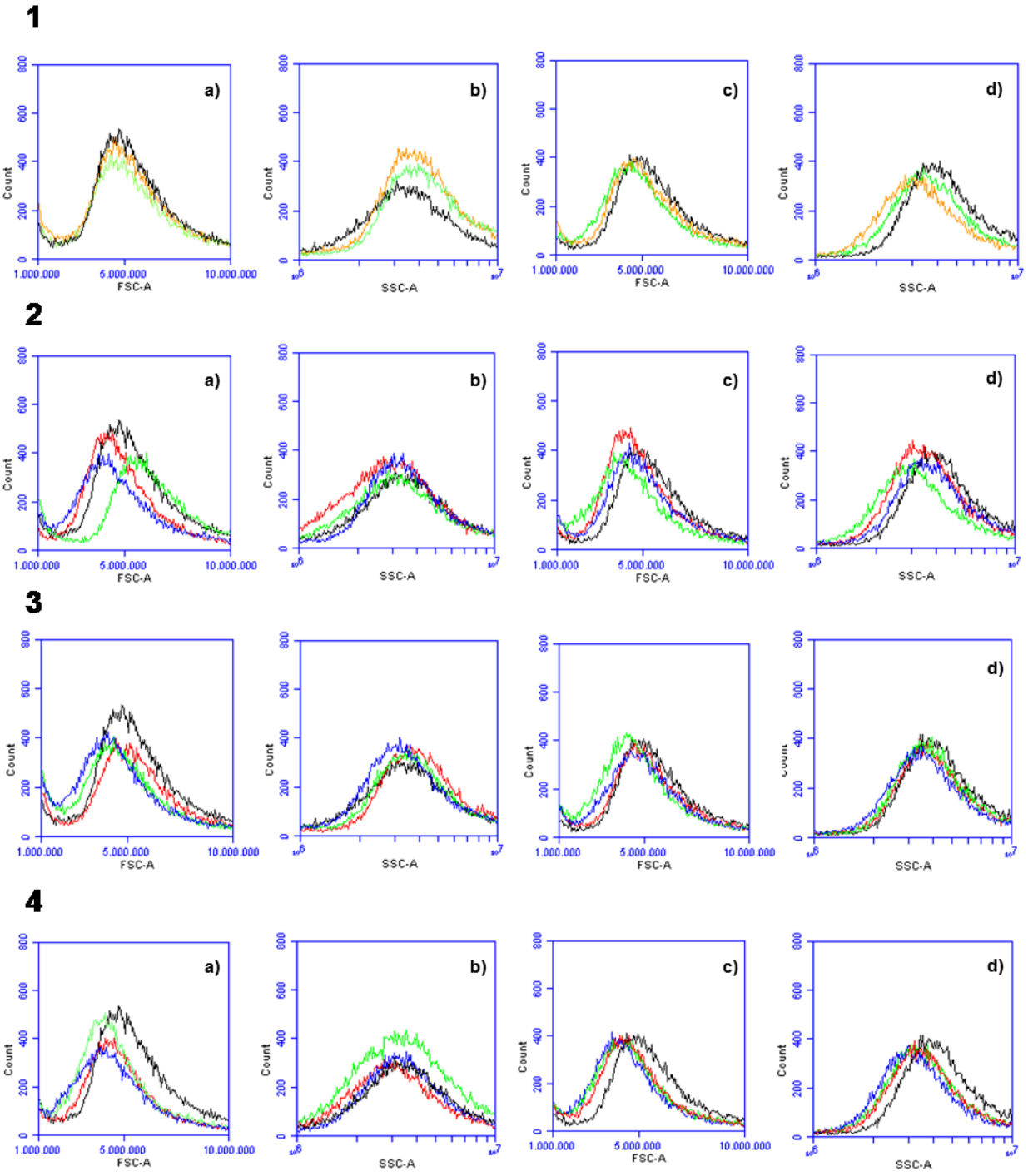
The uptake of AuNPs and AgNPs was analysed by flow cytometry by comparing differences in size (FSC) and complexity (SSC) between control and NPs-exposed cells either in synchronized or non-synchronized cultures. The results are presented in **Table 10 and 11.**

Table 10 - Gold nanoparticles (AuNPs) uptake determined by flow cytometry analysis of cell size (FSC) and complexity (SSC) in synchronized and non-synchronized cultures, after 24h of exposure.

NP	Concentration (μM)	Synchronized culture		Non-Synchronized culture	
		FSC (Mean ± SEM) (x 10^6)	SSC (Mean ± SEM) (x 10^6)	FSC (Mean ± SEM) (x 10^6)	SSC (Mean ± SEM) (x 10^6)
Control		3.53 ± 0.11	2.63 ± 0.08	3.47 ± 0.03	2.53 ± 0.02
Vehicles (H_2O)	**1%**	3.41 ± 0.18	2.57 ± 0.07	3.20 ± 0.10	2.38 ± 0.03
Cit-AuNPs	**1**	3.22 ± 0.06	2.48 ± 0.02	3.99 ± 0.21	2.48 ± 0.07
	3	3.14 ± 0.23	2.40 ± 0.13	3.41 ± 0.08	2.51 ± 0.04
	10	3.37 ± 0.15	2.59 ± 0.10	3.31 ± 0.07	2.49 ± 0.02
CALNN-AuNPs	**1**	3.03 ± 0.20	2.34 ± 0.07	3.32 ± 0.26	2.47 ± 0.13
	3	3.26 ± 0.09	2.40 ± 0.05	3.24 ± 0.18	2.45 ± 0.07
	10	3.09 ± 0.12	2.39 ± 0.06	3.02 ± 0.22	2.40 ± 0.08
CALNS-AuNPs	**1**	3.30 ± 0.01	2.37 ± 0.02	3.29 ± 0.10	2.47 ± 0.04
	3	3.09 ± 0.08	2.30 ± 0.04	2.98 ± 0.17	2.28 ± 0.08
	10	3.52 ± 0.01	2.32 ± 0.08	3.35 ± 0.12	2.51 ± 0.09
CALND-AuNPs	**1**	3.27 ± 0.31	2.48 ± 0.18	3.01 ± 0.16	2.37 ± 0.05
	3	3.51 ± 0.12	2.59 ± 0.07	3.10 ± 0.14	2.36 ± 0.05
	10	2.98 ± 0.16	2.37 ± 0.11	3.20 ± 0.14	2.45 ± 0.10

Note: Data represents the mean ± standard error of the mean (SEM) of three independent experiments (n = 2 per group). Statistical analysis was performed by using non-parametric Kruskal-Wallis test followed by the post-hoc Dunn's test applied for multiple comparisons. Significance was accepted at a P-value ≤ 0.05. No differences in size (FSC) and the complexity (SSC) were found in AuNPs-exposed cells comparing with controls (untreated cells).

No significant differences in the size (FSC) and complexity (SSC) between AuNPs-treated cells and control cells were observed. The same findings were obtained for AgNP-exposed cells. As expected, vehicle-treated cells did not show significant differences in size and complexity compared to control cells. Moreover, no difference was found in the SSC and FSC values between synchronized and non-synchronized cultures. In **Figures 19 and 20,** the FSC and SSC histograms of control and NPs-exposed Caco-2 cells stained with PI are represented.



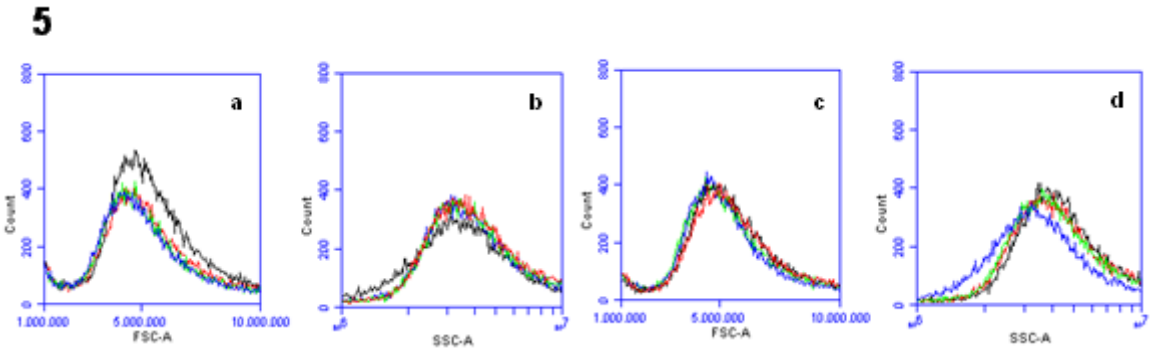


Figure 19 - Caco-2 cells histograms of size (FSC) and complexity (SSC) of synchronized (a and b) and non-synchronized (c and d) cultures obtained after exposure to differently coated AuNPs. 1) vehicles (H_2O and citrate), 2) Cit-AuNPs, 3) CALNN-AuNPs, 4) CALNS-AuNPs, 5) CALND-AuNPs, at the concentrations of 1 μM (red line), 3 μM (green line) and 10 μM (blue line) compared to control cells (black line).

Table 11 - Silver nanoparticles (AgNPs) uptake determined by flow cytometry analysis of cell size (FSC) and complexity (SSC) in synchronized and non-synchronized cultures, after 24h of exposure.

NP	Concentration (μg/mL)	Synchronized culture		Non-Synchronized culture	
		FSC (Mean ± SEM) ($x 10^6$)	SSC (Mean ± SEM) ($x 10^6$)	FSC (Mean ± SEM) ($x 10^6$)	SSC (Mean ± SEM) ($x 10^6$)
Control		3.53 ± 0.11	2.63 ± 0.08	3.47 ± 0.03	2.53 ± 0.02
Vehicle (Citrate)	**5**	3.30 ± 0.12	2.42 ± 0.08	3.45 ± 0.24	2.49 ± 0.14
Cit-AgNPs	**1**	3.15 ± 0.25	2.35 ± 0.08	3.22 ± 0.31	2.26 ± 0.12
	2.5	3.03 ± 0.14	2.40 ± 0.07	3.53 ± 0.06	2.58 ± 0.11
	5	3.15 ± 0.09	2.42 ± 0.08	2.98 ± 0.19	2.38 ± 0.06
$AgNO_3$	**1**	3.22 ± 0.01	2.46 ± 0.09	2.97 ± 0.13	2.26 ± 0.04
	2.5	3.17 ± 0.16	2.39 ± 0.03	3.28 ± 0.16	2.47 ± 0.14
	5	3.32 ± 0.13	2.47 ± 0.06	3.21 ± 0.14	2.37 ± 0.07

Note: Data represents the mean ± standard error of the mean (SEM) of three independent experiments (n = 2 per group). Statistical analysis was performed by using non-parametric Kruskal-Wallis test followed by the post-hoc Dunn's test applied for multiple comparisons. Significance was accepted at a P-value ≤ 0.05. No differences in size (FSC) and the complexity (SSC) were found in AuNPs-exposed cells comparing with controls (untreated cells).

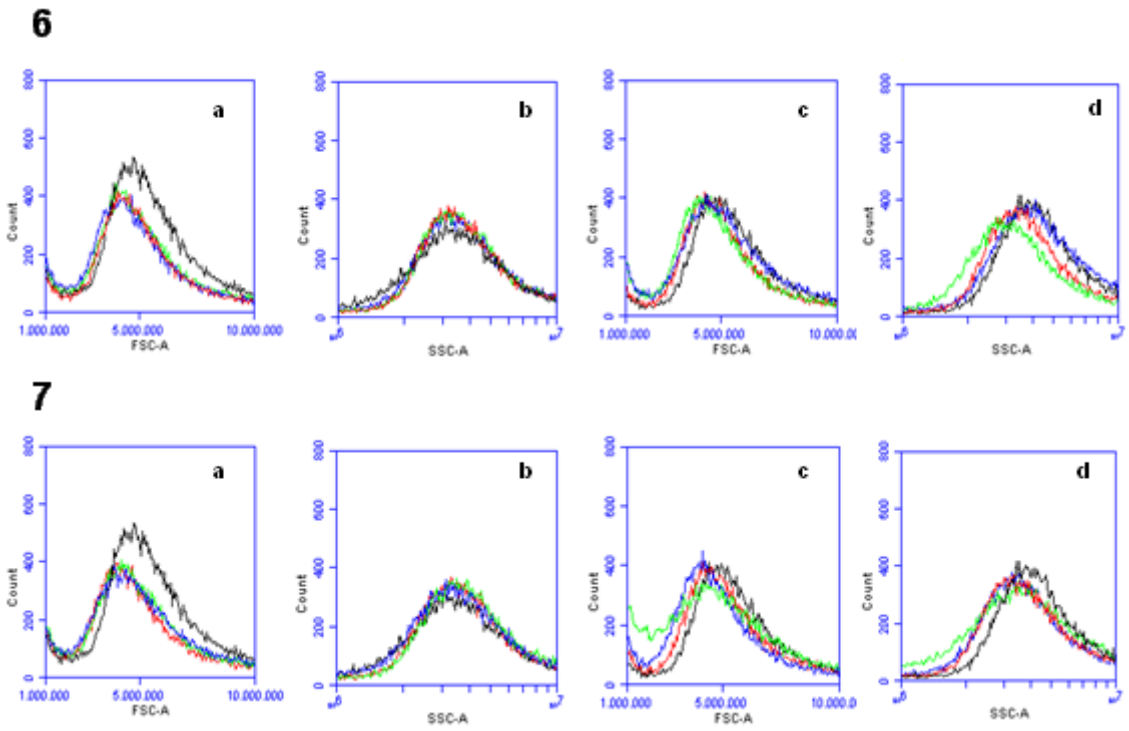


Figure 20 - Representative histograms of AgNPs uptake in Caco-2 cells by flow cytometry analysis of cell size (FSC) and complexity (SSC) of synchronized (a and b) and non-synchronized culture (c and d), after exposure of 6) Cit-AgNPs and 7) $AgNO_3$at the concentrations of 1 µg/mL (red line), 2.5µg/mL (green line) and 5µg/mL (blue line) comparing to control cells (black line).

4.3.2. Cell cycle analysis

Cell cycle distribution was evaluated by flow cytometry in DNA-stained Caco-2 cells incubated for 24 h with non-toxic concentrations of AuNPs and AgNPs. In the **Tables 12 - 15** the flow cytometry cell cycle results are presented. The sub-G1 phase is not particularly evident in the histograms **(Figures 21 and 22)** but this population was detected in all the analysed samples. As shown in **Figures 21 and 22**, synchronized cultures produced a ”cleaner” histogram than non-synchronized cultures, where the different phases of the cell cycle could be visualized more clearly. In the representative histograms of control cells in synchronized and non-synchronized cultures, the cells distribution differs slightly. In synchronized culture the G1 and G2/M phase peak are prominent whereas the gap (S phase) is almost imperceptible. In non-synchronized cells this gap is more evident, while G2/M peak is unnoticeable. No differences were found in cell cycle distribution of AuNPs- and AgNPs-exposed cells comparing to control cells, either in synchronized and non-synchronized cultures. *(In this section the AuNPs histograms represented pertain only to the highest concentration tested, while for AgNPs*

histograms all the concentrations were tested. The respective histograms of lower concentrations of AuNPs are presented in Supplement 1).

Table 12 - Effect of 24h-exposure to AuNPs on cell cycle distribution (%) in synchronized Caco-2 cultures.

	NPs	Concentration (μM)	Sub-G1 (Mean ± SEM)	G1 (Mean ± SEM)	S (Mean ± SEM)	G2/M (Mean ± SEM)
Synchronized Cultures	Control		7.60 ± 1.01	38.37 ± 1.43	29.65 ± 2.13	24.00 ± 3.44
	H_2O	1%	9.31 ± 3.10	37.84 ± 1.71	29.50 ± 3.10	22.13 ± 1.75
	Cit-AuNPs	1	8.12 ± 0.76	40.65 ± 1.81	31.62 ± 3.06	19.82 ± 1.41
		3	8.45 ± 1.54	43.00 ± 2.66	25.63 ± 4.10	21.45 ± 1.49
		10	8.53 ± 1.06	38.15 ± 0.39	31.57 ± 2.19	20.07 ± 1.82
	CALNN-AuNPs	1	7.68 ± 0.64	39.32 ± 2.73	28.18 ± 2.46	23.28 ± 1.74
		3	7.67 ± 0.33	35.80 ± 2.95	34.32 ± 1.89	20.41 ± 1.70
		10	7.34 ± 1.04	39.43 ± 1.31	29.13 ± 2.01	23.60 ± 2.54
	CALNS-AuNPs	1	7.63 ± 1.73	39.33 ± 5.07	29.20 ± 4.53	19.62 ± 1.95
		3	7.66 ± 0.66	37.57 ± 2.49	32.63 ± 1.81	20.86 ± 0.58
		10	7.49 ± 0.87	36.33 ± 3.83	31.72 ± 2.63	19.84 ± 1.26
	CALND-AuNPs	1	6.67 ± 0.62	38.12 ± 1.87	30.30 ± 1.45	23.34 ± 2.00
		3	7.31 ± 1.40	34.55 ± 3.38	32.78 ± 2.60	23.47 ± 2.35
		10	7.81 ± 0.94	41.38 ± 3.04	27.48 ± 2.68	21.59 ± 1.79

Note: Data represents the mean ± standard error of the mean (SEM) of three independent experiments (n = 2 per group). Statistical analysis was performed by using non-parametric Kruskal-Wallis test followed by the post-hoc Dunn's test applied for multiple comparisons. Significance was accepted at a P-value ≤ 0.05. No differences were found in AuNPs-exposed cells comparing with controls (untreated cells).

Table 13 - Effect of 24h-exposure to AuNPs on cell cycle distribution (%) in non-synchronized Caco-2 cultures.

	NPs	Concentration (μM)	Sub-G1 (Mean ± SEM)	G1 (Mean ± SEM)	S (Mean ± SEM)	G2/M (Mean ± SEM)
Non-Synchronized cultures	Control		7.94 ± 1.70	36.78 ± 2.70	27.28 ± 1.48	26.40 ± 2.16
	H_2O	1%	10.07 ± 3.60	41.14 ± 2.57	25.90 ± 3.19	21.56 ± 2.45
	Cit-AuNPs	1	7.29 ± 1.09	39.88 ± 3.67	21.10 ± 5.20	30.27 ± 4.08
		3	7.23 ± 0.82	36.92 ± 2.06	29.02 ± 2.41	25.05 ± 2.38
		10	9.54 ± 1.16	39.02 ± 1.96	26.68 ± 3.18	22.97 ± 2.06
	CALNN-	1	5.21 ± 0.58	39.00 ± 1.74	25.44 ± 1.04	27.55 ± 2.02

	AuNPs	**3**	6.74 ± 0.92	35.97 ± 1.95	30.33 ± 2.02	25.12 ± 1.54
		10	7.60 ± 1.17	34.92 ± 2.32	29.25 ± 1.42	26.16 ± 1.75
	CALNS-AuNPs	**1**	6.31 ± 0.69	42.92 ± 1.64	23.48 ± 2.56	25.62 ± 2.20
		3	9.78 ± 2.63	36.92 ± 4.20	29.03 ± 4.05	22.64 ± 2.95
		10	7.12 ± 1.39	39.95 ± 2.10	27.87 ± 1.77	23.33 ± 1.44
	CALND-AuNPs	**1**	7.33 ± 1.01	43.42 ± 2.70	22.60 ± 3.04	24.97 ± 1.39
		3	7.61 ± 1.27	38.50 ± 1.78	26.57 ± 1.34	25.42 ± 2.19
		10	6.20 ± 0.97	41.60 ± 2.84	23.40 ± 2.39	26.96 ± 2.76

Note: Data represents the mean ± standard error of the mean (SEM) of three independent experiments (n = 2 per group). Statistical analysis was performed by using non-parametric Kruskal-Wallis test followed by the post-hoc Dunn's test applied for multiple comparisons. Significance was accepted at a P-value ≤ 0.05. No were found in AuNPs-exposed cells comparing with controls (untreated cells).

Table 14 - Effect of 24h-exposure to AgNPs and $AgNO_3$ on cell cycle distribution (%) in synchronized Caco-2 cultures.

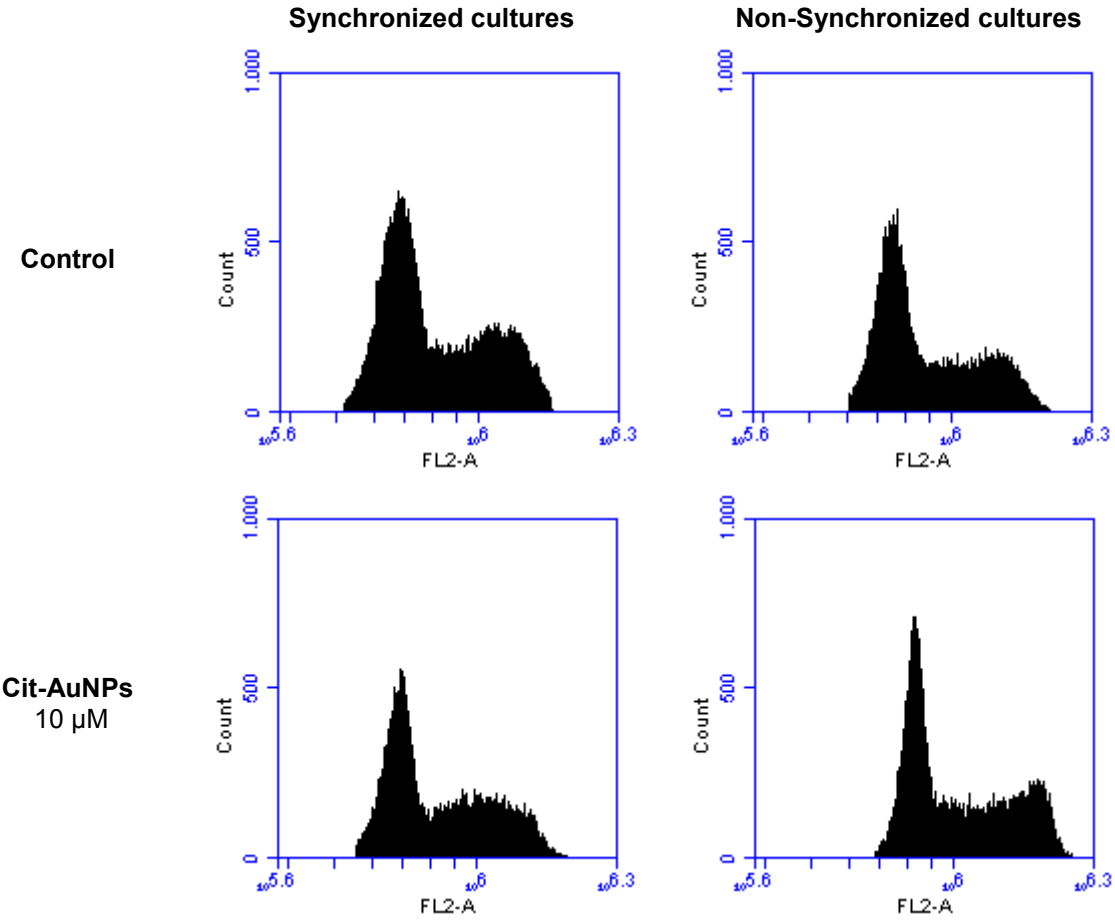
	NPs	**Concentration (µg/mL)**	**Sub-G1 (Mean ± SEM)**	**G1 (Mean ± SEM)**	**S (Mean ± SEM)**	**G2/M (Mean ± SEM)**
Synchronized Cultures	**Control**		7.60 ± 1.01	38.37 ± 1.43	29.65 ± 2.13	24.00 ± 3.44
	Citrate	**5**	9.07 ± 1.74	38.60 ± 2.18	27.32 ± 1.62	23.41 ± 2.21
	Cit-AgNPs	**1**	8.97 ± 0.46	38.12 ± 1.92	31.65 ± 1.16	19.40 ± 1.84
		2.5	8.01 ± 1.18	34.92 ± 1.86	31.46 ± 2.12	21.67 ± 2.45
		5	10.39 ± 2.53	33.55 ± 2.08	34.03 ± 3.00	20.70 ± 3.45
	$AgNO_3$	**1**	6.67 ± 1.27	38.62 ± 1.27	25.82 ± 2.71	27.22 ± 3.31
		2.5	7.45 ± 1.11	38.13 ± 2.27	25.85 ± 2.52	26.88 ± 1.87
		5	7.90 ± 1.10	33.52 ± 1.79	30.50 ± 2.84	26.47 ± 2.53

Note: Data represents the mean ± standard error of the mean (SEM) of three independent experiments (n = 2 per group). Statistical analysis was performed by using non-parametric Kruskal-Wallis test followed by the post-hoc Dunn's test applied for multiple comparisons. Significance was accepted at a P-value ≤ 0.05. No differences were found in AgNPs-exposed cells comparing with controls (untreated cells).

Table 15 - Effect of 24h-exposure to AgNPs and $AgNO_3$ on cell cycle distribution (%) in non-synchronized Caco-2 cultures.

	NPs	Concentration (µg/mL)	Sub-G1 (Mean ± SEM)	G1 (Mean ± SEM)	S (Mean ± SEM)	G2/M (Mean ± SEM)
Non-Synchronized Cultures	Control		7.94 ± 1.70	36.78 ± 2.70	27.28 ± 1.48	26.40 ± 2.16
	Citrate	5	6.77 ± 0.90	41.53 ± 2.64	22.87 ± 4.24	24.35 ± 1.96
	Cit-AgNPs	1	8.59 ± 1.95	36.82 ± 4.19	32.03 ± 3.11	21.40 ± 0.95
		2.5	9.08 ± 1.25	35.05 ± 1.57	33.17 ± 2.03	21.39 ± 1.07
		5	8.77 ± 1.67	37.08 ± 1.52	26.37 ± 2.96	25.92 ± 3.72
	$AgNO_3$	1	6.78 ± 0.72	38.57 ± 2.70	29.17 ± 1.25	24.09 ±2.81
		2.5	6.59 ±0.58	37.92 ± 3.55	28.58 ± 2.25	25.47 ± 2.43
		5	8.17 ± 1.19	33.25 ± 2.17	28.73 ± 3.44	28.37 ± 5.07

Note: Data represents the mean ± standard error of the mean (SEM) of three independent experiments (n = 2 per group). Statistical analysis was performed by using non-parametric Kruskal-Wallis test followed by the post-hoc Dunn's test applied for multiple comparisons. Significance was accepted at a P-value ≤ 0.05. No differences were found in AgNPs-exposed cells comparing with controls (untreated cells).



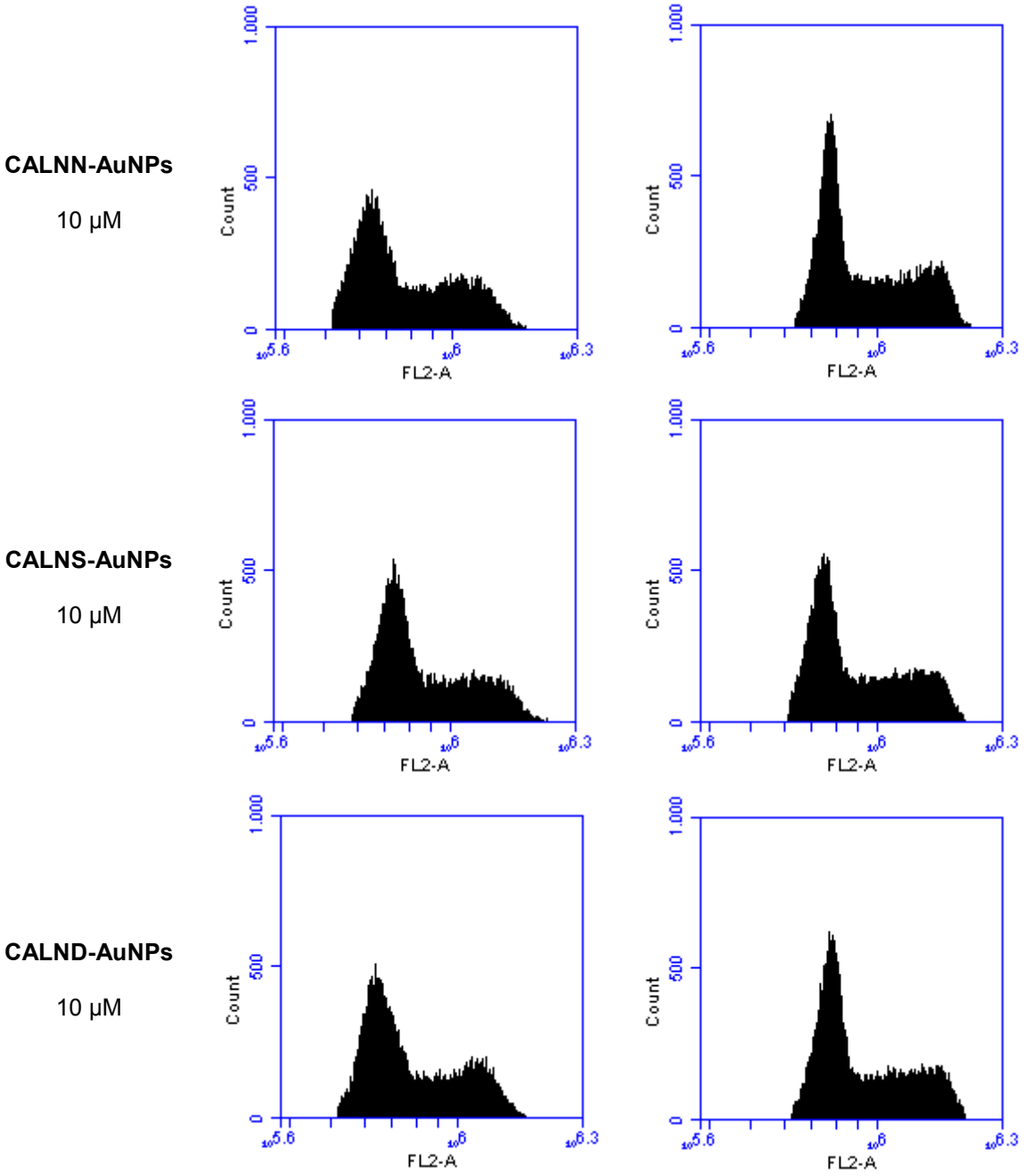
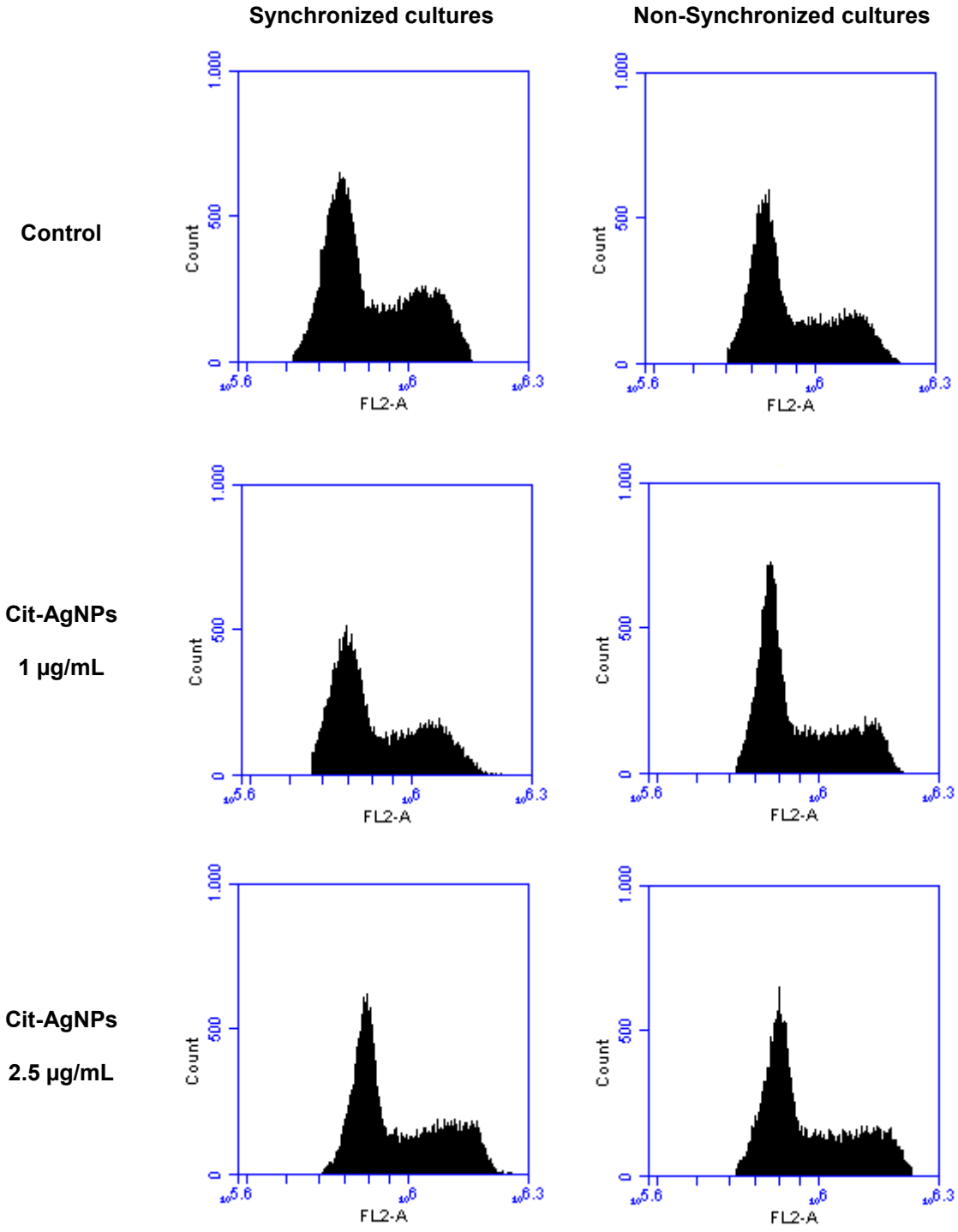
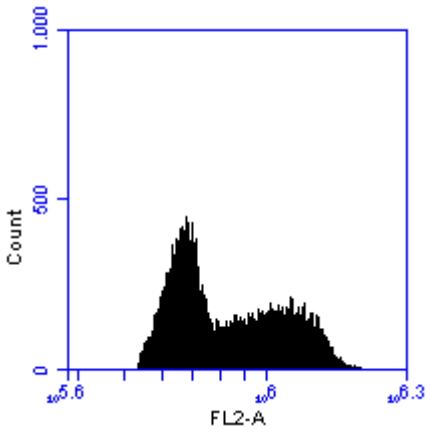


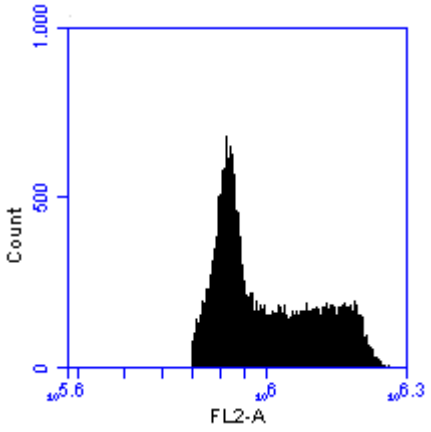
Figure 21 - Representative PI fluorescence (DNA content) histograms of the Caco-2 cells (synchronized and non-synchronized cultures) after 24 h of exposure to AuNPs (10 μM).


Synchronized cultures
Non-Synchronized cultures
Control
Cit-AgNPs
1 µg/mL
Cit-AgNPs
2.5 µg/mL
Count
FL2-A
1.000
500
0

Cit-AgNPs

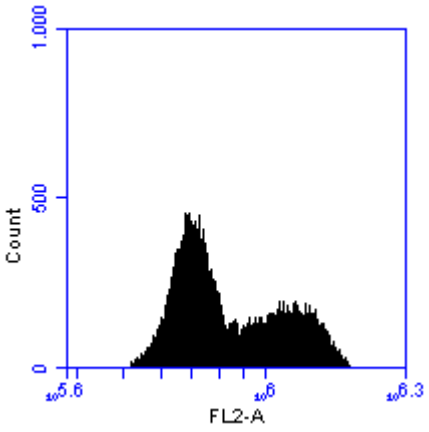
5 µg/mL

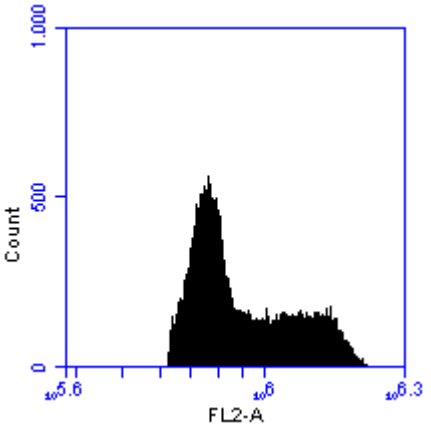




$AgNO_3$

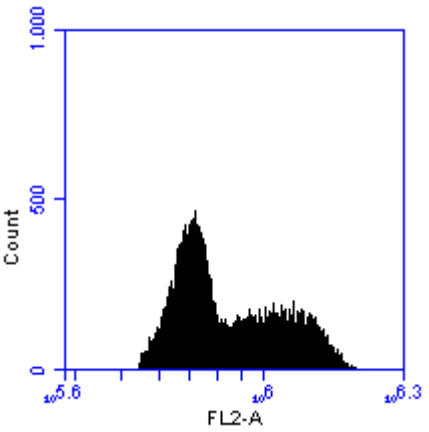
1 µg/mL

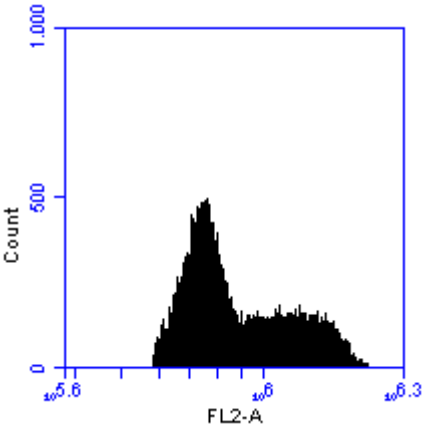




$AgNO_3$

2.5 µg/mL





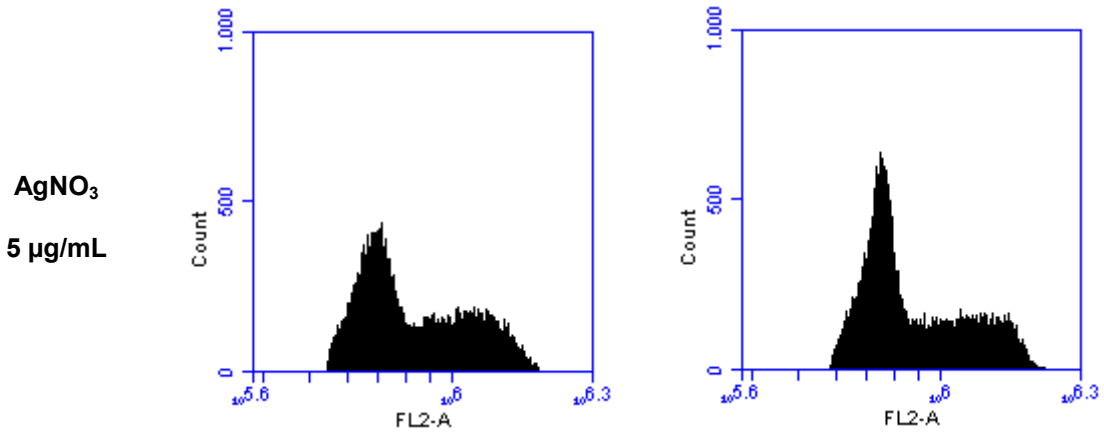


Figure 22 - Representative PI fluorescence (DNA content) histograms of the Caco-2 cells (synchronized and non-synchronized cultures) after 24 h of exposure to 1, 2.5 and 5 µg/mL Cit-AgNPs and $AgNO_3$ comparing to control cells (synchronized and non-synchronized cultures).

Chapter 5

Discussion

Discussion

In the present work, it was examined the *in vitro* cytotoxicity and cell cycle effects of AuNPs, capped with citrate (Cit-AuNPs) or a pentapeptide (CALNN, CALNS or CALND), and citrate-AgNPs. All these metallic NPs have potential application in food and feed.

This study was performed in Caco-2 cells, a well-established model of human intestinal epithelial cells. To investigate the potential AuNPs cytotoxic effects on Caco-2 cells, esterase activity, plasma and lysosomal membrane integrity were assessed.

Overall, the cytotoxicity data demonstrated that AuNPs, independently of their coating, did not cause significant toxicity in Caco-2 cells. A small significant decrease of lysosomal membrane integrity was detected, however did not conduct to a decrease in cell viability.

The biocompatibility of AuNPs is controversial. In previous studies, AuNPs have proven to be biocompatible and non-cytotoxic (Connor et al., 2005, Patra et al., 2007, Fraga et al., 2013). However, increasing evidence supports that the surface coating could influence AuNPs toxicological potential (Connor et al., 2005). Different sensitivity of the cell models used for cytotoxicity assessment of the AuNPs may also account for the discrepancy in the results. Our study supports the view that AuNPs are non-cytotoxic. The toxicity of Cit-AgNPs was evaluated in parallel with the toxicity of $AgNO_3$, a source of bulk Ag. The cytotoxicity was assessed by the NR uptake and MTT reduction assays. In both assays, a concentration-dependent decrease in cell viability was observed following incubation with either Cit-AgNPs or $AgNO_3$.

Cells treated with $AgNO_3$ showed more marked cell viability decreases than AgNPs-treated cells.

Unlike the AuNPs, AgNPs are often associated with cytotoxicity. Many studies have reported that AgNPs can induce significant toxicity (Arora et al., 2009, AshaRani et al., 2009, Beer et al., 2012).

Theodoro et al. found that AgNPs compromised the mitochondrial activity and thus interrupted the energy metabolism in isolated rat liver mitochondria cells (Teodoro et al., 2011). Since NR uptake into the lysosomes is energy-mediated, and in this study, the same reduction appears in both NR and MTT assay after treatment with AgNPs and Ag^+ ions, it is possible that the reduction of NR uptake is a consequence of the loss of mitochondrial activity.

Foldbjerg et al. also found that bulk Ag reduced viability (mitochondrial activity) of monocytes in a higher degree than AgNPs (Foldbjerg et al., 2009).

Beer et al. also demonstrated that concentrations higher than 10 µg/mL, significantly decrease viability of rat brain endothelial (RBE-4) cells, as assessed by the NR uptake assay, following 24 h of exposure to Cit-AgNPs. These authors also evaluated the contribution of Ag^+ ions present in the AgNPs suspensions for the toxicity of the AgNPs as these NPs easily dissolve. They demonstrated that toxicity was induced by the particles itself and not by the ions released in solution (Beer et al., 2012). However, contradicting data has been presented in other studies that show that Ag^+ ions are the ones responsible for the AgNPs-induced toxicity (Miura and Shinohara, 2009, Li et al., 2010).

In the present study, dissolution of the tested AgNPs is unlikely to occur due to the citrate capping. In addition, the tested Cit-AgNPs have "Biopure" grade, which means the free of contaminants in solution.

Regarding the of the Cit-AgNPs study, to compare the toxicity of AgNPs to Ag^+ ions it was used $AgNO_3$ as an Ag^+ ion source. The use of both nanoparticle and ion aimed to compare our results with those of the literature.

The toxicity mechanisms of metal NPs can be associated with ROS production. In the present study, no significant differences in the ROS levels of AuNPs-exposed cells were detected comparing with control cells. However, other study contradicts this result, in which AuNPs induced high levels of ROS after 2 h of exposure in rainbow trout hepatocytes (Farkas et al., 2010). Chompoosor et al. also found high levels of ROS in HeLa cells after 24 h of exposure with cationic AuNPs (Chompoosor et al., 2010)

On the other hand, significant changes in ROS levels were observed after 72 h of exposure to Cit-AgNPs and to the bulk Ag immediately after 6 h of exposure. These results are concomitant with the ones from previous studies, in which Ag, both bulk and nanoparticulate, induced oxidative stress (AshaRani et al., 2009, Piao et al., 2011).

The phase contrast microscopy observations supported the cytotoxicity data. Both Au- and Cit-AgNPs did not induce the loss of the monolayer integrity in the early times of exposure, however, the presence of NP agglomerates were observed on the top of the cells incubated with the highest concentrations. After 72 h of exposure, the highest tested concentration of AgNPs and $AgNO_3$ (40 µg/mL) caused loss of the monolayer integrity.

The study of the cytotoxicity of AuNPs and AgNPs was also based on the evaluation of the impact of these NPs in the cellular morphology. For this it was used the phase contrast microscopy after 6, 24, 48 and 72 h of exposure. It can be noticed that both Au- and AgNPs did not induce the loss of the monolayer integrity in the early times of exposure, however, the presence of NP agglomerates were observed on the cells incubated with the highest concentration. At 72 h of exposure, highest tested

concentration of AgNPs and $AgNO_3$ caused the loss of the monolayer integrity. This observation is consistent with a previous study, in Caco-2 cells after 24 h of exposure with peptide (L-cysteine L-lysine L-lysine) coated AgNPs. In the study, AgNPs led to the loss of adherence capacity of the cells and formed spherical forms (Bohmert et al., 2012).

Overall, AgNPs toxicity mechanisms can be associated with ROS production, reduction of mitochondrial activity and loss of lysosomal integrity which is responsible for the degradation of xenobiotics once inside the cell. However more tests need to be performed for a better interpretation of these results and the mechanisms of toxicity of these NPs.

The cellular uptake of AuNPs and AgNPs, and the subsequent effects of the internalized NPs on cell cycle progression of Caco-2 cells were analyzed by flow cytometry. Exposure to Cit-, pentapeptide-AuNPs and Cit-AgNPs did not induce any significant changes in the size and complexity of Caco-2 cells given by FSC and SSC values, respectively.

Analysis of the uptake of NPs by flow cytometry has been previously performed. Paino et al observed an increase in the complexity of HepG2 cells following incubation with poly(amidoamine) (PAMAM)-AuNPs (Paino et al., 2012).

In our study, no alteration in the complexity and size of Caco-2 cell exposed to the tested NPs was detected. This might be explained by the low NPs concentrations tested. In fact, non-cytotoxic concentrations were selected, since the same samples were submitted to cell cycle analysis.

One of the reasons underlying this discrepancy of results may be that our concentrations were lower than the concentrations used in the Paino et al. study, and for these low concentrations the flow cytometry analysis may not be capable of detecting small changes in size and complexity.

Moreover, no differences in size and complexity were observed between non-synchronized and synchronized cultures. This might be due to the fact that synchronized cultures are incubated with the NPs in complete DMEM for 24 h. This 24h-period seems to be sufficient to promote cell division and attenuate differences between cultures.

The impact of AuNPs in the cell cycle progression has been previously addressed. In this context, Roa et al. evaluated the effect of Glu-AuNPs in the cell cycle of synchronized and non-synchronized cultures of human prostate cancer DU-145 cells. These authors observed an arrest in G2/M phase in non-synchronized cultures (Roa et al., 2009).

No significant differences were found in the cell cycle distribution between NPs-exposed and control cells, both in synchronized and non-synchronized cultures.

Again, this may be due to the concentrations used in this study. As previously mentioned, the choice of the low concentrations was based on the need to avoid cytotoxicity and possible interferences of the NPs in the PI fluorescence, which would interfere in the flow cytometry analysis, of both uptake and cell cycle experiments.

However noticeable changes were observed between the histograms of synchronized and non-synchronized cells. Generally it was noticed that the synchronized cells were accumulated in G1 phase and G2/M phase (not significant yet noticeable). Non-synchronized cells showed accumulation in S phase compared to the synchronized population.

Chapter 6

Conclusion

Conclusion

In conclusion, the present study has demonstrated the lack of toxicity of AuNPs and the toxicity of AgNPs at long exposure times. Regarding AuNPs experiments, even though some cytototoxicity assays demonstrated absence of cytotoxicity (Calcein-AM and PI), slight changes in ROS and lysosomal integrity were observed, and most of these changes were detected in cells treated with pentapeptide-AuNPs.

The AgNPs induced a concentration-dependent toxicity, and mediated by a reduction of mitochondrial activity and loss of lysosomal membrane integrity. Although, ROS production has been reported to be the most likely toxicity mechanism of AgNPs, in this study, high levels of ROS were only detected after 72 h of AgNPs incubation. On the other hand, $AgNO_3$ used as an Ag^+ ions source, demonstrated a concentration-dependent toxicity at all time-points tested.

In flow cytometry analysis, no significant changes were detected in cellular uptake and cell cycle progression, but for a better understanding of these results more flow cytometry studies need to be performed.

Overall, the cytotoxic effects of metallic NPs remain controversial and more studies need to be carried out in order to understand more accurately the toxicity mechanisms of these metallic NPs.

Chapter 7

References

References

Ahamed M, Alsalhi MS, Siddiqui MK (2010) Silver nanoparticle applications and human health. *Clin Chim Acta* 411:1841-1848.

Ahamed M, Karns M, Goodson M, Rowe J, Hussain SM, Schlager JJ, Hong Y (2008) DNA damage response to different surface chemistry of silver nanoparticles in mammalian cells. *Toxicol Appl Pharm* 233:404-410.

Alkilany AM, Thompson LB, Boulos SP, Sisco PN, Murphy CJ (2012) Gold nanorods: Their potential for photothermal therapeutics and drug delivery, tempered by the complexity of their biological interactions. *Adv Drug Deliver Rev* 64:190-199.

Arora S, Jain J, Rajwade JM, Paknikar KM (2009) Interactions of silver nanoparticles with primary mouse fibroblasts and liver cells. *Toxicol Appl Pharm* 236:310-318.

Arora S, Rajwade JM, Paknikar KM (2012) Nanotoxicology and in vitro studies: The need of the hour. *Toxicol App Pharm* 258:151-165.

AshaRani PV, Low Kah Mun G, Hande MP, Valiyaveettil S (2008) Cytotoxicity and Genotoxicity of Silver Nanoparticles in Human Cells. *ACS nano* 3:279-290.

AshaRani PV, Low Kah Mun G, Hande MP, Valiyaveettil S (2009) Cytotoxicity and genotoxicity of silver nanoparticles in human cells. *ACS nano* 3:279-290.

Ashby MF, Ferreira PJ, Schodek DL (2009) Chapter 6 - Nanomaterials: Classes and Fundamentals. In: Nanomaterials, Nanotechnologies and Design, pp 177-197 Boston: Butterworth-Heinemann.

Balansky R, Longobardi M, Ganchev G, Iltcheva M, Nedyalkov N, Atanasov P, Toshkova R, De Flora S, Izzotti A (2013) Transplacental clastogenic and epigenetic effects of gold nanoparticles in mice. *Mutat Res-Fund Mol M* 751–752:42-48.

Beer C, Foldbjerg R, Hayashi Y, Sutherland DS, Autrup H (2012) Toxicity of silver nanoparticles - nanoparticle or silver ion? *Toxicol Lett* 208:286-292.

Bohmert L, Niemann B, Thunemann AF, Lampen A (2012) Cytotoxicity of peptide-coated silver nanoparticles on the human intestinal cell line Caco-2. *Arch Toxicol* 86:1107-1115.

Bystrzejewska-Piotrowska G, Golimowski J, Urban PL (2009) Nanoparticles: Their potential toxicity, waste and environmental management. *Waste Manage* 29:2587-2595.

Chernousova S, Epple M (2013) Silver as antibacterial agent: ion, nanoparticle, and metal. *Angew Chem Int Edit* 52:1636-1653.

Chithrani BD, Chan WCW (2007) Elucidating the Mechanism of Cellular Uptake and Removal of Protein-Coated Gold Nanoparticles of Different Sizes and Shapes. *Nano Lett* 7:1542-1550.

Cho EC, Au L, Zhang Q, Xia Y (2010) The effects of size, shape, and surface functional group of gold nanostructures on their adsorption and internalization by cells. *Small* 6:517-522.

Choi SY, Jeong S, Jang SH, Park J, Park JH, Ock KS, Lee SY, Joo SW (2012) In vitro toxicity of serum protein-adsorbed citrate-reduced gold nanoparticles in human lung adenocarcinoma cells. *Toxicol In Vitro* 26:229-237.

Chompoosor A, Saha K, Ghosh PS, Macarthy DJ, Miranda OR, Zhu Z-J, Arcaro KF, Rotello VM (2010) The Role of Surface Functionality on Acute Cytotoxicity, ROS Generation and DNA Damage by Cationic Gold Nanoparticles. *Small* 6:2246-2249.

Chuang SM, Lee YH, Liang RY, Roam GD, Zeng ZM, Tu HF, Wang SK, Chueh PJ (2013) Extensive evaluations of the cytotoxic effects of gold nanoparticles. *Biochim Biophys Acta* 1830:4960-4973.

Chueh PJ, Liang RY, Lee YH, Zeng ZM, Chuang SM (2014) Differential cytotoxic effects of gold nanoparticles in different mammalian cell lines. *J Hazard Mater* 264:303-312.

Connor EE, Mwamuka J, Gole A, Murphy CJ, Wyatt MD (2005) Gold Nanoparticles Are Taken Up by Human Cells but Do Not Cause Acute Cytotoxicity. *Small* 1:325-327.

Corma A, Garcia H (2008) Supported gold nanoparticles as catalysts for organic reactions. *Chem Soc rev* 37:2096-2126.

de Lima R, Seabra AB, Duran N (2012) Silver nanoparticles: a brief review of cytotoxicity and genotoxicity of chemically and biogenically synthesized nanoparticles. *J Appl Toxicol* 32:867-879.

Dusinska M, Magdolenova Z, Fjellsbø L (2013) Toxicological Aspects for Nanomaterial in Humans. In: Nanotechnology for Nucleic Acid Delivery, vol. 948 (Ogris, M. and Oupicky, D., eds), pp 1-12: *Humana Press*.

Dziendzikowska K, Gromadzka-Ostrowska J, Lankoff A, Oczkowski M, Krawczynska A, Chwastowska J, Sadowska-Bratek M, Chajduk E, Wojewodzka M, Dusinska M, Kruszewski M (2012) Time-dependent biodistribution and excretion of silver nanoparticles in male Wistar rats. *J Appl Toxicol* 32:920-928.

Elechiguerra JL, Burt JL, Morones JR, Camacho-Bragado A, Gao X, Lara HH, Yacaman MJ (2005) Interaction of silver nanoparticles with HIV-1. *J Nanobiotechnology* 3:6.

Elsaesser A, Howard CV (2012) Toxicology of nanoparticles. *Adv Drug Deliver Rev* 64:129-137.

Enustun BV, Turkevich J (1963) Coagulation of Colloidal Gold. *J Am Chem Soc* 85:3317-3328.

European Commission (2011) Commission Recommendation of 18 October 2011 on the definition of nanomaterial. *Official Journal of the European Union*.

Fadeel B, Feliu N, Vogt C, Abdelmonem AM, Parak WJ (2013) Bridge over troubled waters: understanding the synthetic and biological identities of engineered nanomaterials. *Wiley Interdisciplinary Reviews: Nanomedicine and Nanobiotechnology* 5:111-129.

Faramarzi MA, Sadighi A (2013) Insights into biogenic and chemical production of inorganic nanomaterials and nanostructures. *Adv Colloid Interfac* 189–190:1-20.

Fathi-Azarbayjani A, Qun L, Chan YW, Chan SY (2010) Novel vitamin and gold-loaded nanofiber facial mask for topical delivery. *AAPS PharmSciTech* 11:1164-1170.

Foldbjerg R, Olesen P, Hougaard M, Dang DA, Hoffmann HJ, Autrup H (2009) PVP-coated silver nanoparticles and silver ions induce reactive oxygen species, apoptosis and necrosis in THP-1 monocytes. *Toxicol Lett* 190:156-162.

Foley S, Crowley C, Smaihi M, Bonfils C, Erlanger BF, Seta P, Larroque C (2002) Cellular localisation of a water-soluble fullerene derivative. *Biochem Bioph Res Co* 294:116-119.

Fraga S, Faria H, Soares ME, Duarte JA, Soares L, Pereira E, Costa-Pereira C, Teixeira JP, de Lourdes Bastos M, Carmo H (2013) Influence of the surface coating on the

cytotoxicity, genotoxicity and uptake of gold nanoparticles in human HepG2 cells. *J Appl Toxicol* 33:1111-1119.

Freese C, Uboldi C, Gibson MI, Unger RE, Weksler BB, Romero IA, Couraud PO, Kirkpatrick CJ (2012) Uptake and cytotoxicity of citrate-coated gold nanospheres: Comparative studies on human endothelial and epithelial cells. *Part Fibre Toxicol* 9:23.

Gao C, Lu Z, Liu Y, Zhang Q, Chi M, Cheng Q, Yin Y (2012) Highly Stable Silver Nanoplates for Surface Plasmon Resonance Biosensing. *Angew Chem Int Edit* 51:5629-5633.

Garcia-Leis A, Garcia-Ramos JV, Sanchez-Cortes S (2013) Silver Nanostars with High SERS Performance. *J Phys Chem C* 117:7791-7795.

Green DR (1998) Apoptotic Pathways: The Roads to Ruin. *Cell* 94:695-698.

Greulich C, Diendorf J, Simon T, Eggeler G, Epple M, Koller M (2011) Uptake and intracellular distribution of silver nanoparticles in human mesenchymal stem cells. *Acta biomaterialia* 7:347-354.

Grigg J, Tellabati A, Rhead S, Almeida GM, Higgins JA, Bowman KJ, Jones GD, Howes PB (2009) DNA damage of macrophages at an air-tissue interface induced by metal nanoparticles. *Nanotoxicology* 3:348-354.

Grosse S, Evje L, Syversen T (2013) Silver nanoparticle-induced cytotoxicity in rat brain endothelial cell culture. *Toxicol In Vitro* 27:305-313.

Grzelczak M, Perez-Juste J, Mulvaney P, Liz-Marzan LM (2008) Shape control in gold nanoparticle synthesis. *Chem Soc Rev* 37:1783-1791.

Hajnóczky G, Csordás G, Das S, Garcia-Perez C, Saotome M, Sinha Roy S, Yi M (2006) Mitochondrial calcium signalling and cell death: Approaches for assessing the role of mitochondrial Ca2+ uptake in apoptosis. *Cell Calcium* 40:553-560.

I. Pratt CA, W. Anderson, G. Chambers, M. Davoren, K. Dawson, R. Evans, M. Fenelon, T. Harty, L. Hyde, S. Lawrie, I. Lynch, P. O'Mahony, M. Radmoski, A (2008) The Relevance for Food Safety of Applications of Nanotechnology in the Food and Feed Industries. *Food Safety*.

Iversen T-G, Skotland T, Sandvig K (2011) Endocytosis and intracellular transport of nanoparticles: Present knowledge and need for future studies. *Nano Today* 6:176-185.

Jeyaraj M, Arun R, Sathishkumar G, MubarakAli D, Rajesh M, Sivanandhan G, Kapildev G, Manickavasagam M, Thajuddin N, Ganapathi A (2014) An evidence on G2/M arrest, DNA damage and caspase mediated apoptotic effect of biosynthesized gold nanoparticles on human cervical carcinoma cells (HeLa). *Mater Res Bull* 52:15-24.

Jiang X, Foldbjerg R, Miclaus T, Wang L, Singh R, Hayashi Y, Sutherland D, Chen C, Autrup H, Beer C (2013) Multi-platform genotoxicity analysis of silver nanoparticles in the model cell line CHO-K1. *Toxicol Lett* 222:55-63.

Kamat JP, Devasagayam TP, Priyadarsini KI, Mohan H (2000) Reactive oxygen species mediated membrane damage induced by fullerene derivatives and its possible biological implications. *Toxicol* 155:55-61.

Karlsson HL (2010) The comet assay in nanotoxicology research. *Anal Bioanal Chem* 398:651-666.

Kaur J, Tikoo K (2013) Evaluating cell specific cytotoxicity of differentially charged silver nanoparticles. *Food Chem Toxicol* 51:1-14.

Khlebtsov N, Dykman L (2011) Biodistribution and toxicity of engineered gold nanoparticles: a review of in vitro and in vivo studies. *Cheml Soc Rev* 40:1647-1671.

Khoury CG, Vo-Dinh T (2008) Gold Nanostars For Surface-Enhanced Raman Scattering: Synthesis, Characterization and Optimization. *J Phys Chem C* 112:18849-18859.

Kim JA, Aberg C, Salvati A, Dawson KA (2012) Role of cell cycle on the cellular uptake and dilution of nanoparticles in a cell population. *Nat Nanotechnol* 7:62-68.

Kim ST, Saha K, Kim C, Rotello VM (2013) The role of surface functionality in determining nanoparticle cytotoxicity. *Accounts Chem Res* 46:681-691.

Kimling J, Maier M, Okenve B, Kotaidis V, Ballot H, Plech A (2006) Turkevich Method for Gold Nanoparticle Synthesis Revisited. *J Phys Chem B* 110:15700-15707.

Kittler S, Greulich C, Diendorf J, Köller M, Epple M (2010) Toxicity of Silver Nanoparticles Increases during Storage Because of Slow Dissolution under Release of Silver Ions. *Chem Mater* 22:4548-4554.

Kruszewski M, Grądzka I, Bartłomiejczyk T, Chwastowska J, Sommer S, Grzelak A, Zuberek M, Lankoff A, Dusinska M, Wojewódzka M (2013) Oxidative DNA damage corresponds to the long term survival of human cells treated with silver nanoparticles. *Toxicol Lett* 219:151-159.

Levy R, Thanh NT, Doty RC, Hussain I, Nichols RJ, Schiffrin DJ, Brust M, Fernig DG (2004) Rational and combinatorial design of peptide capping ligands for gold nanoparticles. *J Am Chem Soc* 126:10076-10084.

Li P-W, Kuo T-H, Chang J-H, Yeh J-M, Chan W-H (2010) Induction of cytotoxicity and apoptosis in mouse blastocysts by silver nanoparticles. *Toxicol Lett* 197:82-87.

Li X, Fang P, Mai J, Choi E, Wang H, Yang X-f (2013) Targeting mitochondrial reactive oxygen species as novel therapy for inflammatory diseases and cancers. *Journal of Hematology & Oncology* 6:19.

Li Y, Chen DH, Yan J, Chen Y, Mittelstaedt RA, Zhang Y, Biris AS, Heflich RH, Chen T (2012) Genotoxicity of silver nanoparticles evaluated using the Ames test and in vitro micronucleus assay. *Mutat Res-Gen Tox Env* 745:4-10.

Mahmoudi M, Azadmanesh K, Shokrgozar MA, Journeay WS, Laurent S (2011) Effect of nanoparticles on the cell life cycle. *Chem Rev* 111:3407-3432.

McBride HM, Neuspiel M, Wasiak S (2006) Mitochondria: More Than Just a Powerhouse. *Curr Biol* 16:R551-R560.

Meng H, Xia T, George S, Nel AE (2009) A predictive toxicological paradigm for the safety assessment of nanomaterials. *ACS nano* 3:1620-1627.

Mihranyan A, Ferraz N, Strømme M (2012) Current status and future prospects of nanotechnology in cosmetics. *Prog Mater Sci* 57:875-910.

Miura N, Shinohara Y (2009) Cytotoxic effect and apoptosis induction by silver nanoparticles in HeLa cells. *Biochem Bioph Res Co* 390:733-737.

Monteiro-Riviere NA, Samberg ME, Oldenburg SJ, Riviere JE (2013) Protein binding modulates the cellular uptake of silver nanoparticles into human cells: Implications for in vitro to in vivo extrapolations? *Toxicol Lett* 220:286-293.

Morais T, Soares ME, Duarte JA, Soares L, Maia S, Gomes P, Pereira E, Fraga S, Carmo H, Bastos MdL (2012) Effect of surface coating on the biodistribution profile of gold nanoparticles in the rat. *Eur J Pharm Biopharm* 80:185-193.

Nel A, Xia T, Mädler L, Li N (2006) Toxic Potential of Materials at the Nanolevel. *Science* 311:622-627.

Nel AE, Madler L, Velegol D, Xia T, Hoek EMV, Somasundaran P, Klaessig F, Castranova V, Thompson M (2009) Understanding biophysicochemical interactions at the nano-bio interface. *Nat Mater* 8:543-557.

Nelson BC, Petersen EJ, Marquis BJ, Atha DH, Elliott JT, Cleveland D, Watson SS, Tseng IH, Dillon A, Theodore M, Jackman J (2013) NIST gold nanoparticle reference materials do not induce oxidative DNA damage. *Nanotoxicology* 7:21-29.

Ng KW, Khoo SP, Heng BC, Setyawati MI, Tan EC, Zhao X, Xiong S, Fang W, Leong DT, Loo JS (2011) The role of the tumor suppressor p53 pathway in the cellular DNA damage response to zinc oxide nanoparticles. *Biomaterials* 32:8218-8225.

Nymark P, Catalán J, Suhonen S, Järventaus H, Birkedal R, Clausen PA, Jensen KA, Vippola M, Savolainen K, Norppa H (2013) Genotoxicity of polyvinylpyrrolidone-coated silver nanoparticles in BEAS 2B cells. *Toxicol* 313:38-48.

Paino IMM, Marangoni VS, de Oliveira RdCS, Antunes LMG, Zucolotto V (2012) Cyto and genotoxicity of gold nanoparticles in human hepatocellular carcinoma and peripheral blood mononuclear cells. *Toxicol Lett* 215:119-125.

Pan Y, Leifert A, Ruau D, Neuss S, Bornemann J, Schmid G, Brandau W, Simon U, Jahnen-Dechent W (2009) Gold Nanoparticles of Diameter 1.4 nm Trigger Necrosis by Oxidative Stress and Mitochondrial Damage. *Small* 5:2067-2076.

Park EJ, Yi J, Kim Y, Choi K, Park K (2010) Silver nanoparticles induce cytotoxicity by a Trojan-horse type mechanism. *Toxicol In Vitro* 24:872-878.

Patra HK, Banerjee S, Chaudhuri U, Lahiri P, Dasgupta AK (2007) Cell selective response to gold nanoparticles. *Nanomed - Nanotechnol* 3:111-119.

Peralta-Videa JR, Zhao L, Lopez-Moreno ML, de la Rosa G, Hong J, Gardea-Torresdey JL (2011) Nanomaterials and the environment: A review for the biennium 2008–2010. *J Hazard Mater* 186:1-15.

Pernodet N, Fang X, Sun Y, Bakhtina A, Ramakrishnan A, Sokolov J, Ulman A, Rafailovich M (2006) Adverse effects of citrate/gold nanoparticles on human dermal fibroblasts. *Small* 2:766-773.

Piao MJ, Kang KA, Lee IK, Kim HS, Kim S, Choi JY, Choi J, Hyun JW (2011) Silver nanoparticles induce oxidative cell damage in human liver cells through inhibition of reduced glutathione and induction of mitochondria-involved apoptosis. *Toxicol Lett* 201:92-100.

Qu Y, Lu X (2009) Aqueous synthesis of gold nanoparticles and their cytotoxicity in human dermal fibroblasts-fetal. *Biomed Mater* 4:025007.

Ravindran A, Chandran P, Khan SS (2013) Biofunctionalized silver nanoparticles: Advances and prospects. *Colloid Surface B* 105:342-352.

Roa W, Zhang X, Guo L, Shaw A, Hu X, Xiong Y, Gulavita S, Patel S, Sun X, Chen J, Moore R, Xing JZ (2009) Gold nanoparticle sensitize radiotherapy of prostate cancer cells by regulation of the cell cycle. *Nanotechnology* 20:375101.

Roy R, Kumar S, Tripathi A, Das M, Dwivedi PD (2014) Interactive threats of nanoparticles to the biological system. *Immunol Lett* 158:79-87.

Sablina AA, Budanov AV, Ilyinskaya GV, Agapova LS, Kravchenko JE, Chumakov PM (2005) The antioxidant function of the p53 tumor suppressor. *Nat Med* 11:1306-1313.

Saidin NA (2008) Cytotoxicity of extract of Malaysian Mitragyna speciosa Korth and its dominant alkaloid mitragynine. In: Department of Biomolecular Medicine, vol. Doctor of philosophy: Faculty of Medicine, Imperial College of London.

Siegel RW (1994) Nanophase materials. In: In Encyclopedia of applied physics, vol. 11, pp 1-27 Weinheim: G.L. Trigg,.

Singh N, Manshian B, Jenkins GJS, Griffiths SM, Williams PM, Maffeis TGG, Wright CJ, Doak SH (2009) NanoGenotoxicology: The DNA damaging potential of engineered nanomaterials. *Biomaterials* 30:3891-3914.

Singh RP, Ramarao P (2012) Cellular uptake, intracellular trafficking and cytotoxicity of silver nanoparticles. *Toxicol Lett* 213:249-259.

Singh S, D'Britto V, Prabhune AA, Ramana CV, Dhawan A, Prasad BLV (2010) Cytotoxic and genotoxic assessment of glycolipid-reduced and -capped gold and silver nanoparticles. *New J Chem* 34:294-301.

Stern S, Adiseshaiah P, Crist R (2012) Autophagy and lysosomal dysfunction as emerging mechanisms of nanomaterial toxicity. *Part Fibre Toxicol* 9:20.

Sun L, Liu D, Wang Z (2008) Functional Gold Nanoparticle−Peptide Complexes as Cell-Targeting Agents. *Langmuir* 24:10293-10297.

Sun Y, Wiederrecht GP (2007) Surfactantless Synthesis of Silver Nanoplates and Their Application in SERS. *Small* 3:1964-1975.

Teodoro JS, Simoes AM, Duarte FV, Rolo AP, Murdoch RC, Hussain SM, Palmeira CM (2011) Assessment of the toxicity of silver nanoparticles in vitro: a mitochondrial perspective. *Toxicol In Vitro* 25:664-670.

Tolaymat TM, El Badawy AM, Genaidy A, Scheckel KG, Luxton TP, Suidan M (2010) An evidence-based environmental perspective of manufactured silver nanoparticle in syntheses and applications: A systematic review and critical appraisal of peer-reviewed scientific papers. *Sci Total Environ* 408:999-1006.

Verma A, Stellacci F (2010) Effect of surface properties on nanoparticle-cell interactions. *Small* 6:12-21.

Vousden KH, Lane DP (2007) p53 in health and disease. Nat Rev Mol Cell Biol 8:275-283.

Wu Y-L, Putcha N, Ng KW, Tai Leong D, Lim CT, Loo SCJ, Chen X (2012) Biophysical Responses upon the Interaction of Nanomaterials with Cellular Interfaces. *Accounts Chem Res* 46:782-791.

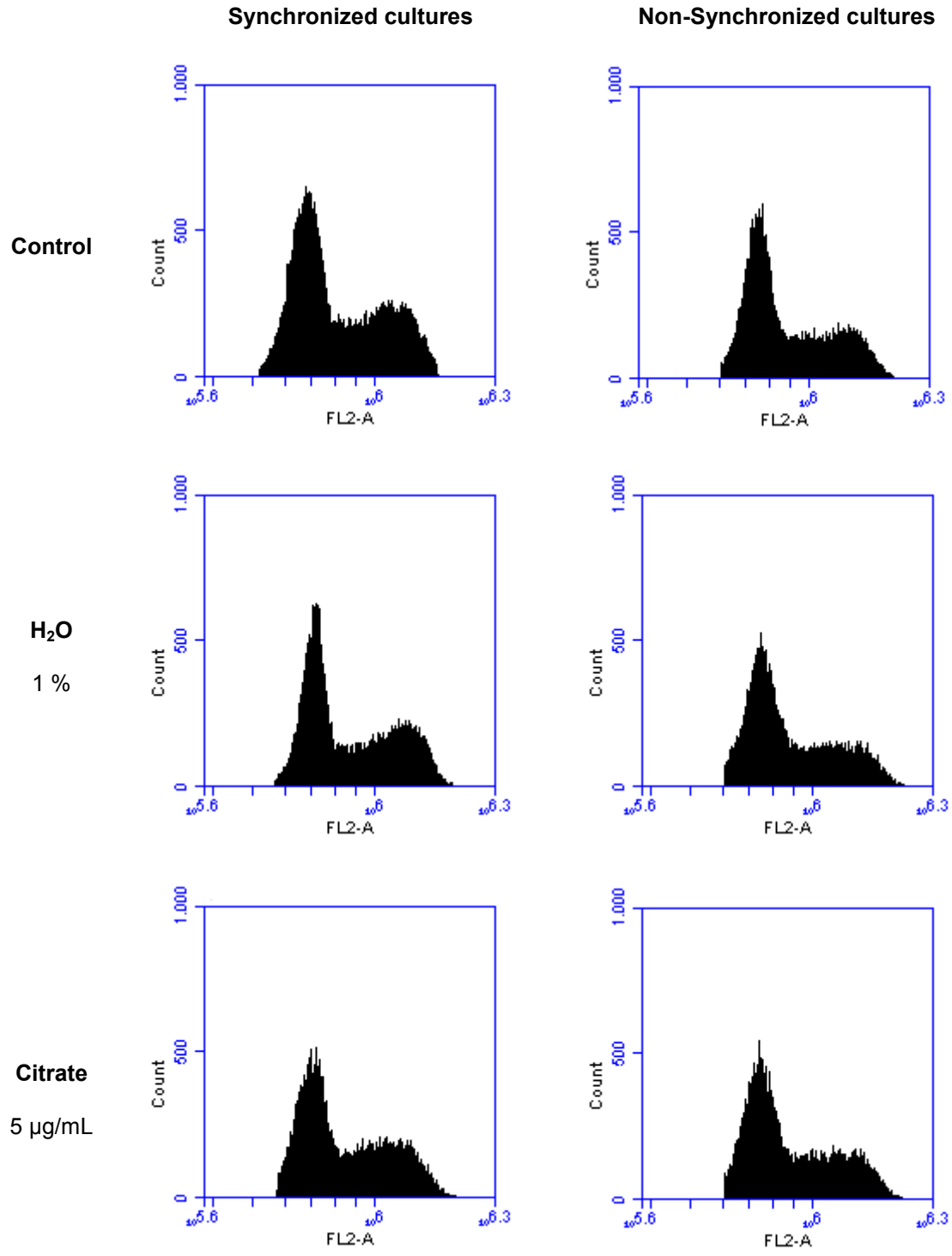
Xia T, Kovochich M, Liong M, Madler L, Gilbert B, Shi H, Yeh JI, Zink JI, Nel AE (2008) Comparison of the mechanism of toxicity of zinc oxide and cerium oxide nanoparticles based on dissolution and oxidative stress properties. *ACS nano* 2:2121-2134.

Zhang X-P, Liu F, Wang W (2010) Coordination between Cell Cycle Progression and Cell Fate Decision by the p53 and E2F1 Pathways in Response to DNA Damage. *J Biol Chem* 285:31571-31580.

Zhang X-Q, Xu X, Bertrand N, Pridgen E, Swami A, Farokhzad OC (2012) Interactions of nanomaterials and biological systems: Implications to personalized nanomedicine. *Adv Drug Deliver Rev* 64:1363-1384.

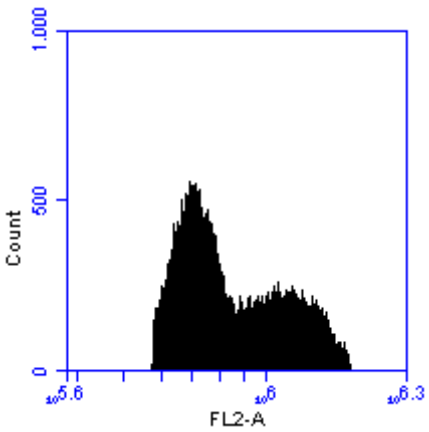
Zheng Q, Yang H, Wei J, Tong JL, Shu YQ (2013) The role and mechanisms of nanoparticles to enhance radiosensitivity in hepatocellular cell. *Biomed Pharmacother* 67:569-575.

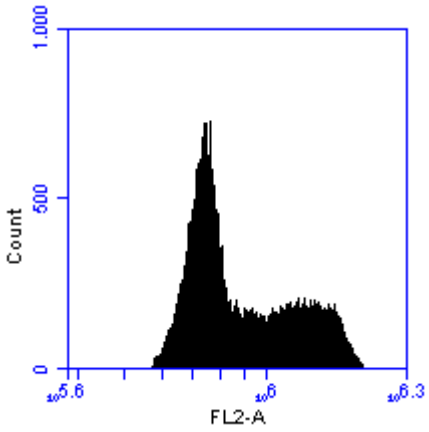
Supplement 1


Synchronized cultures
Non-Synchronized cultures
Control
H2O
1 %
Citrate
5 µg/mL
Count
FL2-A
1.000
500
0

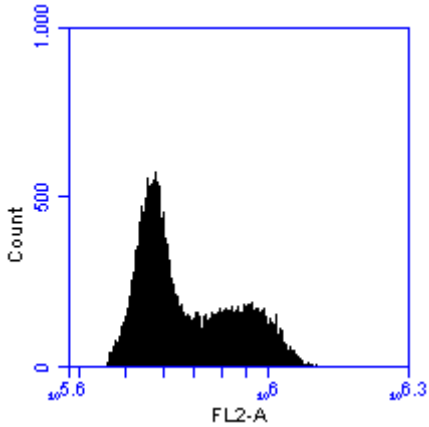
Cit-AuNPs

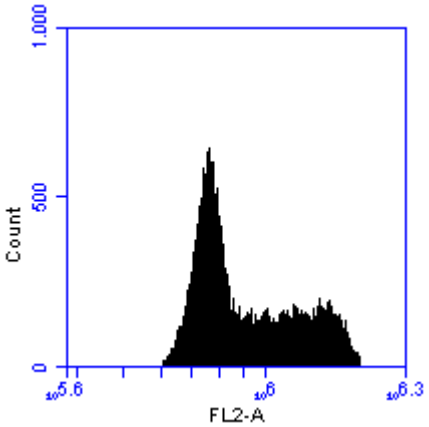
1 µM



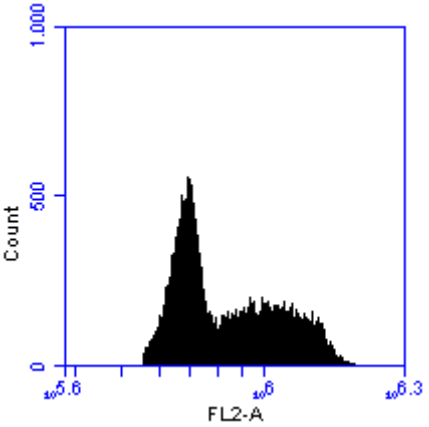


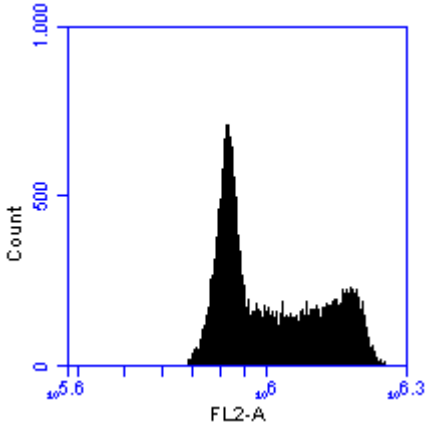
Cit-AuNPs 3 µM





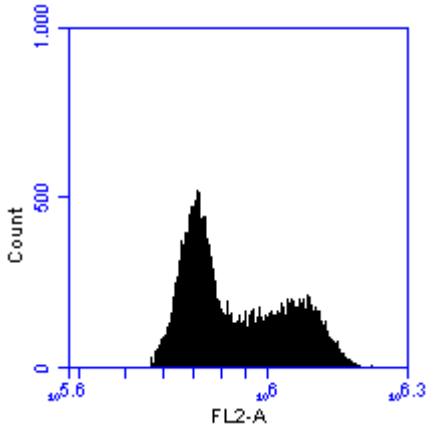
Cit-AuNPs 10 µM

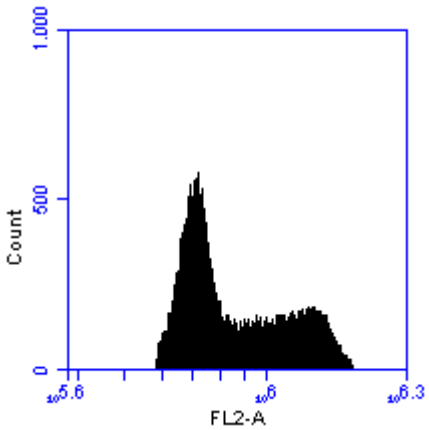




CALNN-AuNPs

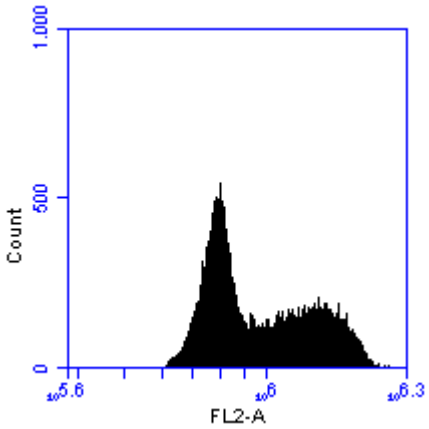
1 µM

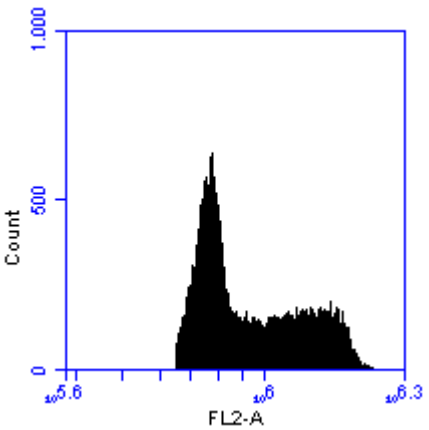




CALNN-AuNPs

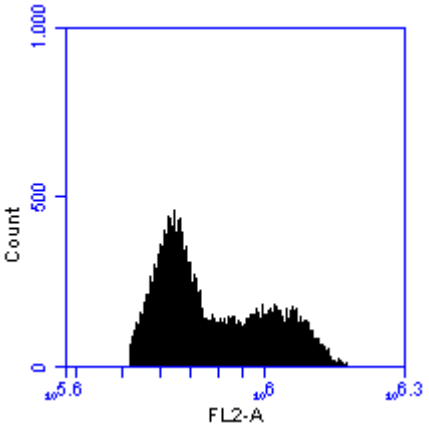
3 µM

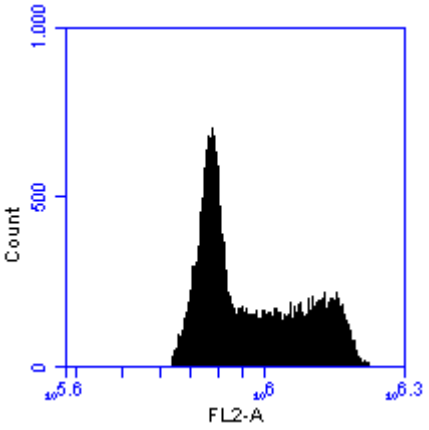




CALNN-AuNPs

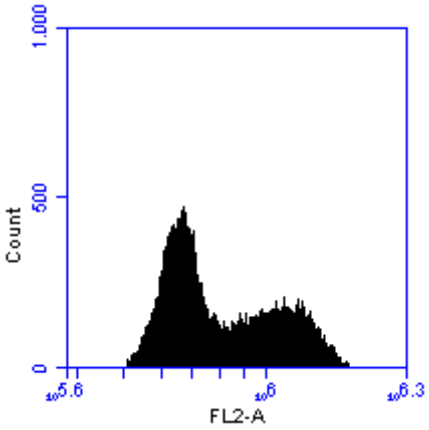
10 µM

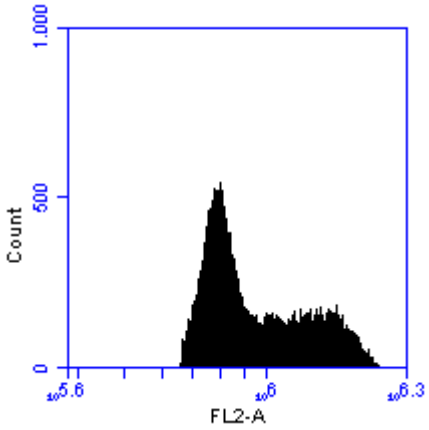




CALNS-AuNPs

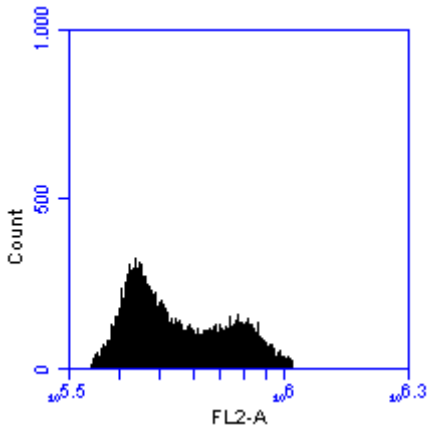
1 µM

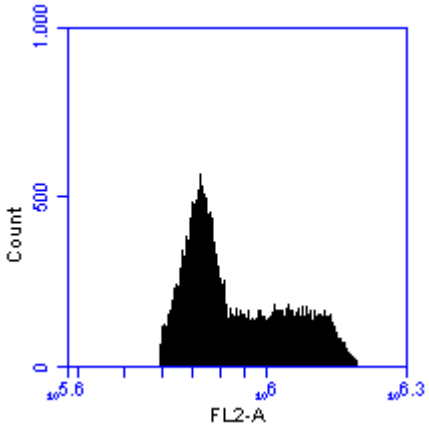




CALNS-AuNPs

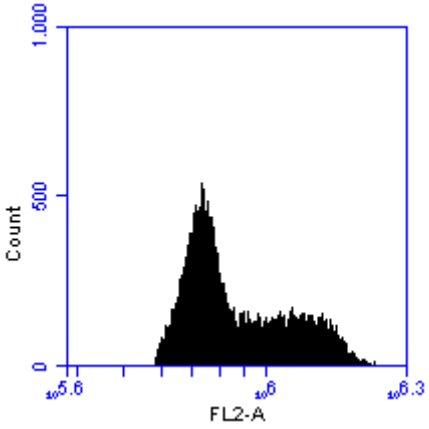
3 µM

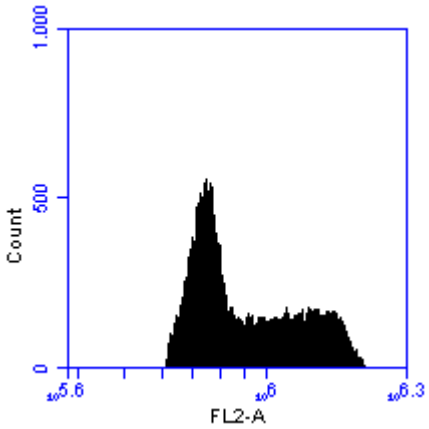




CALNS-AuNPs

10 µM





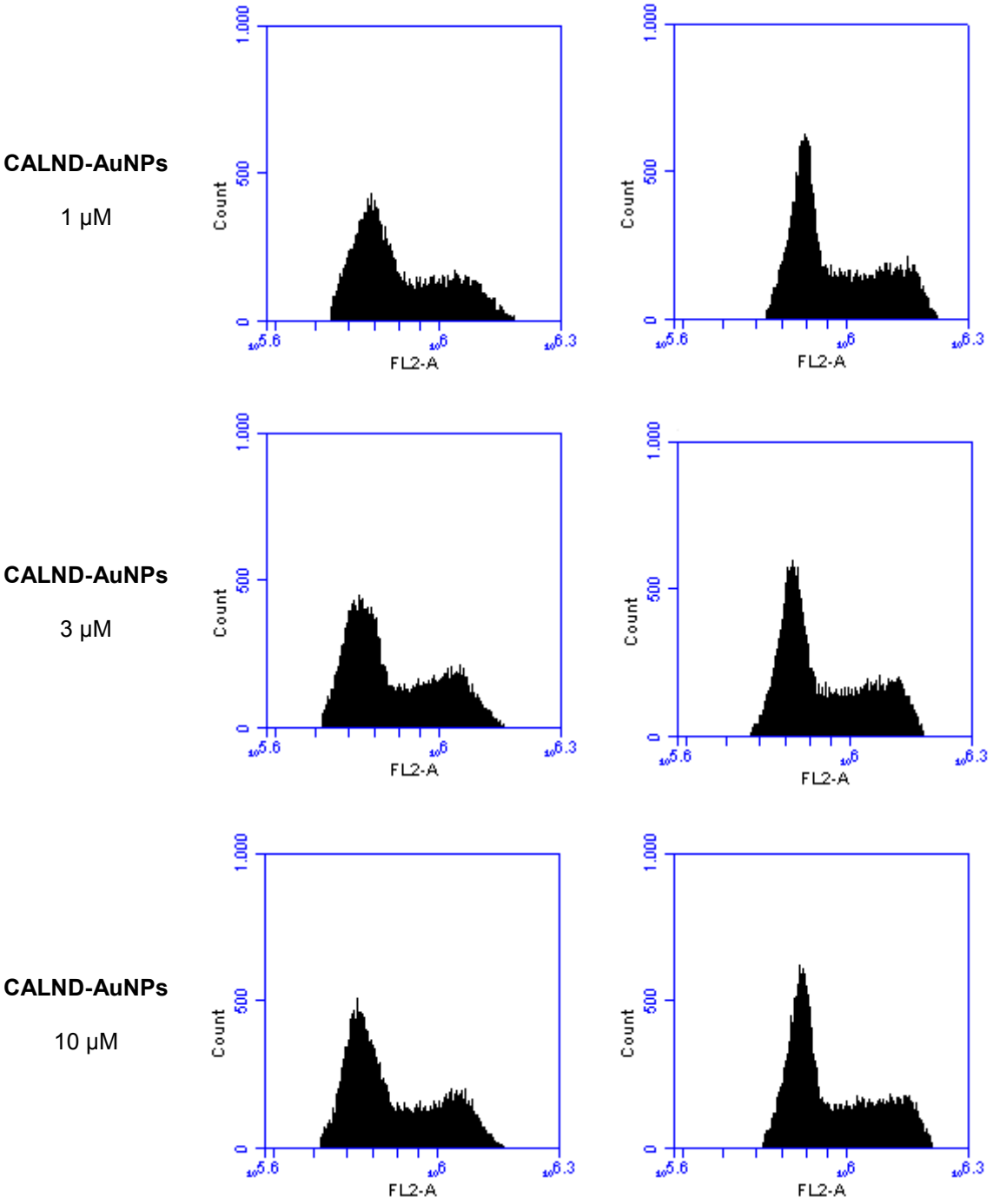


Figure 23 - Representative histograms of the Caco-2 cell cycle analysis by flow cytometry after 24 h of exposure with Cit-, CALNN-, CALNS- and CALND-AuNPs (1, 3 and 10 µM), comparing to control cells (synchronized and non-synchronized culture).